NTNU – Trondheim
Norwegian University of
Science and Technology

Evaluation of Methods for Detecting and Locating Faults in HVDC Grids

Erik Martinsen

Master of Energy and Environmental Engineering
Submission date: June 2014
Supervisor: Hans Kristian Høidalen, ELKRAFT
Co-supervisor: Salvatore D'Arco, SINTEF

Norwegian University of Science and Technology
Department of Electric Power Engineering

Problem description

Protection in HVDC networks is more difficult than in AC networks, both due to the low impedance and lack of changes in current polarity. Very fast tripping of DC interruption devices is required in order to avoid harmful stress to the converters. A project at SINTEF energy Research addresses protection and fault handling in offshore DC grids, but with main focus on power converter performance.

In order to investigate different protection principles, a simple Multi Terminal High Voltage Direct Current (MTDC), radial cable based system is to be modeled in PSCAD. Simulation models are obtainable from SINTEF, but this should be tested and extended. The model should incorporate full switching, two level voltage source converters and a cable model suiatble for simulations of direct current. The finished model is to be used for investigating fault currents and voltages in the MTDC system.

Once fault characteristics have been established, different fault localisation principles shall be implemented in the MTDC system model. Traditional methods which should be considered for implementation include:

- Overcurrent and undervoltage protection
- Differential protection
- Voltage derivative protection

In addition, newer localisation methods based on signal processing should also be investigated, especially the following two methods:

- Travelling wave protection
- Fault location algorithms, for instance Wavelet transforms

Goal of the project is to implement these methods in the PSCAD model and evaluate them under different fault conditions. Following this evaluation, a protection scheme which will meet requirements for fast and precise fault detection and localisation for all faults should be implemented if possible.

Abstract

In this thesis work, different proposed methods for detecting and locating short circuit faults in Multi Terminal HVDC grids have been evaluated by implemenation and transient simulations in PSCAD. The research has been limited to cable based systems.

HVDC grids have seen increasing interest in recent years, but have yet to be fully realised. Suitable converter technology was introduced in 1997 and has been further developed since, while switches able to interrupt large DC currents were introduced in June 2013. One of the major issues left is fault localisation. Due to the low impedance in HVDC cable systems, fault currents rise to severe magnitudes system wide in a matter of a few milliseconds. This may cause damage to the converter diodes if not dealt with quickly.

In order to obtain a better understanding of the fault propagation, research into the subject is presented. It is found that the capacitors in the converters is a main source of large fault currents, and fast fault detection is essential for protection of converter components. Time between first detection of fault until current interruption should be within a few milliseconds.

Different methods have been proposed for localisation of faults in recent years. These are presented together with traditional fault localisation methods, and briefly discussed with the intent of deciding which to implement and evaluate in PSCAD.

Protection based on current derivative and wavelet transformation, as well as travelling wave protection is chosen and implemented in a three converter VSC system. Different fault types are applied at various locations with varying system capacitance and up to 16 Ω fault impedance. The results indicate that none of the three methods are able to detect and locate all impedance faults on their own. The travelling wave protection is suitable for short lines, but fails when exposed to high fault impedances and distances.

By using derivative polarity to determine direction of fault and wavelet magnitude to determine distance, faults are successfully located in a high capacitance system within a respectable time. It is concluded that all the three tested methods should be considered for implementation when designing a future HVDC protection system.

Sammendrag

I denne avhandlingen er forskjellige foreslåtte metoder for å bestemme feillokasjon i flerterminals HVDC systemer presentert og undersøkt ved hjelp av simuleringer i PSCAD. Simuleringene har tatt for seg et radielt kabelsystem med tre VSC omformere.

Interessen for flerterminals HVDC systemer har økt de siste årene, men et større system har enda ikke blitt realisert. Passende omformerteknologi ble innført i 1997 og har blitt utviklet videre i senere tid. Brytning av store likestrømmer har lenge vært umulig, men ny bryterteknologi med dette formålet ble introdusert i juni 2013. En av de største gjenværende utfordringene er feillokalisering. På grunn av lav impedans i kabelbaserte HVDC systemer stiger feilstrømmer raskt til nivåer som kan forårsake skade på komponenter i systemet.

For å oppnå en bedre forståelse av hvordan feil sprer seg i nettet blir nyere forskning på feltet presentert. Det konkluderes med at filterkapasitansen i de nye omformerne er en hovedårsak til store feilstrømmer, og rask feillokalisering er essensielt for å unngå skade på komponenter i omformerne. For å unngå dette bør feilen klareres innen få millisekunder.

Forskjellige metoder for å gjennomføre feillokalisering i HVDC nett på en rask og sikker måte har blitt foreslått i nyere tid. Noen av disse er presentert sammen med tradisjonelle metoder for feillokalisering med det formål å bestemme hvilke som skal implementeres i PSCAD.

Lokaliseringsmetoder basert på derivering av strøm, wavelet transformasjon og vandrebølger blir implementert i et radielt HVDC system med tre VSC omformere. Forskjellige feiltyper blir lagt inn ved forskjellige lokasjoner i nettet, med varierende kapasitans ved omformerne og opptil 16 Ω feilimpedans. Resultatene indikerer at ingen av de tre systemene kan lokalisere feilen på egenhånd, uavhengig av feilimpedans og avstand til feil. Vandrebølgemetoden er egnet for linjer med begrenset lengde, men klarer ikke å oppdage feil over lengre distanse med høy impedans.

Ved å benytte polariteten til den deriverte av strømmen for å bestemme feilretning og wavelet koeffisienten til å bestemme avstand lykkes det å detektere feil raskt og sikkert i et system med høy kapasitans for alle feildistanser og –impedanser. Alle de tre systemene anses som egnet til å være del av en endelig lokaliseringsløsning for HVDC nett.

Acknowledgements

There are many who deserve thanks for helping me through the last five years of studying, and especially with the last semester of writing this thesis.

First of all I must thank my two supervisors, professor Hans Kristian Høidalen at NTNU and Salvatore D'Arco at SINTEF Energy, for this interesting and challenging work. You have laid the foundation and supported me in uncertain times, and been there for me when I had questions.

A big thank you also goes to other employees at SINTEF energy, namely John Are Suul and Andrzej Holdyk who have provided me with the necessary simulation models and always been available for explanations of difficult questions.

I must also thank my fellow students at NTNU and the city of Trondheim for good times and many wonderful memories. Especially those I have been spending most time with. Ole, Marielle, Truls, Richard and Hanne, it would have been awfully boring without you.

Lastly, I thank my father and brother who always believe in me, even when I do not.

Trondheim June 2014 Erik Martinsen

Contents

List of Figures

List of Tables

Abbreviations

HVDC	**H**igh **V**oltage **D**irect **C**urrent
HVAC	**H**igh **V**oltage **A**lternating **C**urrent
MTDC	**M**ulti **T**erminal High Voltage **D**irect **C**urrent
MMC	**M**odular **M**ultilevel **C**onverter
HBSM	**H**alf **B**ridge **S**ub **M**odule
FBSM	**F**ull **B**ridge **S**ub **M**odule
C-DSM	**C**lamped-**D**double **S**ub **M**odule
VSC	**V**oltage **S**ource **C**onverter
CSC	**C**urrent **S**ource **C**onverter
ANN	**A**rtificial **N**eural **N**etworks
OCT	**O**ptical **C**urrent **T**ransducer

Chapter 1

Introduction

1.1 Background and motivation

With the ever increasing demand for electrical power and construction of renewable energy, there is a need for increased power transmission capacity over long distances. Implementing the increased power generation into an existing power system, such as in Europe or North America, represents a challenge for the mature HVAC network [1]. To overcome this challenge, increased interconnection of load centers with the use of HVDC has been proposed as an efficient and economical solution. Classic HVDC systems are point-to-point systems, but great advantages could be obtained by the implementation of an interconnected HVDC grid [2].

For the implementation of a full HVDC grid, voltage Source Converters (VSCs) are favored over traditional Current Source Converters (CSCs) [1]. This is primarily due to the VSCs capability of changing power flow by reverting current direction, as opposed to the CSC which changes voltage polarity. However, there are several challenges related to the development of a multi-converter, complex HVDC grid based on VSCs. Amongst the most serious of these is fault handling [2]. The low impedance in HVDC grids coupled with the lack of changing current polarity makes both locating and interrupting a fault more difficult than in HVAC networks. Compared to a CSC, the VSC has a very low inductance, making it more susceptible to damage during DC faults.

For the last decade, several methods for locating DC short circuit faults have been proposed. While there are some very promising solutions, very few have been tested for various fault locations and fault types. When implementing a fault detection system, it is important to know that the system will be able to detect all faults regardless of fault location and impedance. It is also of interest to determine what system parameters limits the implementation of the different systems.

1.2 Scope and limitations

For this thesis, different proposed fault localisation methods will be presented. Some of the presented methods are implemented in a computer model of a power system in PSCAD. Faults will be applied at various locations and with varying fault impedance. In addition, parameters of the grid which may affect the results are varied.

There are multiple goals with the simulations. First, the simulated fault currents and voltages will be compared to results obtained in previous literature to confirm the behaviour of the model. Second, the results will determine how the different methods perform under different conditions. It is especially interesting to determine weaknesses and limits of each method. Lastly, the results will be used to propose a detection system using one or more of the implemented methods.

The simulations and investigations are limited to detecting and locating the fault. Current interruption and isolation of fault will not be simulated, merely discussed.

The implemented model does not contain any overhead HVDC lines, only cables. Overhead lines have different characteristics than cables, including higher inductance and lower capacitance, which will influence fault behaviour.

Faults are only applied in DC cables and the converters. It will not be tested whether the different methods are able to differentiate between AC and DC faults, nor are the effects of DC faults on the AC system investigated.

1.3 Thesis structure

The thesis is structured in 8 chapters and five appendices, following this introduction which is the first chapter.

The second chapter describes how the HVDC grid can be built, with an emphasis on the components and different construction schemes. This is based on literature regarding classic HVDC systems as well as various studies into the feasibility of HVDC grids.

In the third chapter, theory regarding fault currents is introduced. Results from several papers which have investigated faults in HVDC grids are also presented. Emphasis is on determining how fast a protection system must act to avoid system damage, and also what parameters influences the fault currents.

In the fourth chapter, different methods for fault detection are presented, and evaluated for use in HVDC systems. Both traditional and newly proposed fault location methods are examined, and some of these are later picked for implementation in PSCAD.

The fifth chapter describes the implemented PSCAD model and detection methods together with the planned simulations and expectations of results.

The sixth chapter contain results from the simulations, and also explanations to some of the observations, as well as a discussion of the different detection methods.

Based on the results in chapter six, the possibility of a detection system based around those methods is discussed in chapter seven.

Conclusions and proposal for further work are then presented in chapters eight and nine.

1.4 Procedure for writing the thesis

The basis of this thesis will be the results obtained from simulations of faults in PSCAD. PSCAD is a very advanced and widely used power transient simulation software, containing one of the worlds most accurate cable models for simulating power transients. The implemented VSC model is provided by SINTEF energy

research, including the control system. SINTEF has also provided parameters for the cable model.

In order to plot the results in a presentable manner, MATLAB is used to post-process the results from PSCAD. MATLAB is also used for other forms of post-processing, which will be detailed in chapter five.

A literature study into the construction of HVDC grids, fault propagation, and fault detection in HVDC grids was undertaken prior to writing this thesis. This work forms the main body of chapters two through four.

Chapter 2

The Multi terminal HVDC system

2.1 History of HVDC and the road to an HVDC grid

HVDC systems have a long history in electrical engineering. In the early age of electricity, all distribution systems were DC. However, as the electrical grid grew there was an increasing demand for higher voltage and power levels, making HVAC systems the norm [1]. In more recent years however, HVDC systems have seen an increase in popularity, and is a popular choice for several applications. These are mainly bulk power transmission across long distances, and the interconnection of HVAC systems operating at different frequencies from one another, known as asynchronous networks [1]. HVDC is also often preferred over HVAC for use in cables, as this drastically decreases voltage loss.

So far all HVDC systems, with a few exceptions, are point to point systems, meaning the power transfer is merely between two converter stations, either connected with cable or overhead line. With recent increase in power demand and production, and especially the increasing renewable share, serious effort has been devoted to examine the feasibility of more complex HVDC systems with several converters interconnected. Such a system is known as a Multi Terminal HVDC (MTDC) system. There are a few in current operation, with the three converter Canadian

FIGURE 2.1: The Quebec-New England MTDC transmission line. Taken from [3]

Quebec-New England connection being amongst the first. This is illustrated in figure 2.1, albeit two of the converters shown are no longer in operation [1].

The future HVDC grid is envisioned to fulfil a larger amount of different tasks than the traditional HVDC connections. Some of these are presented in [1]:

- Supply power to urban load centres
- Interconnection of offshore installations, especially wind farms and oil/gas platforms
- Bulk power transfer between countries and continents

An HVDC grid can be imagined both as an independent grid, or as an overlay grid alleviating the strain on existing HVAC grids which are close to their maximum operating point [1]. There are several advantages for choosing HVDC over HVAC for the future expansion of the high voltage power transmission [1]:

- Lower number of cables and reduced visual impact
- Enables power exchange between asynchronous networks
- Lower losses over long distances
- Improves performance in parallel HVAC grid

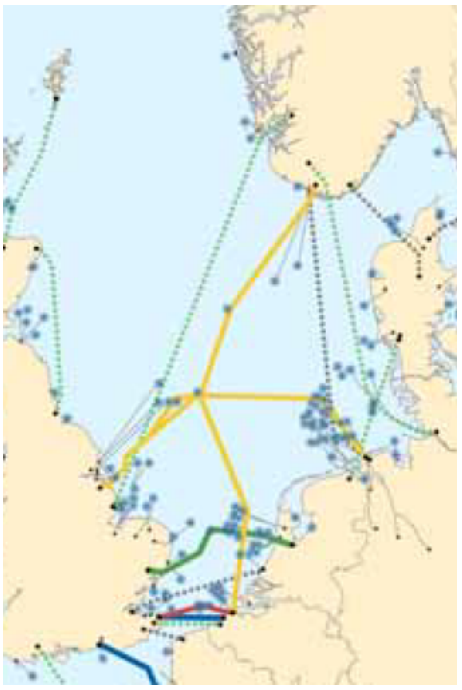

FIGURE 2.2: Proposed topology for MTDC system in the North Sea. Dotted lines are existing HVDC interconnections. Taken from [2]

However, there are technical challenges which must be overcome before the realisation of MTDC systems is feasible. Important steps have been made in recent decades, especially with the introduction of new converter technology in 1997 by ABB [4], known as Voltage Source Converter (VSC). Among the remaining challenges, fault handling is considered one of the major ones [2, p. 83] [1, 5].

The possibility of a European HVDC supergrid has been investigated in [2], where different design possibilities are discussed. Different system topologies for an MTDC system in the North Sea are proposed, one of which is illustrated in figure 2.2. Varying power and voltage ratings are also proposed. Due to constraints in development of converter technology, it is assumed that power rating in a VSC based network will be limited to 1.2 GW until year 2020, and increase to 2 GW in the year 2030. Voltage rating for the 1.2 GW system is proposed to $\pm$320 kV, and increased to $\pm$500 kV for a 2 GW system [2, p. 115]. Current ratings in these systems would be 1.875 kA and 2 kA, respectively.

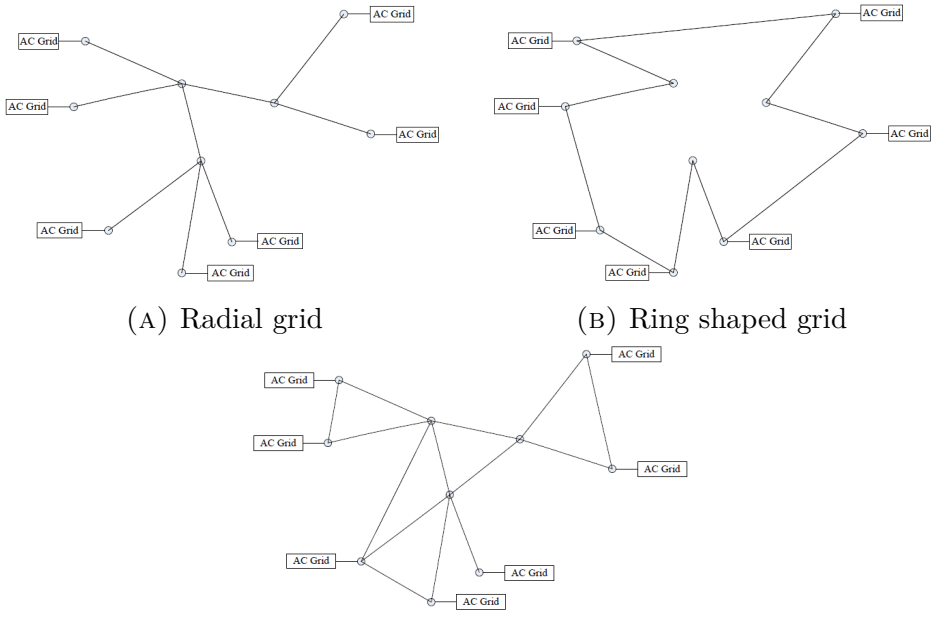

(A) Radial grid

(B) Ring shaped grid

(C) Meshed grid

FIGURE 2.3: Different grid topologies

2.2 Different system topologies

There are basically three different topologies for multi terminal grids; radial, ring shaped and meshed. These concepts are illustrated in figure 2.3. Advantages and disadvantages are summarised in table 2.1, based on information in [6].

TABLE 2.1: Advantages and disadvantages with different grid topologies

Topology	Meshed	Ring shaped	Radial
Redundancy	High. All loads have alternative feeding line	Some. A fault may cause overload in some lines and increase transmission distance and losses	Low. Loads are primarily only fed through a single line, and will lose power in case of fault
Complexity	High	Low	Low
Cost	High	Medium	Low

Choice of grid topology also affect severity of fault currents, with the meshed grid leading to larger currents and more complicated fault localisation [6].

2.3 HVDC system configurations

There are different ways of connecting converters together in a DC system. A distinction is made between monopolar and bipolar systems [1, 7–9], with the monopolar systems further distinguished as either asymmetrical or symmetrical. These different configurations will be presented in the following sections.

2.3.1 Monopolar systems

In monopolar systems, each converter station consists of a single converter. The resulting maximum system voltage and power is thus equal to the maximum rating of the converter. Most submarine cable HVDC systems using classical converter technology are monopoles [9]. The highest monopolar VSC system contracted is Skagerrak 4 at 500 kV and a power rating of 715 MW, with a possibility of upgrading to 800 kV [10].

2.3.1.1 Asymmetrical monopoles

With an asymmetric monopole, each converter is connected to a high voltage conductor at one pole, while the other pole is grounded [1]. Power is transmitted through the high voltage conductor, while current return path can either be through earth, or the grounded points of each converter can be interconnected via a low voltage conductor [8]. The latter configuration is called asymmetrical monopole with metallic return, while the former is known as asymmetrical monopole with earth return, both illustrated in figure 2.4 [1]. Earth return is cheaper, as there is only a single conductor which needs to be installed, but it leads to a continuous flow of current through earth. This is not acceptable in all parts of the world, as parts of the environment can be damaged by these currents [1, 7]. With the metallic earth return, the continuous earth currents are avoided, but losses will increase due to the resistance in the return conductor [1].

2.3.1.2 Symmetrical monopoles

In symmetrical monopoles, both poles are connected to high voltage conductors, illustrated in figure 2.5. Each conductor will then carry half the rated power

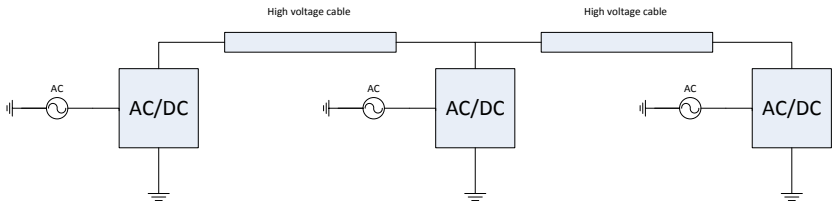

(A) Earth return

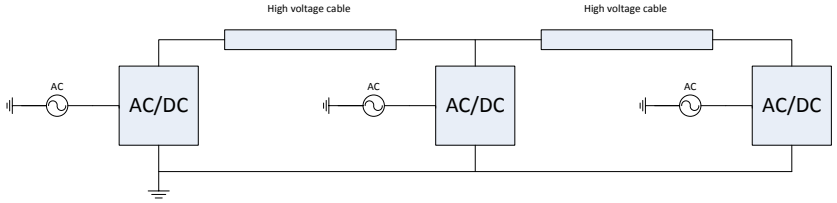

(B) Metallic return

FIGURE 2.4: Asymmetric monopoles with three converters

and be subjected to half the system voltage [7]. The conductors are at equal, but opposite polarity [8]. Neutral point can then be provided in different ways, including grounding of the mid point, grounding at the AC side through reactors and grounding on the DC poles through large resistors [1]. Since the currents in each conductor are equal and opposite under normal operation, the ground current is zero, and so there is no need for a metallic return path. Most of the VSC systems currently installed are symmetrical monopoles [1]

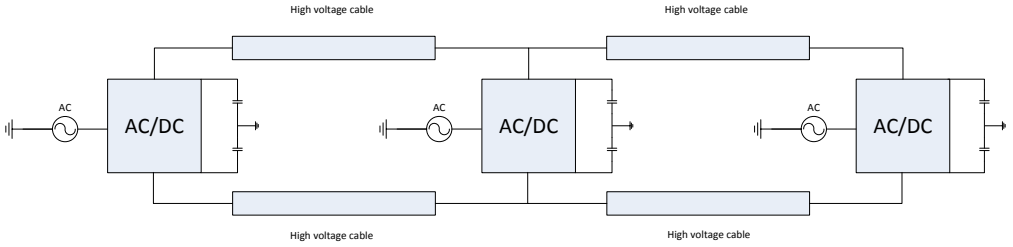

FIGURE 2.5: Symmetrical monopole with grounded midpoint and earth return

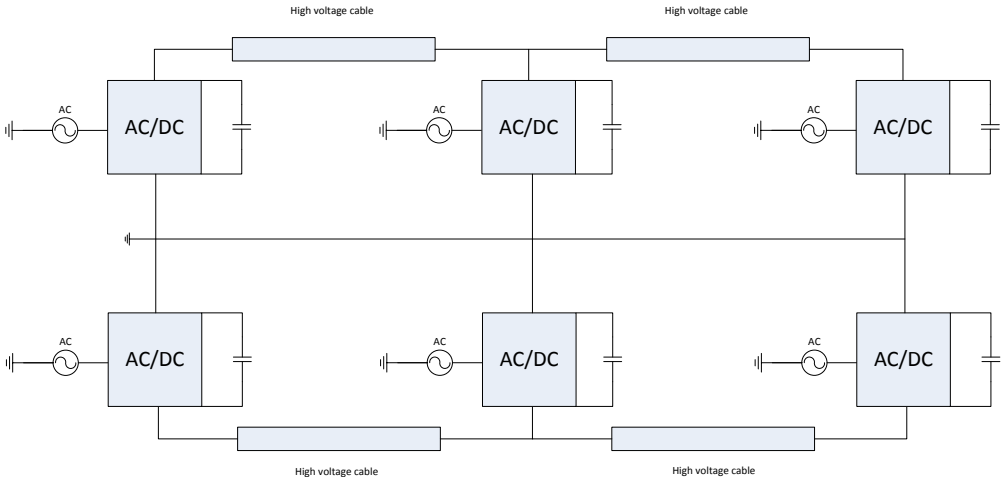

FIGURE 2.6: Bipolar system with grounded midpole and metallic return

2.3.2 Bipolar system

If voltage and power rating is to be increased beyond what is possible for a single converter, two converters can be connected together in a bipolar configuration, which is illustrated in figure 2.6. The bipolar configuration is basically two monopolar systems operating in parallel [9], at equal voltage levels but with opposite polarity from one another [7]. The bipolar system is similiar to the symmetrical monopole, but the extra converter operating in parallel ensures increased

redundancy, allowing the system to continue operation at half the rated voltage in case of a fault on either pole [1]. Bipolar systems are grounded at the DC mid point between the converters to provide a neutral point. The neutral points of each converter can be connected together with metallic return, but during normal operation of both poles the neutral current will be zero [1].

2.3.3 Comparison of the possible configurations

When considering offshore cable based sytems, the asymmetrical monopole with earth return is the simplest and least costly solution, as there is only need for the laying of a single cable [1]. However, it is getting increasingly difficult to attain permission to build systems with earth return, and so a low voltage conductor must be laid down in addition. The laying cost of a second conductor is quite substantial, making the cost difference between a low voltage metallic return and a high voltage conductor used in symmetrical monopoles relatively small [1]. When considering interconnection of several stations into an MTDC grid, the bipolar configuration with a metallic return path seems to offer the best solution [1]. This is due to several factors listed below.

- Higher voltage means lower currents and therefore lower losses and thermal stress [1]
- Higher capacity makes it easier to connect smaller systems [1]
- It is possible to connect monopolar converter stations between the metallic return path and high voltage conductor [1]

The last point is illustrated in figure 2.7. Connecting monopole converter stations to a larger bipolar system reduce cost and the need for extra space compared to a full bipolar station. This is especially interesting for offshore oil platforms and wind farms, since it is expensive to provide the extra room needed for a second converter when building in the ocean.

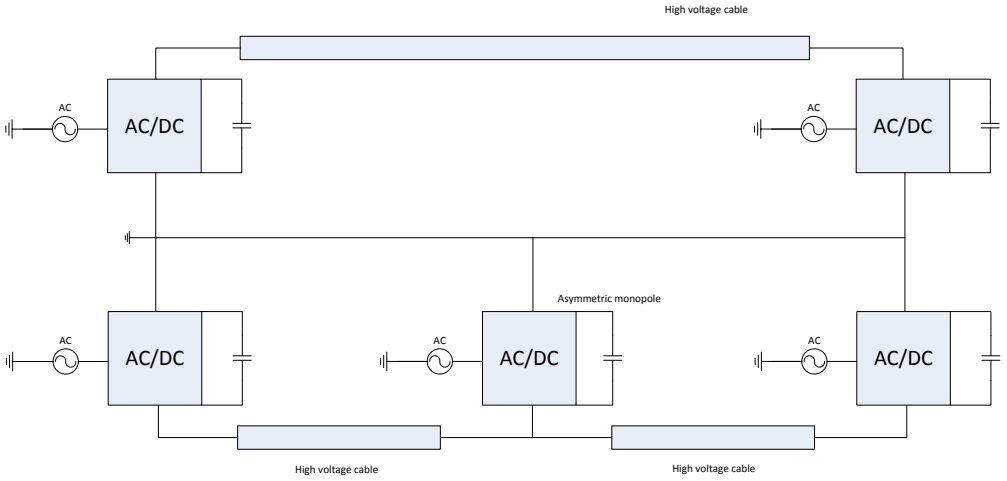

FIGURE 2.7: Asymmetric monopole connected to a two converter bipolar system

2.4 Converter technologies in an MTDC system

2.4.1 Current Source Converters and Voltage Source Converters

As mentioned earlier, a new converter technology was introduced in 1997, known as Voltage Source Converters (VSC), or Self Commutated Converters (SCC). Prior to this, converter stations used in power transmission were so called Current Source Converters (CSC), also known as Line Commutated Converters (LCC). The CSC uses thyristors arranged in a so called Graetz bridge for commutating current from the different phases in an AC system [7]. The layout is illustrated in figure 2.8.

The thyristors used in CSCs can be made conducting by applying a control signal, but in order to stop conducting, the AC current must naturally approach zero [11, p. 18]. This means the CSC is reliant on an operating AC grid to turn off its semiconductors. Also, if the charges left in the thyristor after being turned off are not removed properly, a rising voltage at the anode may cause a misfire, potentially short circuiting the DC terminals of the CSC [12]. This is known as a

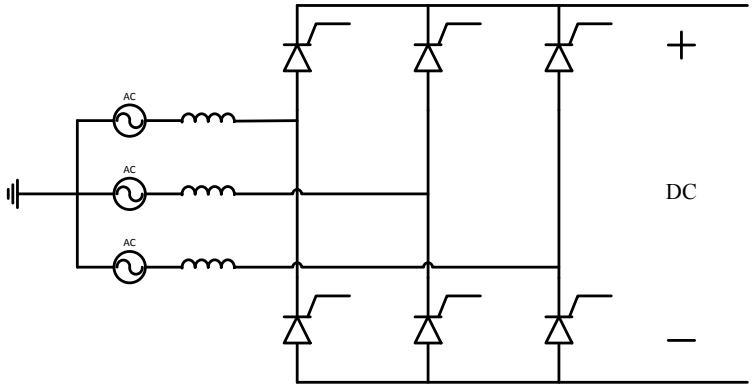

FIGURE 2.8: 6-pulse Current Source Converter - Arrangement of thyristors

commutation failure and may occur as a consequence of AC voltage disturbances [1].

A VSC is made up of transistor and diode pairs, arranged in a similar manner to the thyristors of a CSC. The layout is illustrated in figure 2.9. Different transistors can be used, but the most common for power transmission is the Insulated Gate Bipolar Transistor (IGBT). Unlike thyristors, transistors can be turned both on and off by a command signal [11, p.27].

The use of IGBTs gives the VSC several advantages compared to the CSC. Some of the advantages most relevant for an MTDC system are given in [1] and listed below:

- Black start capability of islanded grid
- No chance of commutation failure during AC grid faults
- Control of both active and reactive power
- Power direction is changed by reversing current direction rather than changing polarity

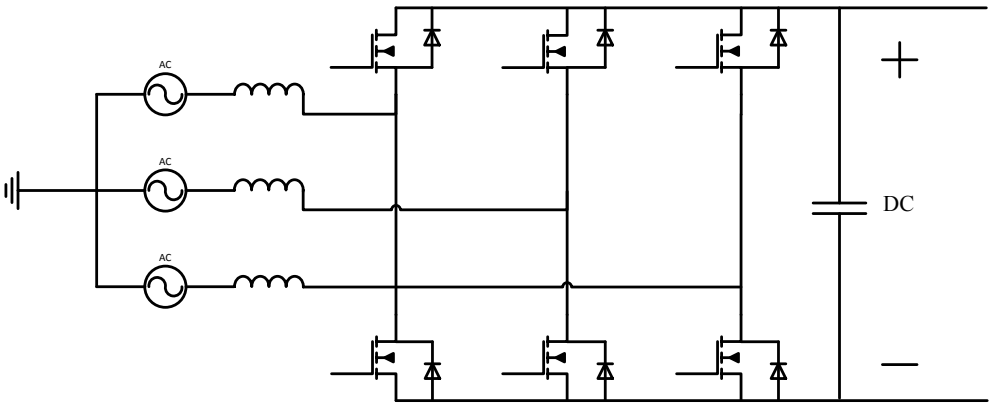

FIGURE 2.9: 6-pulse Voltage Source Converter - Arrangement of transistors

For these reasons, it is generally accepted that a future MTDC system will have to be based around the VSC. However, while superior to the CSC when considering operational characteristics, the VSC is very vulnerable to DC side short circuit failures [1]. This is primarily due to the filtering DC capacitor and the diodes installed in the Gratz bridge, and will be further explained in the following sections.

2.4.2 VSC configurations

The diodes and IGBTs can be arranged in different ways. The different constructions can be divided in two basic groups; based around the classic Graetz bridge design, or as a Modular Multilevel Converter (MMC) [13]. Different variations of both designs are presented in this section.

2.4.2.1 Two-level VSC

The half bridge two-level VSC is the simplest design available. It involves six diode and IGBT pairs arranged in a Graetz bridge, as was shown in figure 2.9 on page 15. In addition to the semiconductors, there is also DC side filter capacitance. In order to increase the voltage blocking capability of the VSC, each valve arm will typically consist of several IGBT/diode pairs connected in series, operating in unison [9].

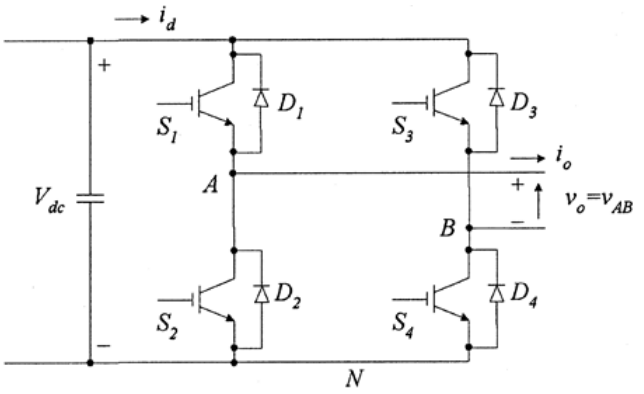

FIGURE 2.10: The full bridge VSC for connection to a single phase. Taken from[18]

AC voltage produced by the half-bridge two-level VSC varies between the voltage levels of either DC terminal. By adding an additional IGBT/diode pair, the full bridge VSC is realised [14, p. 10], depicted in figure 2.10. The full bridge VSC can output AC voltage amplitude twice as large as that of the half bridge VSC, giving a better utilization of the DC voltage and switch cells [14, p. 10].

Since the voltage level can only be varied between two different levels, there is substantial need for filtering [15]. On the DC side, filtering depends on a rather large capacitor which will be discharged during a DC fault, causing large initial fault currents [9, 16]. Also, if a DC fault occurs, there is no way to completely block current through the converter, as the diodes will continue conducting, even after the IGBTs have been blocked [17]. On the other hand, the two-level converter is the simplest VSC available, making it both cheaper to construct and easier to operate than any alternative.

2.4.2.2 Multi level VSC

By connecting extra diodes to the valve arms as illustrated in 2.11, a multilevel VSC is realised. When such a converter is operating as an inverter, the produced AC voltage will have reduced harmonic distortion compared to the two-level VSC. This is because the AC voltage waveform can be made up in several steps rather than just two [19, p.221]. The trade off for this improved AC voltage is an increase in equipment complexity and cost. In addition, controlling such devices will be more difficult than the simple two-level VSC [19, p. 219]. Also, as with the two-level VSC, the large DC capacitor and free current path through the diodes makes the design vulnerable to DC faults.

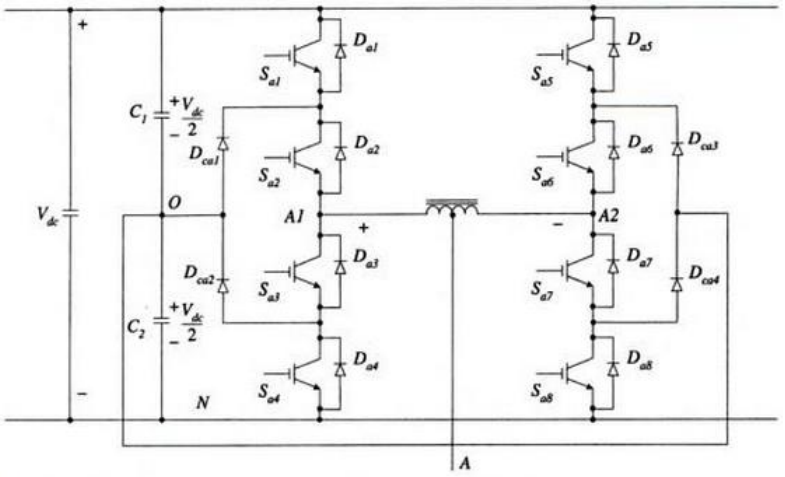

FIGURE 2.11: Five-level VSC phase leg. Taken from [19, p. 218]

2.4.2.3 Modular Multilevel Converter

The MMC is made up of several sub modules connected in series, each series connection making up one leg of the converter [13]. The design is illustrated in figure 2.12. There are different sub module designs available, the simplest being the half bridge sub module which is depicted in figure 2.13. Other examples of sub modules are the full-bridge sub module in figure 2.14 and clamp-double sub module in figure 2.15 [20]. The clamped-double sub module is similar to the full-bridge, but the extra diode reduce the number of IGBTs that current must flow through during normal operation, thus reducing on-state losses. All the alternatives have an incorporated capacitance in each sub module. This means there is no need for a separate DC side capacitor for filtering and energy storage [13].

The multi level arrangement of sub modules allows the MMC to access several DC voltage levels when acting as an inverter, giving it the same advantage as the multi level VSC [13]. In addition, since there is no large DC capacitor, the issue of a large initial current transient is removed [13]. Also, if the sub modules used are either full-bridge or clamped-double sub modules, the MMC is capable of completely blocking AC current from flowing into a DC fault [20]. However, these advantages come at the expense of increased complexity, cost and size of the converter [15].

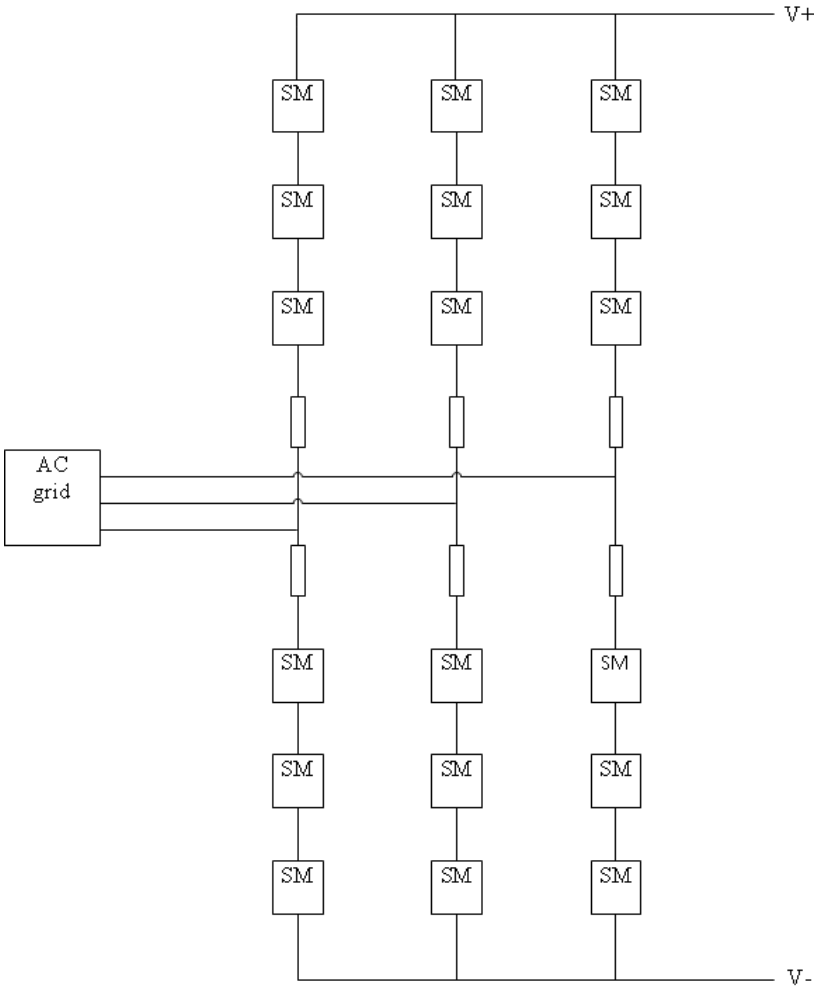

FIGURE 2.12: The modular multilevel converter, placement of submodules (SM)

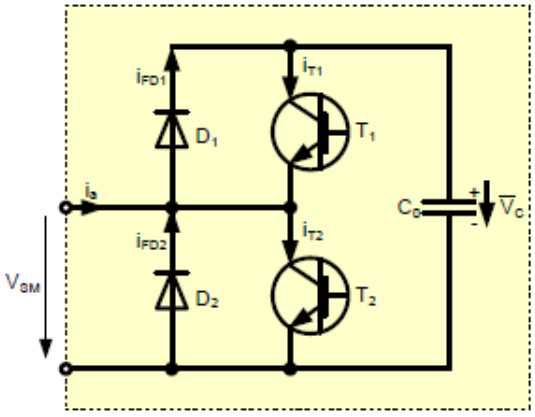

FIGURE 2.13: Design of half bridge MMC sub module. Drawing found in [20]

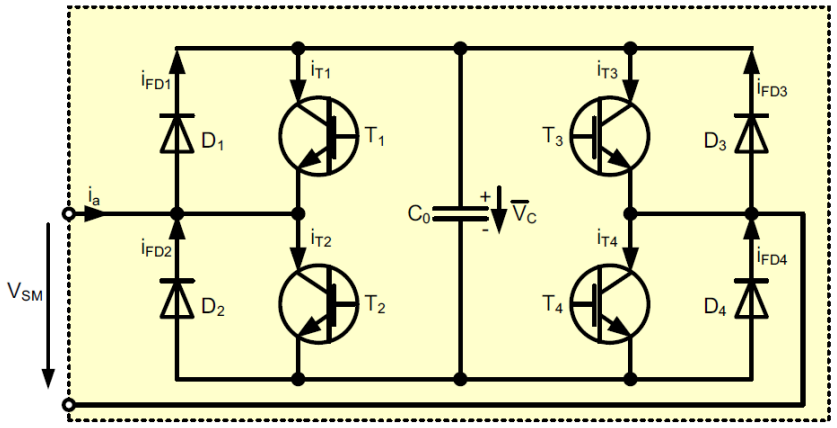

FIGURE 2.14: The full bridge sub module as proposed in [20]

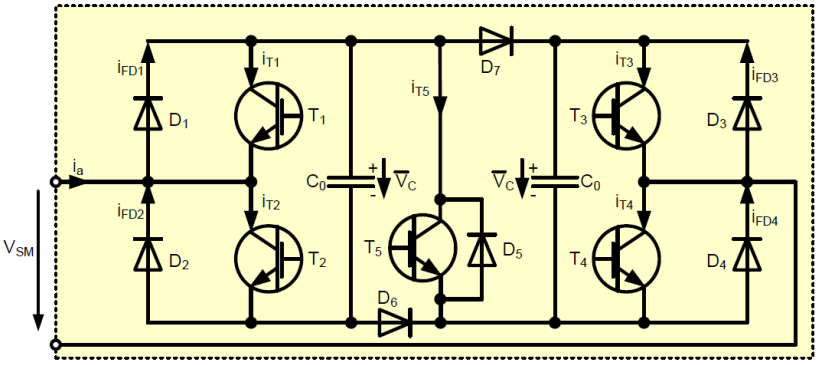

FIGURE 2.15: The clamped double sub module as proposed in [20]

2.5 Cable design

Most HVDC cables in use today are so called mass impregnated cables, insulated by oil impregnated paper. An alternative to this is extruded cables, isolated with polymers. Cables insulated with polymers, such as XLPE for example, are generally lighter and less expensive than expensive than the mass impregnated ones. However, polymers are dielectrics, so when exposed to a voltage difference, all the charges in the polymer align. Changing polarity of the voltage can cause electrical trees to form in the insulation, shortening the cable life time and possibly causing DC ground fault [7]. This is a problem when using CSC, as power reversal is done by changing voltage polarity. With the use of VSC, this is no longer an issue, and polymer insulated cables are generally seen as the preferred choice over mass impregnated ones [7].

The cable is constructed in several layers, illustrated in 2.16. The central conductor is made of copper or aluminium, and is insulated by a dielectric polymer,

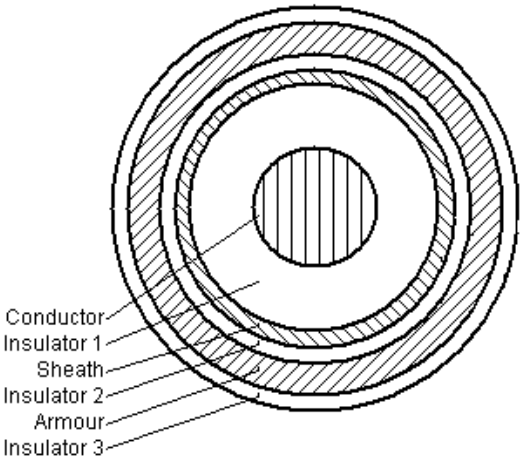

FIGURE 2.16: Cable cross section. Figure from the PSCAD library

for example cross linked polyethylene (XLPE). Outside the insulation is a metal sheath, grounded in either end of the cable [21]. Submarine cables will be subjected to a lot of force, especially during installation. Metal wires known as armour are twisted around the cable to protect it against crushing and twisting forces [21]. The sheath and armour is separated by a second layer of polymer. The whole cable is wrapped in a waterproof material. In between each layer there is usually some sort of filler material, in addition to special tape on the interface between insulation and metal [21]. Naturally, there will be a potential difference between the conductor and the earthed metal sheath. Since these are separated by a dielectric, the cable essentially becomes a large coaxial capacitor.

2.6 Current interruption in HVDC systems

When current is interrupted by separating two conducting contacts, an arc is formed [22]. In AC systems, this is extinguished by the naturally occurring current zero crossing, which is a result of the changing current and voltage polarity. Current interruption is therefore a lot more difficult in DC systems, since there are no polarity variations [22].

Up until very recently, the only option for clearing faults in HVDC systems has been to activate current breakers in the connected AC systems. For use in MTDC systems, such a method is proposed as the ”handshake method” [23]. This method involves momentarily disconnecting the entire MTDC system from connected AC systems and then clearing the fault before reconnecting. The time for clearing

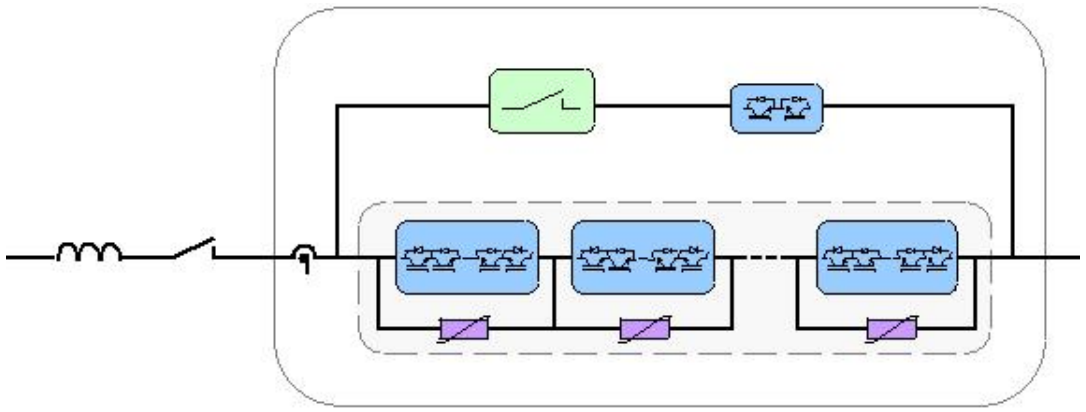

FIGURE 2.17: The DC circuit breaker designed by ABB. Taken from [26]

a fault and restoring grid operation using this method has been reported as 0.5 seconds [23]. If MMCs are used, they can perform current interruption as explained in section 2.4.2.3, which would be much faster than the AC breakers, thus reducing fault clearing time. However, the entire DC grid would still have to be taken momentarily off line.

If the interruption time is to be further reduced and only the faulted part of the grid disconnected, fast acting HVDC breakers must be installed at each line in the MTDC system. Such a breaker would have to incorporate semiconductors for creating an artificial current zero crossing [24], and also be able to withstand fast rising currents and high current levels.

Recent years have seen a large interest in developing a fast and reliable HVDC breaker [1], and in November 2012 ABB announced the release of such a device [25], called a "Proactive hybrid HVDC breaker". This is described in [26] and the design is depicted in figure 2.17. Fast acting mechanical circuit breakers work together with IGBTs in order to commutate and interrupt large fault currents quickly.

The design can be separated into three different sections. First section is the main DC breaker, comprised of several IGBTs connected in series, each connected in parallel with an arrester. The second section is a bypass made up of a single IGBT and a fast mechanical disconnector. This is connected in parallel with the main breaker. The third section is comprised of a reactor connected in series with a mechanical isolator, which in turn are connected in series with the other two sections. This design allows for fast interruption of large fault currents, while keeping on-state losses at a minimum [26].

The proposed solution also has the ability of proactive operation. When a fault occurs, the breaker can be put on standby until it is decided whether it need to be opened or not [26]. If the breaker then needs to operate, current will be interrupted within a few μs. While in standby mode, current flows through the IGBTs of the main breaker, which could operate in a specific way to limit the fault current [26].

In [26], the DC breaker is tested in a setup equivalent to a 320 kV, 2 kA system with fault current rising at a rate of 4.5 kA/ms. Results reported opening times below 2 ms and interruption of currents up to 16 kA.

2.7 Current limiters

Low impedance in DC systems leads to higher fault currents. In order to reduce the currents, current limiters may be installed. These are devices with very low resistance in normal operating circumstances, and which respond to increased current magnitude or frequency with an increased impedance. A few examples of such devices are given below.

2.7.1 Tuned LC circuit

The tuned LC circuit uses a linear inductor connected in series with a parallel connection of capacitor and a nonlinear inductor. This is depicted in figure 2.18. The inductors and capacitor are dimensioned such that the capacitance and linear inductor cancel each other out during normal operation. During fault, the increased current saturates the nonlinear inductor, limiting voltage across the parallel connection. In turn, the tuned LC circuit becomes inductive since contribution from the capacitor is reduced [27]. There is no need for external influence in order to make the device inductive, and it has a very small effect on normal state grid operation. It is also quite cost effective and relies upon familiar technology and devices.

2.7.2 Polymer PTC thermistor

The polymer PTC is a polymer fabricate with embedded conducting particles. During normal state, these particle are in contact with each other, creating a low

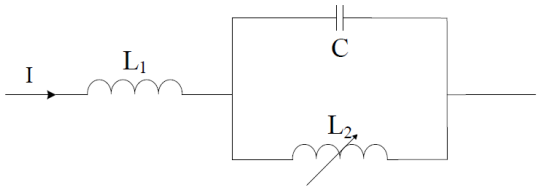

FIGURE 2.18: The concept of a tuned LC circuit

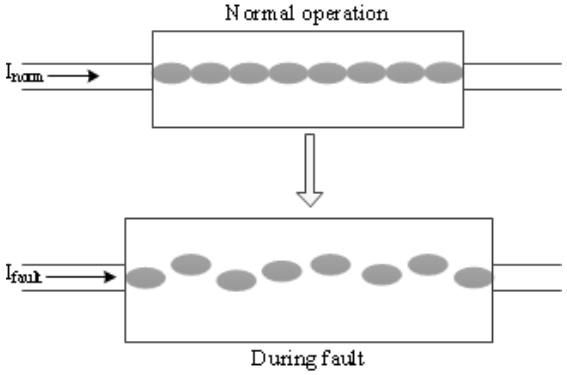

FIGURE 2.19: PTC during normal operation and at fault

resistance current path. With increased current and subsequent increased heat development, the polymer expands, causing the particles to lose contact with each other, illustrated in figure 2.19. The current path then becomes more resistive, limiting the current [27]. Such devices have a nonlinear temperature-resistance characteristic, with the resistance quickly increasing once a certain temperature is reached [28]. Seeing how heat development in the device can be calculated by $Q = RI^2$, it seems clear that the device should be able to quickly limit a rising fault current. Once the fault current has been extinguished, the polymer contracts, reforming the low ohmic path. Polymer PTC resistors are commercially available today, but not for high voltages [27].

2.7.3 Liquid metal

Liquid metal fault current limiters are made by encapsulating liquid metal and placing it in the current path. This has a relatively low resistance. When subjected to a large fault current the metal vapourises due to the increased temperature, increasing resistance of the current path. Once current has been succesfully interrupted, the metal cools back down into its liquid phase [27].

Chapter 3

Fault current transients

As mentioned, the VSC is vulnerable to DC side faults. These may occur in different parts of the system, either on the VSC itself, in grid junctions or on the cable.

3.1 Basic physics of fault currents

3.1.1 Resistive system

Figure 3.1 illustrate a simple system with a voltage source U and a load R_L connected by a transmission line with resistance R_t. Current in the transmission line and load will be given by Ohm's law $I = U/(R_L + R_t)$. When a short circuit fault appears, it is the equivalent of connecting a fault resistance R_f in parallel with R_L and assuming that $R_f << R_L$. As a consequence, system current will rise, as it is now given by $I = U/(R_f + R_t)$. Since faults typically does not occur at the load, R_f will also be somewhat reduced.

Magnitude of the fault current in a transmission line is in other words given by the voltage at feed-in point and total fault path resistance. The latter is the sum of fault resistance and resistanc in the transmission line between feed-in and fault point.

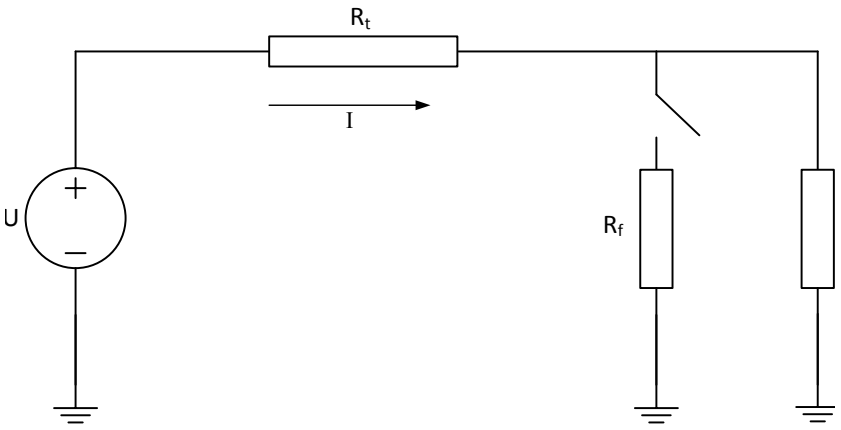

FIGURE 3.1: A simple resistive system with fault

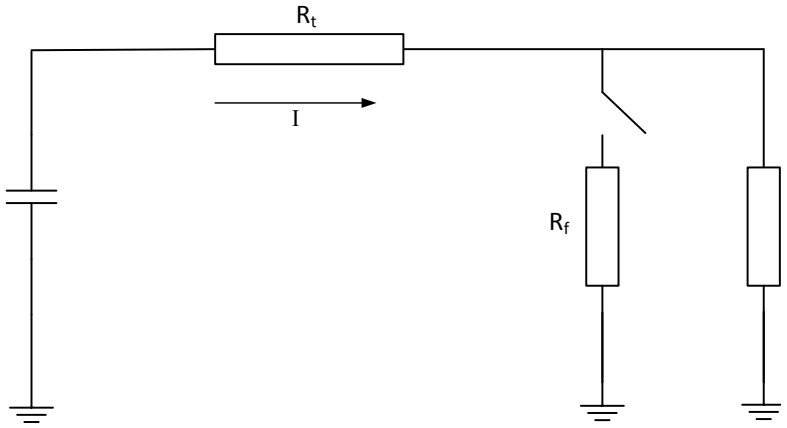

FIGURE 3.2: A capacitive system with fault

3.1.2 Capacitive system

By replacing the voltage source with a capacitor a better understanding of fault currents in a capacitive system can be obtained. This is illustrated in figure 3.2, and is a simplified equivalent of a two-level VSC during fault.

A fault somewhere along the transmission line will trigger a discharge of the capacitor. The voltage producing fault current will then be time dependent, and given by equation (3.1), assuming complete discharge. Current in a capacitor is given by equation 3.2 [29, p. 273].

$$V_C(t) = V_0 e^{-\frac{t}{\tau}} \tag{3.1}$$

$$I_C(t) = C\frac{dV_C}{dt} = -\frac{V_0}{R}e^{-\frac{t}{\tau}} \tag{3.2}$$

Here, t is time after initiating discharge, V_0 is capacitor voltage at fault inception and $\tau = RC$, with $R = R_f + R_t$ and C is size of the capacitor. These equations are plotted with different resistance values in figure 3.3. Discharge time depends on τ, meaning a system with large resistance and/or capacitance will need more time to fully discharge. Both current and voltage derivatives will be large at beginning of the discharge, then gradually decrease.

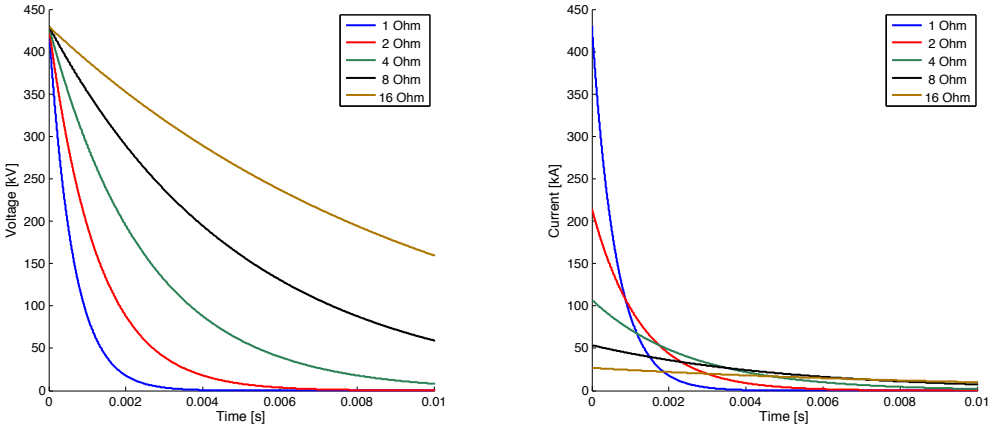

(A) Voltage (B) Current

FIGURE 3.3: Discharge voltage and current of RC circuit with varying resistance

3.1.3 Transmission lines

Transmission lines are conductors with a long length. Faults with low fault path impedance in a capacitive system will experience fault currents that vary greatly within a very short time window. Since electromagnetic waves are prohibited from moving faster than the speed of light, c, it becomes necessary to express current and voltage along the transmission line as functions of not only time, but also place [30, p. 2.1]. This can be done by applying the following two equations [31,

p. 19].

$$\begin{aligned} \frac{\partial U}{\partial x} &= -L\frac{\partial I}{\partial t} \\ \frac{\partial I}{\partial x} &= -C\frac{\partial U}{\partial t} \end{aligned} \tag{3.3}$$

Position on the line is denoted by x. Solving the equations in (3.3) reveal the following voltage and current characteristics;

$$U(x,t) = U_f(x - vt) + U_r(x + vt) \tag{3.4}$$

$$I(x,t) = \frac{1}{Z_c}U_f(x - vt) - \frac{1}{Z_c}U_r(x + vt) \tag{3.5}$$

To get a better understanding of how the electromagnetic waves develop, it is necessary to represent the transmission line with a pi-equivalent instead of a single resistance. The pi-equivalent is illustrated in figure 3.4 [30, p. 2.2]. Capacitance to ground has been added as well as inductance of the conductor. Resistance, inductance and capacitance can be calaculated using equations 3.6-3.8. Transmission lines can be modelled reasonably well by series connecting a large number of these equivalents [32], but fault currents can be sufficiently explained by using only one.

$$R = \frac{\rho}{A} \quad [\Omega/m] \tag{3.6}$$

$$L = \frac{\mu_0}{2\pi} ln \frac{r_y}{r_i} \quad [H/m] \tag{3.7}$$

$$C = \frac{2\pi\varepsilon}{ln\frac{r_y}{r_i}} \quad [F/m] \tag{3.8}$$

By looking at this pi-equivalent connected to a VSC filter capacitor, we can assume that the majority of the system capacitance is located at the converter, and therefore connected in series with the line resistance and inductance. This makes the system a series connected RLC circuit. Such a circuit is shown in figure 3.5 which is used to derive the basic equations explaining currents and voltage during a fault.

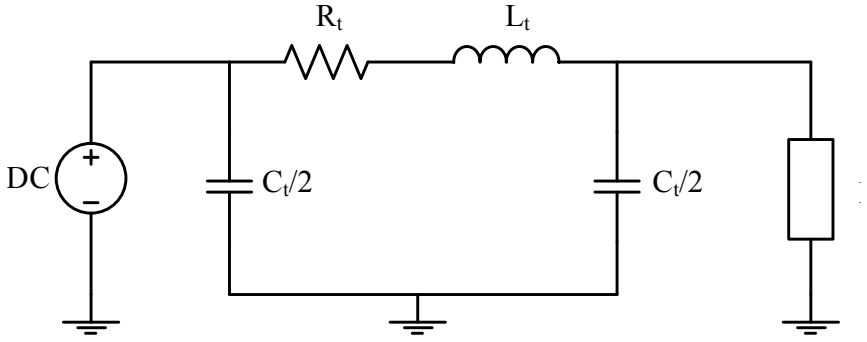

FIGURE 3.4: A pi-equivalent

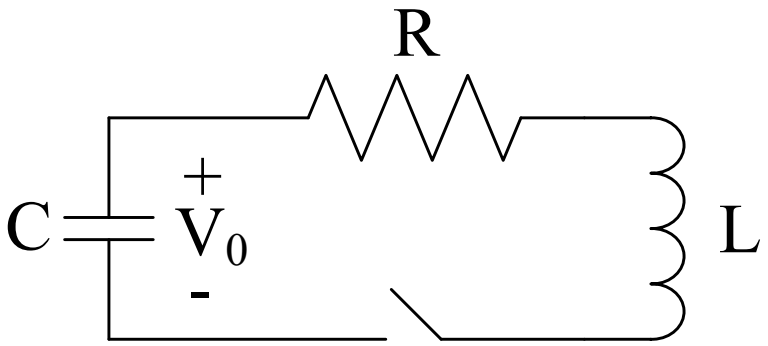

FIGURE 3.5: A series RLC circuit

Applying Kirchoffs voltage law gives the following equation for the discharge of the capacitor [29, p. 355].

$$Ri + L\frac{di}{dt} + \frac{1}{C}\int_0^t i d\tau + V_0 = 0 \tag{3.9}$$

By differentiating with respect to t and rearranging the terms, the characteristic equation for a series RLC circuit is obtained [29, p. 355].

$$\frac{d^2i}{dt^2} + \frac{R}{l}\frac{di}{dt} + \frac{i}{LC} = 0 \tag{3.10}$$

This is a second order differential equation. Its roots are found by the following equation [29, p. 356]:

$$\frac{di}{dt}_{1,2} = -\frac{R}{2L} \pm \sqrt{(\frac{R}{2L})^2 - \frac{1}{LC}} \tag{3.11}$$

The response from an RLC circuit to the discharge of its capacitance is said to be either critically, over or under damped. This is decided by whether the roots are real or complex, and also if they are equal or different. Two equal and real roots leads to a critical system, while uneven real roots leads to an overdamped system and complex roots leads to an underdamped system. As can be seen from equation (3.11), this is decided by the difference between the two expressions in the square root. These are now denoted as β and ω_0, where

$$\beta = \frac{R}{2L} \qquad\qquad \omega_0 = \frac{1}{\sqrt{LC}} \tag{3.12}$$

Damping of the system, basically its ability to dissipate energy in the resistance, is determined by size of β, while ω_0 gives the systems natural frequency [33]. The damping factor is introduced as the ratio between β and ω_0.

$$\zeta = \frac{\beta^2}{\omega_0^2} = \frac{CR^2}{4L} \tag{3.13}$$

Criteria for critically, over- or underdamped systems are given in table 3.1 [29, p. 356], expressed by the damping factor.

Table 3.1: Criteria for damping of RLC circuit

ζ	Damping
1	Critical
>1	Over
<1	Under

The different responses are shown in figure 3.6 [34]. Similar to the response from an RC circuit, the current (and voltage) derivative is larger at beginning of discharge before reducing nearing steady state.

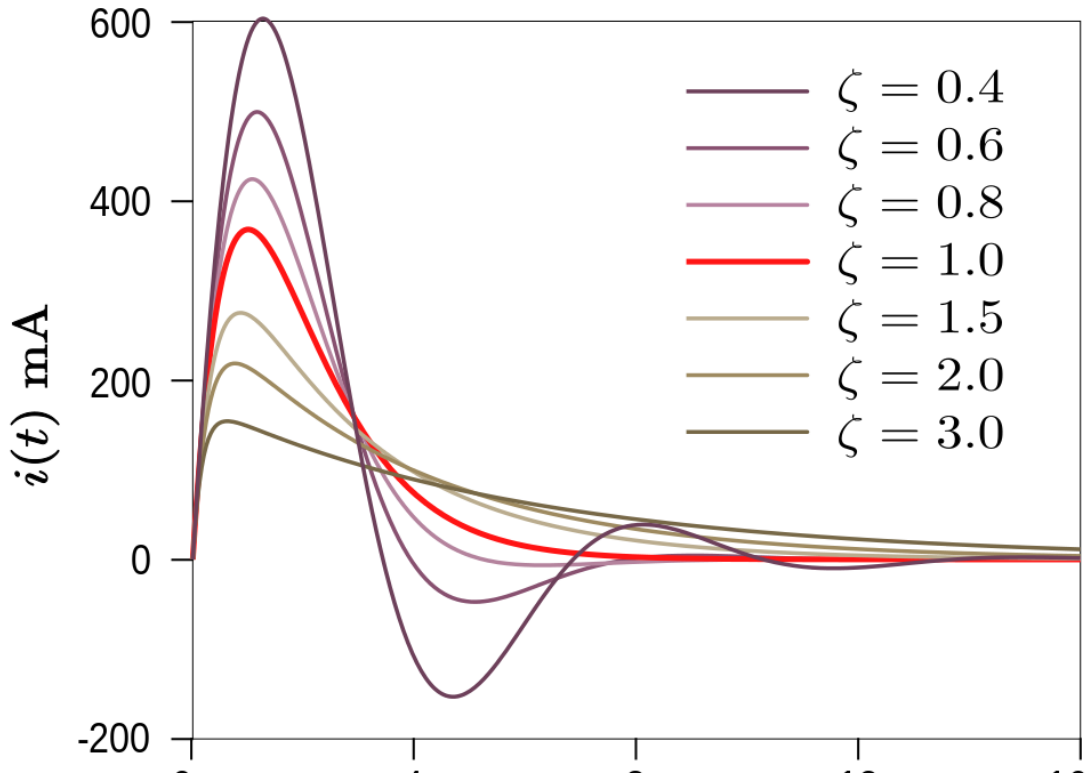

FIGURE 3.6: Natural response of an RLC circuit

3.1.4 Transient waves following fault

A fault to ground at time $t = 0$ cause a local drop in voltage which triggers a discharge of the transmission line capacitance, causing a negative voltage wave to travel away from the fault, illustrated in figure 3.7. As the wave proceeds along the line, cable capacitance is discharged into the fault [16]. This voltage wave travels at a given speed, determined by per length inductance and capacitance of the line. In a loss less line ($R = 0$), wave speed is expressed in equation (3.14)[30, ch. 2.2].

$$v = \frac{1}{\sqrt{LC}} \tag{3.14}$$

Where L and C are inductance and capacitance per length of the transmission line, given by equations 3.7 and 3.8. Once this wave reaches the end of the line, part of it will be reflected back towards the fault, while the rest is transmitted to the other side of the line interface, illustrated in figure 3.8. How much is reflected and transmitted is determined by the reflection and transmission coefficients. These depend on impedance of the line the wave is travelling on and impedance of the

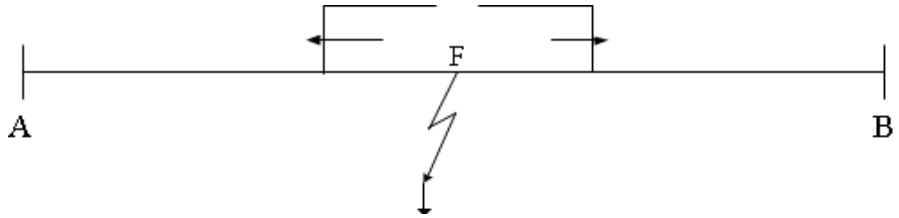

FIGURE 3.7: Wave initialized at ground fault location F

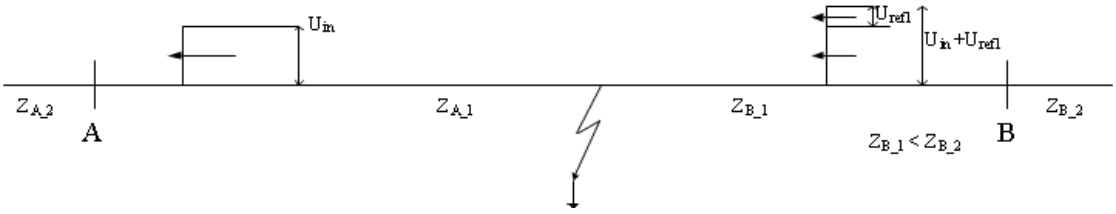

FIGURE 3.8: Wave reflected at converter station B

component it approaches, and are given by equations (3.15) and (3.16) [30, p. 2.12]. Wave impedance of a transmission line is given by equation (3.17) [30, p. 2.6].

$$\rho = \frac{Z_2 - Z_1}{Z_1 + Z_2} \tag{3.15}$$

$$\alpha = \frac{2Z_2}{Z_1 + Z_2} = 1 + \rho \tag{3.16}$$

$$Z_w = \sqrt{\frac{L}{C}} \tag{3.17}$$

In figure 3.9, voltage and current are given subscripts r and f for reverse and forward travelling waves. Reflection and transmission coefficients for both terminals are denoted k_A and k_B, and are determined by equations (3.15) and (3.16). For a system without losses the magnitude of current and voltage waves will only be reduced when reflected/transmitted. In real life, these waves will be attenuated and distorted due to line resistance, corona and other effects [31, p. 21].

3.1.5 Faults in VSC system

In an HVDC grid with VSCs, the first change the voltage wave will encounter is the converter station. A schematic of the system seen from the travelling waves point of

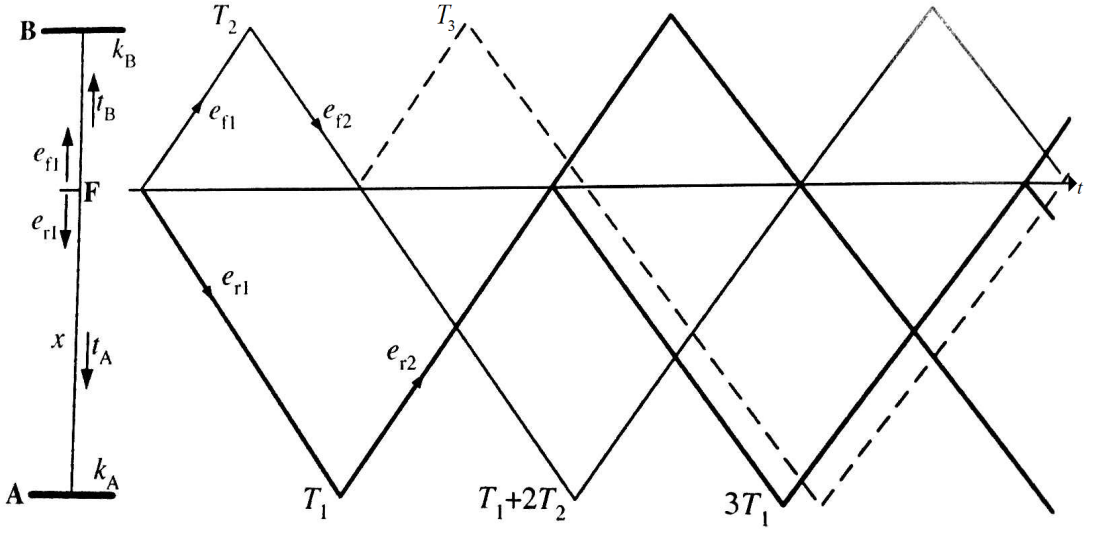

FIGURE 3.9: Lattice diagram showing how waves are reflected between two converters and fault point

view is shown in figure 3.10. It is assumed that the IGBTs will block quickly enough to be considered an open circuit, which is a reasonable assumption according to [6, 16, 17]. The voltage wave then sees a path to ground through the capacitor, connected in parallel to a healthy transmission line with a wave impedance as given by equation 3.17. Impedance of a capacitor is given by $Z_C = (j\omega C)^{-1}$. Total impedance seen by the wave is expressed in (3.18), calculation performed in appendix E.

$$Z_{eq} = Z_w \frac{1 + j\omega Z_w C_{conv}}{1 + (\omega Z_w C_{conv})^2} \tag{3.18}$$

Where Z_w is wave impedance of the healthy line and C_{conv} is the converter capacitance.

Arrival of the negative voltage wave will trigger the discharge of the converter capacitor in a way similar to what was described earlier. This discharge current will contain both high and low frequency components and is discharged towards the fault. Looking at the pi-equivalent, it is clear that impedance along the fault path as well as impedance to ground is dependent on current frequency. Consequently, fault current components with high frequency will experience a large series impedance and relatively small impedances to ground, and opposite for low frequency components [30, p. 2.5]. High frequency components can therefore be expected to reduce faster than low frequency components.

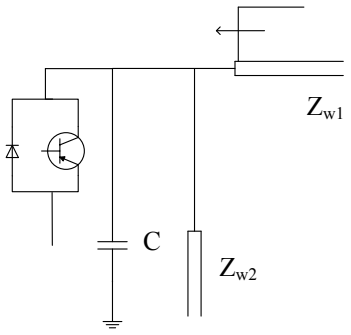

FIGURE 3.10: Wave approaching a VSC station with neighbouring line connected. Z represent the wave impedance of each transmission line, while C is the converter capacitance

The discharge current travels along the line similar to the voltage wave, being reflected at the fault point. Assuming a small fault impedance so that $R_f << Z_w$, reflection coefficient $\rho \simeq -1$ and an equal and opposite wave is reflected back towards the converter, where it is reflected once again with the impedance given in (3.18). With the assumption that $Z_{w1} \simeq Z_{w2}$ this impedance will never be greater than the one the wave is already travelling along, and so the reflection coefficient must be negative. Since a negative current wave travelling in one direction is equivalent to a positive wave travelling in the opposite direction, the current at the converter station increases until the wave energy is dissipated in the line resistance and a steady state is reached. Relating to figure 3.3 of the natural response of a series RLC circuit, it is clear that the current should be decreasing over time. Due to the reflections of the current, this is not the case, and a current development at the converter similar to that of an over voltage following a lightning strike can be expected, as is described in [30, p. 3.55] and illustrated in figure 3.11. The voltage on the other will experience little change in value at reflection, as the positive and negative wave cancel each other out.

During discharge of the filter capacitance, there is no current going through the converter [17]. The diodes will start to conduct a current once the capacitors are discharged [17].

Due to stored energy in the cable inductance, the initial magnitude of diode current may be quite large, potentially damaging the diodes [17]. For a system with half bridge VSCs, it is therefore important to interrupt current before the filter capacitor is fully discharged.

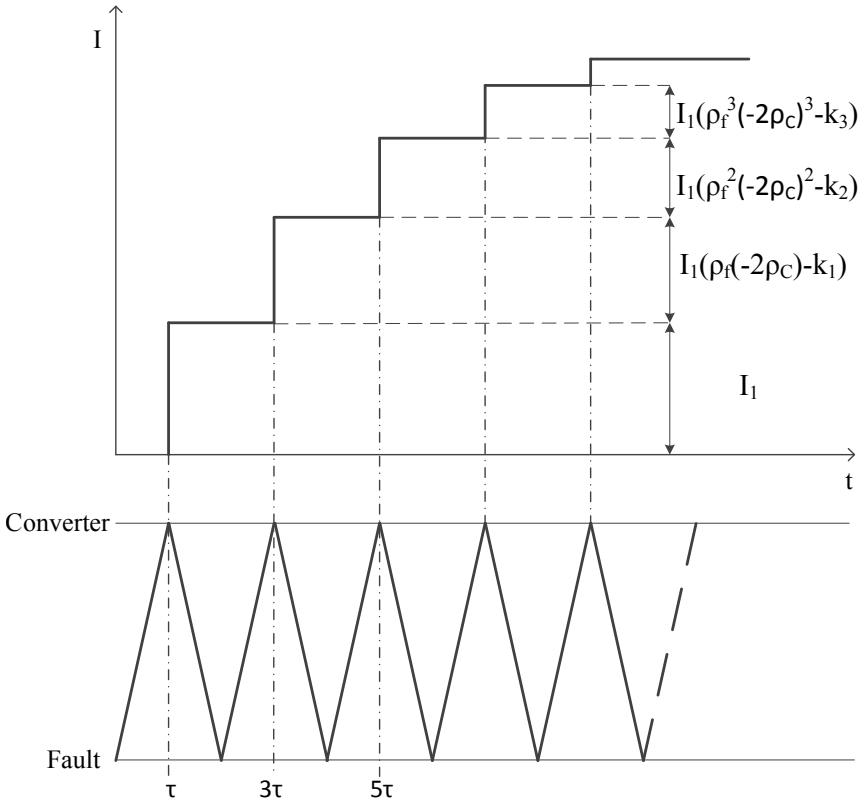

FIGURE 3.11: Build up of current at converter shown together with the Lattice diagram over arriving waves. Time for wave to travel from fault to converter is denoted by τ. The factor k_n is introduced as a damping variable to illustrate the attenuation of the wave.

Once the cable inductance has been discharged as well, the fault current is dominated by contributions from the connected AC grids [16]. After approximately 300 ms, the fault current approaches a steady state value [6].

The different stages of fault development is illustrated in figure 3.13.

3.1.6 Effect of multiple converter stations

With additional converters in the system, there are several point where the wave can be reflected at. Transmission of the fault wave at the point must then also be taken into account. A line with two converters and a fault between them is shown in figure 3.14. The fault is closer to converter A than B, meaning capacitance at this station will be discharged first. Since resistance, inductance and capacitance is evenly distributed along the line, this capacitor will see a smaller resistance and inductance, and therefore experience a larger discharge current. The current

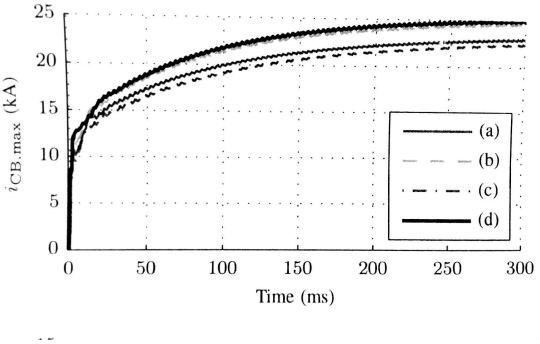

FIGURE 3.12: Fault current development in MTDC grid for different system topologies. a) Radial grid, b) Lightly meshed grid, c) Ring shaped grid, d) Densely meshed grid. Taken from [6]

wave reaching the fault point is mostly reflected, but if the fault impedance is sufficiently large, a significant part is transmitted to the other part of the line. It will eventually reach station B where it causes a drop in the current, as it is travelling in the opposite direction of the fault current from the station. The effect is a much more chaotic fault current which will not only rise, but also drop. However, for this to have a measurable effect, the fault impedance must be very high, compared to the wave impedance of the line. Otherwise, the reflection coefficient at fault point will be close to -1, resulting in a near perfect reflection and no transmitted wave.

3.1.7 Properties of cables and overhead lines

The resistance, inductance and capacitance per unit length in a transmission line are given by equations (3.6), (3.7) and (3.8) respectively [35, p. 282][30, p. 2.7].

Where ρ is resistivity of the conductor, r_y and r_i are the outer and inner radius of the insulation, A is cross sectional area of the conductor, μ_0 is permeability of free space, and $\varepsilon = \varepsilon_0\varepsilon_r$ is the insulation permittivity. The construction of a cable was detailed in section 2.5. An overhead line can be equated to a cable using air as insulation, suspended a certain height over the ground. They have distinct different properties due to this.

As was noted in section 2.5, cables are essentially large coaxial capacitors. The inductance will be low as the relationship between outer and inner radius of the

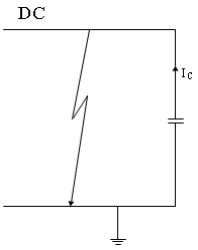

(A) Stage 1, filter capacitance is discharged

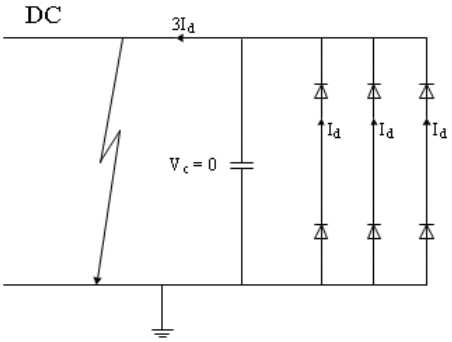

(B) Stage 2, cable discharged through diodes

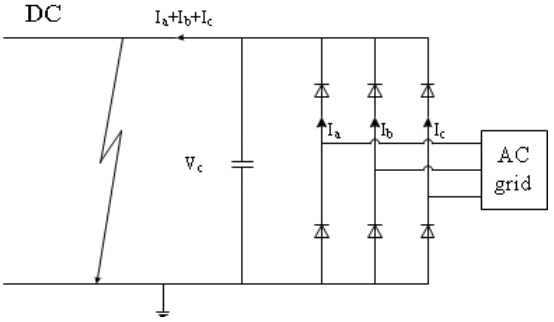

(C) Stage3, The fault is fed by adjacent AC grid through diode bridge

FIGURE 3.13: The three stages of fault development

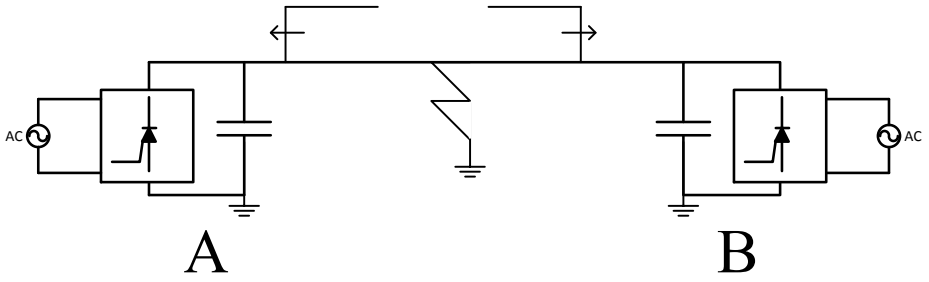

FIGURE 3.14: Two converter system with fault between the converters

insulation is relatively small. The opposite is true for overhead lines, where the large distance to ground gives a large inductance, and in combination with the low permittivity of air ($\varepsilon \simeq 1$) a comparably small capacitance [30, p. 2.9]. Some implications from this are listed below:

- Travelling wave velocity in overhead lines are equal to light speed, while velocity in cables are lower [30, p. 2.8]
- Fault impedance is lower in cables
- Increased capacitance and lowered inductance gives a higher damping coefficient

3.2 Different kinds of faults

In a bipolar system, fault can occur on either of the poles, causing a monopolar fault, or there can be a short circuit between the poles which will lead to a bipolar fault. Faults are more likely to occur along the line rather than in converters or grid junctions [36]. This is also true for cable based systems, where faults can be caused by degradation of insulation or external damage to the cable. In either case, cable faults are always permanent. While bipolar faults are more severe than monopolar faults , they are unlikely in offshore cable systems since the cables are situated relatively far apart. This greatly reduce the risk of simultaneous damage to both cables [16]. For the purpose of describing fault propagation, the monopolar cable fault will therefore be used as an example in the following sections.

3.3 Parameters that influence the fault current

Magnitude of the current during the initial discharge of filter capacitors are mainly decided by the filter and line capacitance and the total impedance between measuring point and fault [16, 32]. The latter is the sum of fault and cable impedance. Reducing the system capacitance will reduce peak value of fault current during the initial phase, and will also shorten discharge time due to the decreased system time constant ($\tau = RC_{filter}$) [16, 32]. Increased fault impedance and distance will reduce peak fault current and increase discharge time [16, 32].

Once the system enter the freewheeling diodes phase, current is caused by the demagnetising of cable inductance and so the fault current will depend on pre-fault current in the cable and short circuit ratio between the DC grid and connected AC grids [32].

During the final stage when the fault current reaches a steady state, its value is depended upon the fault location, impedance and the Short Circuit Ratio (SCR) between the AC and DC systems [16, 32].

In addition to these, the topology of the grid also matter [6]. A more complex DC grid with several junctions and high mesh grade will experience higher fault currents and faster spread of the fault than a simpler system [6].

3.4 Requirements to fault protection system

A modern protection system consists of three main sub systems [37]. First are the relays, where inputs from current transformers are used to monitor the grid and determine if a fault has occurred. Secondly, a communication system is necessary in order to communicate between the relays, possible central decision making units and the system breakers. The third and final system is made up of the devices responsible for interrupting current. In AC grids this is done by mechanical breakers [22]. The proposed methods for clearing faults in an HVDC grid was presented in sections 2.6 and 2.4.2.3. The following is required of a modern protection system, both in AC and DC grids [5].

- **Speed** Fast action is important to prevent the fault from spreading to other parts of the system
- **Sensitivity** The system must detect all faults, and at the same time not trigger during normal operation transients
- **Selectivity** The system must be able to correctly locate the faulted component, and isolate it from the healthy grid
- **Seamless** After fault clearance, the rest of the power system should be able to resume operation

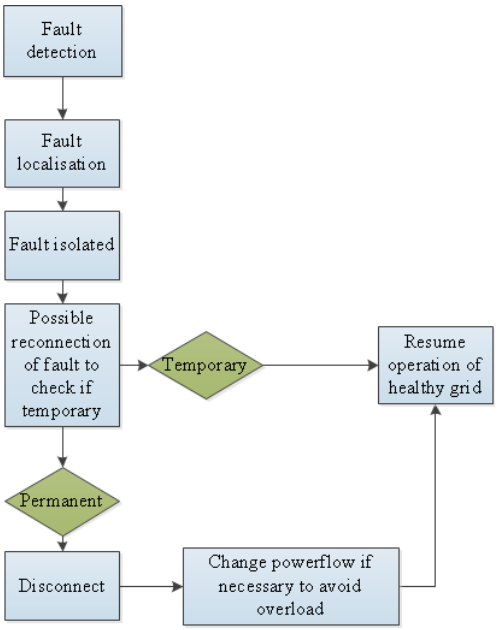

FIGURE 3.15: The process from detecting fault to normal operation is resumed

- **Robustness** In case parts of the protection system is unable to function properly, there should be back-up systems available

The process of fault clearance is illustrated in figure 3.15 from fault detection to restoration of normal system operation.

The process can be divided in two parts. The time up until fault isolation starts is spent by the relays and a data processing unit to locate the fault and decide which measures to take. How long this takes depends on the chosen relay technology, and also the distance of any needed communication. The rest of the process is performed by current interrupting devices which will isolate the fault. In order to achieve the fast acting protection system which is required for a DC system, both parts needs to be optimised in comparison to their present AC equivalents. Since DC systems are typically installed over great distances, communication between relays installed at different nodes may be expected to take a significant portion of the time available. Therefore, relays systems that do not require communication is of particular interest.

Chapter 4

Fault detection and localisation

In a protection system, relays have the task of detecting and locating faults. There are many different kinds of relays being used in HVAC transmission systems today. This chapter aims to present these as well as recently proposed detection methods, and discuss which are most promising to be used in an MTDC system.

4.1 Classification of relays

Different principles are being used in order to detect and locate a fault, and relays can be classified depending on which principle they utilise [37].

- Magnitude relays, which compare the magnitude of an input to a given threshold
- Directional relays, which compare the phase angle of two inputs
- Ratio relays, which respond to the ratio of two inputs
- Differential relays, which takes two or more inputs and checks their algebraic sum
- Pilot relays, which get inputs from remote locations

In addition to these, there are new techniques being developed which may be more suited for DC systems. In [5], travelling wave, voltage and current derivatives, and wavelet analysis is mentioned. These will also be presented in the following sections.

4.2 Recording currents and voltages

When recording current and voltages using a digital relay, the measurements will be discrete, meaning they are a series of snapshots, with the variation between each snapshot assumed small enough to be linearised. In order for this assumption to be valid, it is important that the sampling frequency is high.

Requirement to sampling frequency depends on frequency of the measured signals. According to the sampling theorem put forward by Claude E. Shannon [31, p. 184], sampling frequency must be more than twice the highest signal frequency in order to ensure no information is lost when rebuilding the signal. The frequency $f = 0.5 f_{max}$ is known as the Nyquist frequency.

Currents in HVDC systems are measured using Optical Current Transducers (OCTs) [38]. These devices exploit the Faraday effect, measuring the effects of the conductor current on light being passed through optical fibers wound around the conductor [39].

For voltage measurements, Electro-Optic Voltage Transducers (E-OVTs) can be used [38]. These measure light being passed through one or more crystals which are exposed to the system voltage.

Optical measuement devices are not as exposed to saturation following high current frequencies or magnitudes as more traditional current transformers are.

4.3 Zones of protection

Each relay is designated a given zone of the power system, in which it is responsible for detecting faults. These zones may overlap, but it is important that they cover the entire system without being so large that several relays will perceive a single fault as in ”their” zone. In AC systems, the boundaries of a zone are normally marked by circuit breakers [37].

4.4 Overcurrent and undervoltage protection

The overcurrent and undervoltage relays simply measure current and voltage and compare the inputs to a given threshold. During a fault, line current will rise due to the reduced impedance to ground. Magnitude of the current depends on distance to converter, where the relay is installed, and on the short circuit potential of the connected AC grid [37]. Once input current exceeds the threshold, the relay will send a trip signal to the breaker, disconnecting the faulted line.

Overcurrent protection can only be used in systems where the lowest possible fault current does not exceed the highest possible operational current. For offshore systems connected to windfarms, the fault current potential varies with wind, so a fault current occuring during low wind may produce currents smaller than operational currents during high winds. This method of protection has a very low degree of selectivity, as a fault occurring in a neighbouring zone close to the relay may produce a sufficiently large overcurrent in the relay to make it trip [37].

In addition to producing an overcurrent, a fault will also cause drop in voltage. DC voltage level protection measure voltage over large time intervals in order to detect a lasting voltage drop. Size of the time interval must be large enough that normal operational transients are ignored. In order to improve speed of the relay, a multi level configuration should be implemented, where the relay will react faster to a more severe voltage drop. The threshold for where the voltage is deemed too low should be chosen as high as possible without coming into conflict with operational voltage [40].

Overcurrent and DC voltage level protection are both very reliable and represent mature and simple technology. However, the lack of selectivity means these should be utilized mainly as back-up protection, in case the primary fault detection system should fail.

4.5 Derivative protection

Derivative protection obtain time derivatives of both current and voltage, and is widely used in point to point HVDC protection [1]. In order to determine whether a fault has occurred within the given protection zone, the weighted sum of the

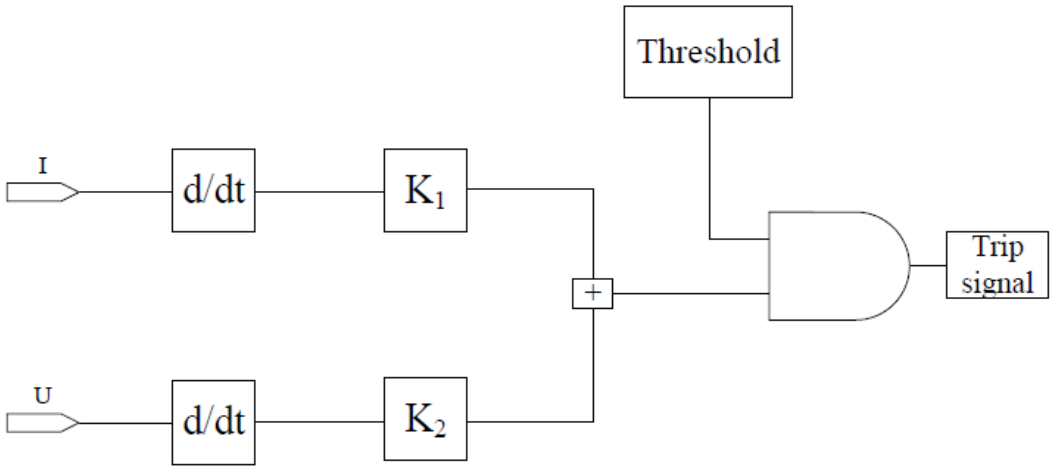

FIGURE 4.1: Operational process of voltage derivative protection. Voltage and current time derivatives are summarized and compared to a given threshold.

derivatives is compared to a given threshold. Weighting and summarisation of the derivatives are given by equation (4.1). Sign of the current derivative indicate fault direction, which increase selectivity compared to the overcurrent protection. For bipolar systems, protection is installed at all converter stations and on both poles in case a monopolar fault induces overvoltage on the healthy pole. Detection time is usually in the order of 2-3 ms [40].

$$\epsilon = K_1 \frac{di}{dt} + K_2 \frac{dU}{dt} \tag{4.1}$$

Even if VDP is a fast method that is already widely used in existing systems and also indicates direction of fault, it has a few disadvantages. Correct tuning of the threshold and weighting of derivatives require extensive network studies [40]. Also, since the voltage derivative is damped by impedance, this method may have difficulty detecting high impedance faults and faults that occur close to inverters [40]. Operational process of the VDP is illustrated in figure 4.1.

4.6 Differential protection

Differential protection applies Kirchoff's current law, and measures current going in and out of a line or other component. According to Kirchoff's law, these currents

will be the same during normal operation. If there is a variation in the currents exceeding a set threshold for a certain time, the relay is tripped [40].

In order to compare the two measurements, the relays need to be able to communicate, which introduce a time delay that has to be made up for by the relay receiving information. For cable systems, and especially long cables, there will be naturally occurring current differences during voltage variations, due to the charging and discharging of cable capacitance. Because of this, the sensitivity of the relay must be reduced, which reduce its capability of detecting high impedance faults [40].

Differential protection offers a very high degree of selectivity, but information must be transferred from one end of the line to the other. If the cables are very long, which is likely in an offshore system, sensitivity is lowered, while response time increases due to the increased communication time. This protection is also very vulnerable to errors in the communication system, and is mostly used for protection of local components such as converter transformers [1].

4.7 Distance relays

Distance relays are installed in many AC transmission lines today. The basic principle behind their operation is the determination of line impedance using current and voltage measurements [37]. During a ground fault, the effective length of a transmission line is shortened, resulting in reduced total impedance. For AC systems, line impedance is fairly constant per unit length [37], meaning the fault impedance can be used for determining distance to the fault and whether it is within the zone of protection. The impedance characteristic of a system is illustrated by the use of an R-X graph in figure 4.2. Fault is indicated when the operating point lies within the zone of protection [37]. For an AC system, this zone has both an X- and an R-component, but in a DC system under normal operation, there is only an R-component, as DC system impedance is purely resistive.

In AC systems, symmetrical component analysis is used to determine fault location [37], but this is not possible in DC systems. In [41], an alternative method is proposed, taking into account frequency dependent parameters of a DC-line. Due to the skin effect and soil conditions, as well as harmonics in the fault voltage transients, the resistance and inductance varies with frequency. Therefore, in order

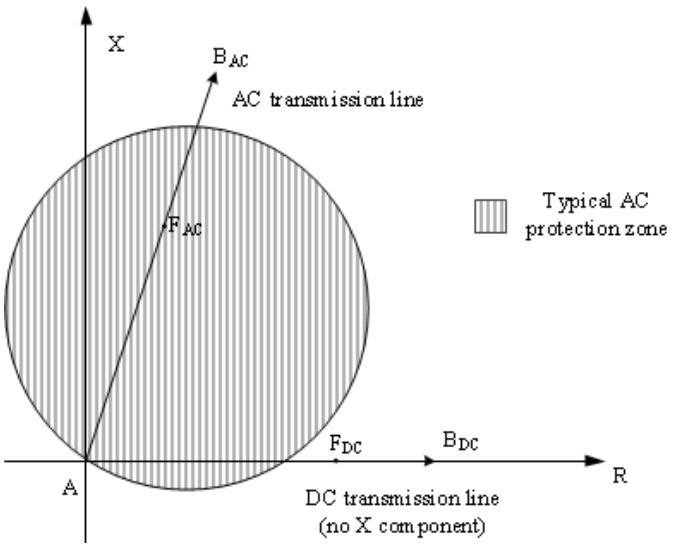

FIGURE 4.2: Typical R-X characteristic of a transmission line between points A and B. Fault indicated at point F.

to accurately determine voltage and current at the relay point, the line transformation matrix is decomposed into two parts. The first is a distributed parameter model with ideal constant parameters. The other is a compensation matrix which takes into account frequency dependent behaviour. While simulations are showing good result, the method requires comprehensive calculations, and further work is needed before implementation is possible [41].

4.8 Travelling wave

As was explained in 3.1.4, a fault occurring along the line cause transient waves to travel along the line in each direction away from the fault, being reflected between the fault and converter until its energy is dissipated in the line resistance. These waves can be registered at the relay, and the time difference between each arrival used to determine distance to the fault, as the wave velocity is dependent on geometry of the line. Travelling wave protection is considered a very fast form of fault detection, but requires large amounts of computation and possibly communication [31, p. 21].

With present technology, there are three different methods for implementing travelling wave protection [31, p. 23].

- single-ended mode relying on fault generated transients

- double-ended mode relying on fault generated transients
- single-ended mode relying on breaker generated transients

4.8.1 Single-ended mode, fault generated travelling wave

This is also known as type A fault location method, and relies on the assumption that terminal and fault arc impedance are lower than the line surge impedance [31, p. 23]. This results in reflection coefficients close to -1 both at the terminal and at the fault. The time between each wave arrival at the terminal can then be used to determine distance to fault with the following equation [42].

$$d = \frac{T_2 - T_1}{2} v \tag{4.2}$$

Where T_1 and T_2 are arrival time of the first two waves to reach the terminal. Successful detection and localisation hinges on fault arc duration and resistance, as well as the identification of appropriate waves [42].

4.8.2 Double-ended mode, fault generated travelling wave

This method for travelling wave fault detection is also known as type D. With this method, arrival time of the initial transient wave is registered at both line end terminals, and then distance can be calculated in accordance with equation (4.3) [31, p. 23]. Compared to the previous method, type D will work even if the fault arc is extinguished quickly or has a higher resistance than assumed. GPS should be used to obtain the time stamps, and the information sent to a central location [31, p. 23]. The communication process takes time, and communication failure will make the system inoperable. Also, it is important that the sample rate is high enough that the first wave is registered correctly at both terminals.

$$d = \frac{L + v(T_A - T_B)}{2} \tag{4.3}$$

Where $(T_A - T_B)$ is the difference in arrival times at the two stations [42].

4.8.3 Single-ended mode, breaker generated travelling wave

The last travelling wave fault location method used today is known as type E, and measures reflections of a breaker generated transient wave. Distance to changes in impedance can then be calculated based on measured time stamps. This method is mainly used to detect faulted parts of the line, or measure its electric length [42]. Consequently, type E is of lesser interest for fault detection, and also depends on implementation of DC circuit breakers.

4.8.4 Evaluation of travelling wave method

The detection of travelling waves require the relays to have a relatively high sampling frequency. Higher sampling frequencies result in higher accuracy, but also higher demands on data processing equipment [42]. GPS is used for acquiring wave arrival times, and inaccuracy is estimated at 1 μs [31, p. 22]. The resulting uncertainty of fault location is less than $\pm$150 meters, depending on wave velocity. It is very important to have precise information on the speed of the travelling wave. If DC circuit breakers are installed, it should be possible to accurately measure this during construction of the line by operating the breakers and measuring the time until the wave is detected at the other end of the cable. If measurements are not possible, wave velocity must be calculated on basis of line parameters. Correct wave identification is complicated both by the high wave velocity, but also attenuation and dampening of the waves [41]. Type D is generally considered to be more accurate than type A, but does require more installed equipment making it the more expensive alternative [42]. Also, the need for communication slows down the process of deciding upon which protection zone a fault has occured in.

4.9 Wavelet analysis

Transient signals contain valuable information which can be used for fault detection and localisation. A known signal processing method is the Fourier transform, but this has a severe drawback in fault detection application since it requires information about the signal waveform for an unlimited period of time [31, p. 147]. In addition, the Fourier transform loses important information about inception of

a signal and any singularities which may appear. In order to obtain this information, the non stationary signals should be transformed into a joint time and frequency domain. This can be done by a Short-Time Fourier Transform (STFT) [43] [31, p.147]. This is a modification of the classical Fourier transform, where the input signal is multiplied by a window function $w(t-\tau)$ where τ represents a time transition. The resulting transforms can be represented in the time-frequency domain, with time and frequency resolution being related by $\Delta f = \frac{1}{\Delta T}$. This strict relationship cause problems in signal processing, as signals with a short duration and high frequency require a fine time resolution, while longer lasting signals with lower frequencies require a fine frequency resolution [43].

By modifying the window function, the wavelet transformation method is obtained, given by the following equation:

$$W(p,\tau) = \frac{1}{\sqrt{p}} \int_{-\infty}^{\infty} x(t)\psi^*(\frac{t-\tau}{p})dt \tag{4.4}$$

Where $\psi^*(\frac{t-\tau}{p})$ is called the mother wavelet, and p is known as the dilating parameter, which determines size of the time-frequency window[44]. It is important that the mother wavelet is a short duration function with a zero average, and that it quickly decays to zero at each edge [43]. Different wavelets with the same mother wavelet but varying τ and p are grouped together in a "wavelet family" [31, p. 150].

In order to implement wavelet transformation digitally, it must be obtained discretely. This is done with the following equation [43]:

$$DW(m,k) = \frac{1}{\sqrt{p_0^m}} \sum_n x(n)\psi^* \left(\frac{k - np_0^m}{p_0^m}\right) dt \tag{4.5}$$

Here, the translation and dilating parameters are functions of integers m and n; $p = p_0^m$, $\tau = np_0^m$. This alleviates the problems with STFT pointed out earlier.

The implementation of discrete wavelet protection involves successive layers of high- and low-pass filters, where the signal is inputted in the first layer, and dilation of the wavelet window is incremented with each layer. Each layer covers a different frequency spectrum, with the first layers covering the higher frequencies, and the latter layers covering lower frequencies [45]. Each layer outputs a set of wavelet coefficients, with the highest frequency of the samples being half of what they were in the previous layer. Following Nyquist's rule, it is therefore possible

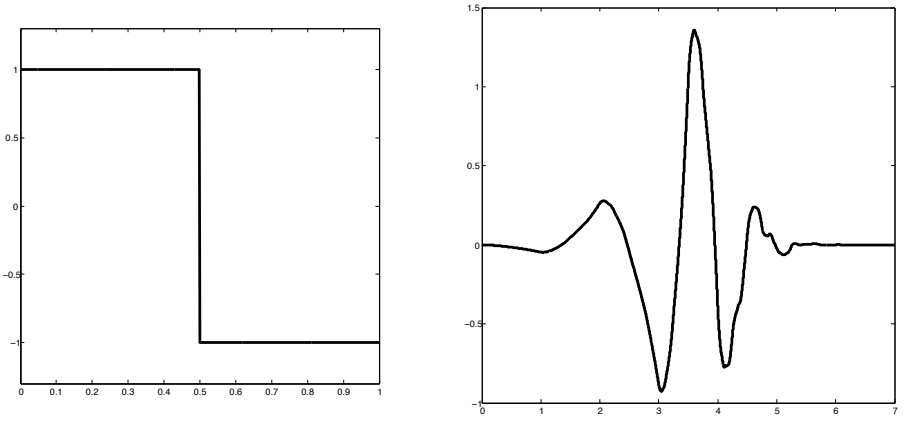

(A) The Haar wavelet (B) The daubechies mother wavelet

FIGURE 4.3: Haar and Daubechies mother wavelets

to discard half the samples of the output [46]. The output from the low pass filter is sent to the next layer of high- and low-pass filters, while the output of each high pass filter together make up the discrete wavelet transform.

However, when comparing transforms obtained from different lines, it is important that both transforms are compared without any shift in time, which is not the case with discrete wavelet transforms. An alternative modification of the discrete transform is the static transform. For this scheme, the dilation parameter p is discreticised, while the transition parameter is kept constant. This results in a stationary transform window which expands for each iteration [44]. When using the static transform, the highest sample frequency is not divided by two for each filter layer, and so Nyquist's rule is not applicable, otherwise the process is similar to the discrete transform. The resulting wavelet and its coefficients will be time invariant [44].

There are several mother wavelets available. In [44], the Haar wavelet is used. This is illustrated in figure 4.3a. For detection of disturbance in electrical systems however, fourth order Daubechies wavelets are reported to be more suited [47], which is illustrated in figure 4.3b.

Different measured values can be used to obtain the wavelet and its coefficients. A fault is characterized by the wavelet coefficients surpassing a specified threshold. Detection time for this method is simulated to below 1 ms [44]. However, the large amount of calculations necessary makes implementation difficult [48].

4.10 Artificial Neural Networks

The basic idea behind Artificial Neural Networks (ANN) is to build a protection system which will learn what different fault currents looks like depending on type of fault and location. To do this, the neural network of a human brain is mimicked by a set of elementary neurons arranged in a layered structure [31, p. 375]. The learning process requires going through several fault cases and feeding the results into the network neurons.

There are different ways of connecting the neurons together, deciding how they interact with each other. One of the more simple architectures is the Feed Forward Network known as perceptron [31, p. 375], illustrated in figure 4.4. Each neuron receives an input and produce an output which is sent to the next layer of the network. The outputs are weighed based on required output during the learning process [31, p. 375]. Input data can be both directly measured signals and features of those signals, while output can be used for tripping command or informing of fault type. For the learning process, the most important system conditions should be covered, both for faults in the protection zone assigned to the network as well as other disturbances [31, p. 377].

Use of ANN for determining fault direction was proposed and investigated in [49], with reported decision time of 2.4 ms based on direct current and voltage measurements in an AC system.

The major disadvantage of ANN is the extensive learning process required. In addition, the internal signals are difficult to interpret, making troubleshooting more difficult. Also, the system is not reported to be especially robust [31, p. 363].

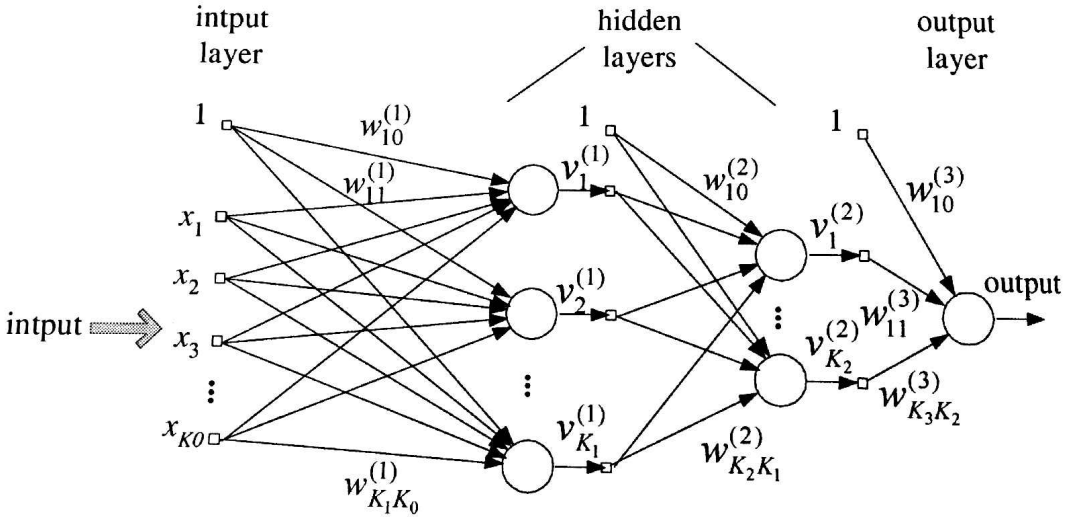

FIGURE 4.4: Forward Feeding Artificial Neural Network structure, taken from [31, p. 376]

Chapter 5

Description of PSCAD model

Of the different proposed detection methods, three were chosen for implementation in a simple MTDC system in PSCAD. SINTEF Energy supplied a PSCAD model of three VSCs connected together with cables in a bipolar scheme. The model included both control system for the VSCs and cable parameters. Some additions were made. Most notably the overcurrent protection of the IGBTs, but also fault locations and the chosen protection methods, as well as breakers connecting the converters to the cables. Some measuring points for voltage and currents were changed and pi equivalents on the AC side of the converters were exchanged with the PSCAD pi section component.

The implemented PSCAD models of converters and cables were provided by SINTEF Energy. and some additions were made, such as overcurrent protection for the converter IGBTs. The system is a simple three station HVDC system with connected AC grids. In this chapter, the system is described in more detail.

5.1 About PSCAD

PSCAD stands for "Power System Computer Aided Design". It is a software for modelling power systems of variable complexity and size, and simulating voltage and current transients in a graphical interface. The program is based on the work in ElectroMagnetic Transient Programming by Hermann Dommel and Scott Meyer [50]. It is now owned by Manitoba Hydro which continue its development.

Changes to the system, such as applying fault or changing certain input parameters to control systems, can be done while the simulations are being run. Currents and voltages can be plotted as they are being calculated.

PSCAD was chosen for this work primarily because it has a very advanced cable model which takes into account the frequency dependency of cable parameters and offer DC correction. This makes it very suitable for modelling fault transients in an HVDC system. It also has an interpolate function for handling switching actions in the system (switching action are for example connecting/disconnecting breakers or turning IGBTs on and off).

5.2 The DC system

The DC system is made up of three converter stations in a bipolar configuration with a total of six VSCs, illustrated in figure 5.1. The figure can also be found in appendix A. Converter stations W and S have a rating of 2400 MVA while station E has a rating of 1600 MVA. AC side transformers are delta-Y wired, with isolated neutral point, in order to avoid circulations of harmonics on the DC line. Since the system is purely bipolar, the converters are individually grounded with no metallic return between them.

In order to apply cable faults in PSCAD, the cables must be divided into sections so the central conductor can be accessed. This is done by making several cable connections and connecting these back to back with the fault in between. There is a total of four possible fault locations in the system. At each location, it is possible to apply positive-pole faults, negative-pole faults and bipolar faults.

The DC-cables are connected to the converters through breakers. They are assumed to be able to interrupt any current regardless of magnitude and polarity, and with an on-state resistance of 5mΩ.

Currents are measured in each breaker, and voltage is measured at all converter stations between each pole and earth. The breaker currents are positive when going into the DC line. During steady state, station W is set to voltage control with the two others controlling power flow. System voltage is $\pm$430 kV.

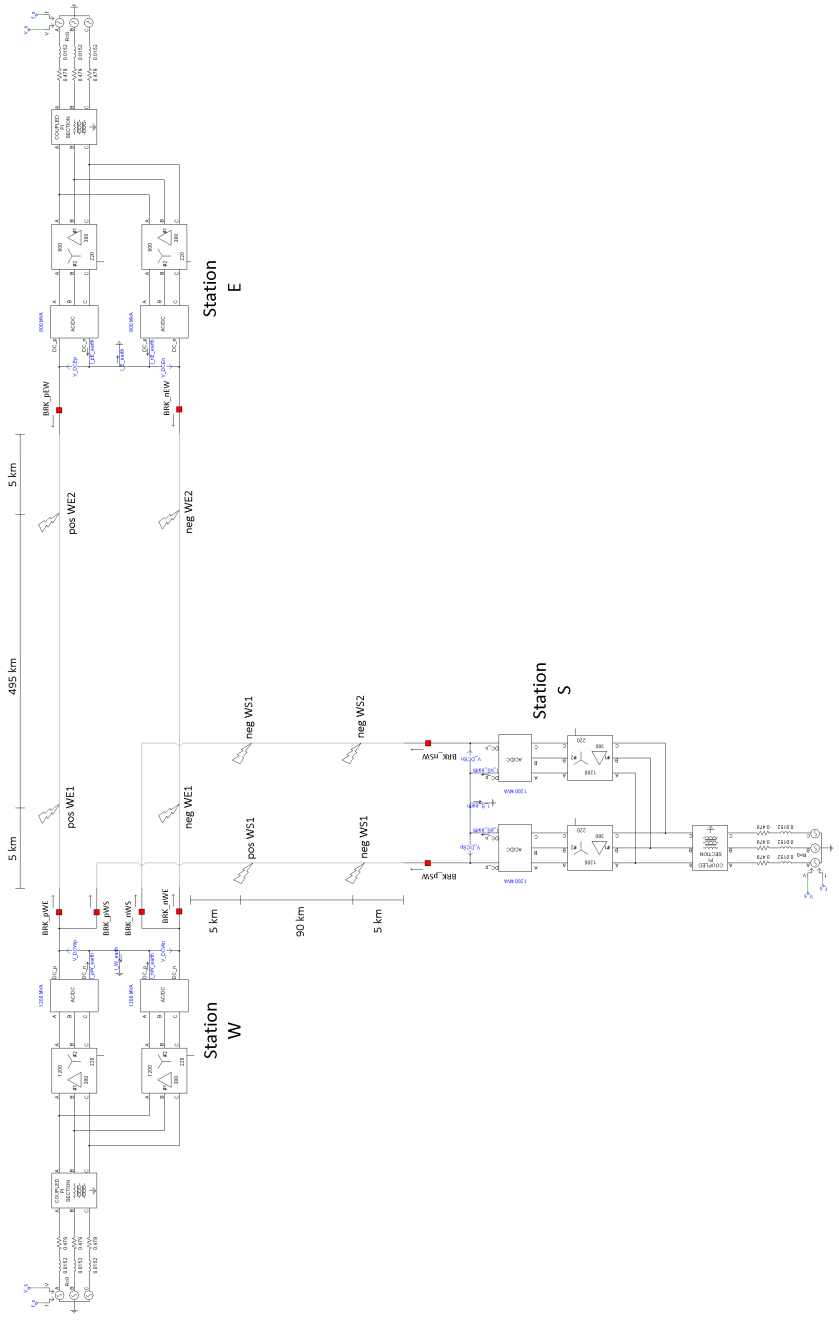

FIGURE 5.1: The MTDC system implemented in PSCAD with all measurement and fault points indicated

5.3 The voltage source converters

The PSCAD converter model is illustrated in figure A.2 in appendix A. On the AC side there is a filter designed to remove harmonics and AC noise. The converter itself is made up of six IGBT and diode pairs. The IGBTs are controlled by PWM, using either voltage or active power as reference. On the DC side, there is a filter

capacitance connected in parallel with a large resistor. This resistor mimics the imperfections of an actual filter capacitance. In addition to the control system, the IGBTs have been given a local overcurrent protection. This is designed to block the IGBTs once the DC current out of the converter exceeds a set threshold, as advised in [1].

5.4 The AC system

There are three AC grids interconnected by the DC system. These are modelled as AC generators connected to the converters with a common aerial line, modelled using the standard PI-equivalent in PSCAD. Generator voltage and frequency are controlled externally. Parameters are given in table 5.1. Each converter is connected to the AC grid by a converter transformer. These are all Delta-Y wired with the AC grid connected to the Delta terminal. The voltage ratio is 380/220.

Table 5.1: AC system parameters

Generator		**PI-equivalent**	
Voltage [kV]	380	Length [km]	100
Frequency [Hz]	50	Resistance [mΩ/km]	17.8
Resistance [mΩ]	15.2	Inductive reactance [Ω/km]	313.88
Inductance [mH]	479	Capacitive reactance [MΩ*m]	273.54

5.5 DC cables

The implemented DC cables are oil filled and insulated using Poly Propylene Laminated Paper (PPLP). Modelling in PSCAD is done using a frequency dependent cable model. According to PSCAD, this is a highly advanced and accurate cable model, especially for modelling transients. The cables used have both a metallic screen and armouring, as they are intended to represent submarine cables. Cable dimensions and design are based on actual 500 kV cables in service today [51]. There are two implemented cable models with power rating 1200 MW and 800 MW for the WS and WE line respectively. A cross section of the cable was illustrated in section 2.5, the cable properties are given in tables 5.2 and 5.3. The

cables screen and armour are assumed perfectly grounded at both ends. The semi-conducting layers between insulation and core/sheath has not been implemented in the model. Instead, permittivity of the insulation has been modified to account for their presence.

Table 5.2: Cable materials

Layer	Material	Resistivity [Ω*m]	Rel. permittivity	Rel. permeability
Core	Copper	18.9×10^{-9}	-	1
Insulation	PPLP	-	3.17	1
Sheath	Lead	220×10^{-9}	-	1
Insulation	PE	-	2.3	1
Armour	Zinc	180×10^{-9}	-	2
Insulation	PE	-	2.3	1

Table 5.3: Cable dimensions

Layer		1200 MW cable	800 MW cable
Core	Inner radius [mm]	12.5	12.5
	Outer radius [mm]	34.7	29.8
Insulation	Outer radius [mm]	57.2	47.3
Sheath	Outer radius [mm]	61.3	51.2
Insulation	Outer radius [mm]	65.1	54.9
Armour	Outer radius [mm]	70.2	58.8
Insulation	Outer radius [mm]	75.0	63.0

With the given parameters cable resistance, capacitance, inducatnce and wave impedance can be calculated using equations (3.6)-(3.8) and equation (3.17). These are listed in table 5.4.

Table 5.4: Cable resistance, capacitance, inductance and wave impedance

	Resistance [mΩ/km]	Capacitance [μF/km]	Inductance [nH/km]	Wave impedance [Ω/km]
800 MW cable	8.221	0.382	92.400	15.569
1200 MW cable	5.741	0.353	99.963	16.843

5.6 Implemented protection methods

There are three fault localisation methods being tested in this model; wavelets, travelling wave and derivative protection. These were presented in chapter 4 along with other proposed methods, and chosen as the most promising alternatives, as previous work indicate they are fast, reliable and does not require communication between relays.

5.6.1 Wavelet protection

The implemented wavelet protection makes use of the discrete wavelet transformation component in PSCAD. In this component, different mother wavelets can be chosen, as well as coefficient levels and desired sampling frequency. There are two output channels from the DWT component. According to the PSCAD Helpsection, one depicts the low frequency content of the input signal, while the other shows the high frequency content. An anti-aliasing filter is applied to the input signal, removing frequencies higher than the Nyquist frequency [31, p. 183].

For these simulations, the mother wavelet chosen was the fourth order Daubechies wavelet, based on recommendations in [47]. It should be noted that other mother wavelets have been used in different studies [44]. Selection of levels is a matter of desired detail. The lower levels represent the highest frequency components of the input signal, while higher levels represent gradually lower frequencies. Coefficients were calculated up to level 6, which is the highest level possible in PSCAD. Sampling frequency has been set to $200kHz$, which is equal to the plot frequency. The calculated wavelets are compared to a set threshold for detection of fault, which is similar to what was done in [44].

5.6.2 Derivative protection

The derivative is calculated by using the *Derivative with Time Constant Component* in PSCAD. The applied time constant scales the signal. In these simulations, the time constant is set at $0.001s$. Only the current derivative is used for determining faulted cable. The voltage is measured at individual DC bars at each converter

station, and is therefore no good indication of which connected cable is faulted. The current derivative is compared to a set threshold for determining whether a fault has occurred in its zone of protection. Polarity of the derivative implies which direction the fault is located. A positive derivative means the fault is in front of the breaker and requires it to trip, while a negative derivative indicates a fault is located behind the breaker and outside its assigned protection zone.

5.6.3 Travelling wave

The travelling wave method is implemented in MATLAB using the equations presented in section 3.1.4. Because the implemented system should not rely on communication, method A has been used. Use of this method assumes a low ohmic fault. The arrival of a transient at a measuring point cause a sudden increase in current. Therefore, the current derivative is used for determining when a transient reaches the breaker. Each detected arrival time is stored in memory. In order to determine fault distance, it must be possible to correctly record arrival times of the first and second transients. Velocity of the travelling wave depends on cable properties. Using equation (3.14) on page 31 and data from table 5.2 the velocity is calculated to 168 497 km/s for both cables. Since sampling time is 5 μs, the margin of error is $5\mu s \times 168.497 m/\mu s = 842 m$.

5.7 Plan for simulations

In chapter 3, it was explained which parameters influence the shape and size of fault currents. In order to test the performance of the different protection methods, these parameters will be varied, and faults at different locations are applied. The different fault locations and their references are indicated in figure A.1 in appendix A. As has been mentioned, sampling frequency is set to 200 kHz, giving a Nyquist frequency of 100 kHz.

5.7.1 The different faults

Both positive pole, negative pole and pole-to-pole faults are applied. In order to apply the pole-to-pole faults, all faults in a single location are activated. For

example, in order to apply pole-to-pole fault WE1, a fault impedance is inserted between the two poles, and between each pole and earth. The fault impedance is the same between the two poles as it is between either pole and earth.

5.7.2 Parameters to vary

According to [32] and [6], the parameters influencing fault currents at converter stations are as follows:

- Fault impedance
- DC filter capacitance
- Distance to fault
- Short Circuit Ratio (SCR) between the AC and DC grids

However, the SCR only affects the second peak of the fault current, which occurs after the diodes have started to conduct [32]. Since the fault should be detected before this time in order to avoid damage to the diodes, the SCR will not be varied in the simulations. In table 5.5, variations in the fault impedance and filter capacitance for each case are given. One parameter is varied during each run and with different fault types and locations.

Table 5.5: Variation of parameters in different simulation cases

Parameter	Base case	Case 1	Case 2	Case 3	Case 4
Capacitance [μF]	631.36	473.52	315.68	157.84	63.14
Fault resistance [Ω]	0.01	2	4	8	16

The three protection methods are evaluated based on the results, and if possible; a protection system will be suggested.

5.7.3 Expectations

During fault the resistance, inductance and capacitance varies as seen from the different converter stations. Each converter will have the same filter capacitance, but line capacitance will vary. This will influence how the system is damped, as

explained in section 3.1.3. The different line parameters during faults are summarised in table 5.6

TABLE 5.6: Distance, resistance, total line inductance and capacitance between each converter and fault points

		Fault location			
Converter	Parameter	WE1	WE2	WS1	WS2
W	Total distance [km]	5.0	495.0	5.0	95.0
	Line resistance [mΩ]	41.1	4069.4	28.7	545.4
	Line inductance [nH]	4.6	457.4	5.0	95.0
	Line capacitance [μF]	1.9	189.1	1.8	33.5
S	Total distance [km]	105.0	595.0	95.0	5.0
	Line resistance [mΩ]	615.2	4643.5	545.4	28.7
	Line inductance [nH]	104.6	557.4	95.0	5.0
	Line capacitance [μF]	37.2	224.4	33.5	1.8
E	Total distance [km]	495.0	5.0	505.0	595.0
	Line resistance [mΩ]	4069.4	41.1	4139.2	4655.9
	Line inductance [nH]	457.4	4.6	467.0	557.0
	Line capacitance [μF]	189.1	1.9	192.8	224.5

Using equation (3.13) from section 3.1.3, the theoretical damping factor can be calculated. Doing this for a single pole fault at WE1 seen from converter W with varying fault resistance and $C_{Conv} = 631.36\mu$F and fault path parameters taken from table 5.6, the values in table 5.7 are obtained. The calculations are done in appendix E, with the assumption that line capacitance can be ignored as it is less than a hundredth of the converter capacitance. This assumption is valid for short fault distances.

TABLE 5.7: Values for damping ratio at different fault impedances, fault distance 5 km on the WE line

Resistance	ζ	Damping
0.01	89.25	Over
2	1.43×10^5	Over
4	5.6×10^5	Over
8	2.22×10^6	Over
16	8.83×10^6	Over

The theoretical values indicate that the system should be overdamped for all fault impedances. A decrease in converter capacitance to $C_{Conv} = 63.14\mu$F means all the damping factors in 5.7 can be divided by ten. The system should still be

overdamped. Since the square of resistance per length is larger than the inductance per length for the cables, damping ratio should increase with increased fault distance. Including the cable capacitance should also increase damping ratios.

Depending on the actual frequency content of the wavelets, some of the levels will register higher than others. Since high frequency components have a smaller impedance to ground and larger on line impedance, the higher wavelet levels will most likely register larger for long distance faults. Frequency content should be closely related to the natural frequency of the RLC circuit. However, due to the distributed capacitance and its effect on the frequency content in the current, the exact values will be difficult to foresee.

It was noted in section 3.1.3 that the current response from an overdamped circuit varied the most at the beginning of capacitor discharge. It is therefore reasonable to assume that the largest current derivative will be recorded at the first arrival of the fault transient at the measuring point. Since an increase in the overall resistance of the fault circuit increase damping which in turn reduce the rise rate of the initial capacitor current, the derivative can be expected to decrease for increasing fault impedances and distance. Further, the arrival of transient waves should be registered as spikes in the derivative. Magnitude of these spikes will decrease as the current wave is attenuated.

The converter diodes are the components with highest exposure to damage from the fault currents. Based on the voltage level of ±430 kV and a maximum load of 1200 MW per converter, these diodes are rated for a current of

$$I_D = \frac{1200\ MW}{430\ kV} = 2.8\ kA \tag{5.1}$$

Assuming they can withstand some overload for a short time, the time between arrival of the first fault transients until diode current reach this level will be the time the protection has to act.

Chapter 6

Simulation results

Results from the previously described simulations are presented in this chapter. First, observed currents and voltages are presented for the different simulation cases, followed by observed wavelets, derivatives and performance of travelling wave protection. The chapter is concluded by a summary of the observations. Unfortunately, it was not possible to reach a steady state for the system with a converter capacitance of 157.84 μF. Influence of capacitance is therefore discussed based on the other three capacitances cases.

The simulations produced a large amount of information and plots. What is presented here is what was determined to be of importance for discussing the different methods. Other plots and tables are located in appendixes C and D, and are referred to when relevant.

The system is illustrated in figure 6.1 with indicated fault points, distances and measuring points.

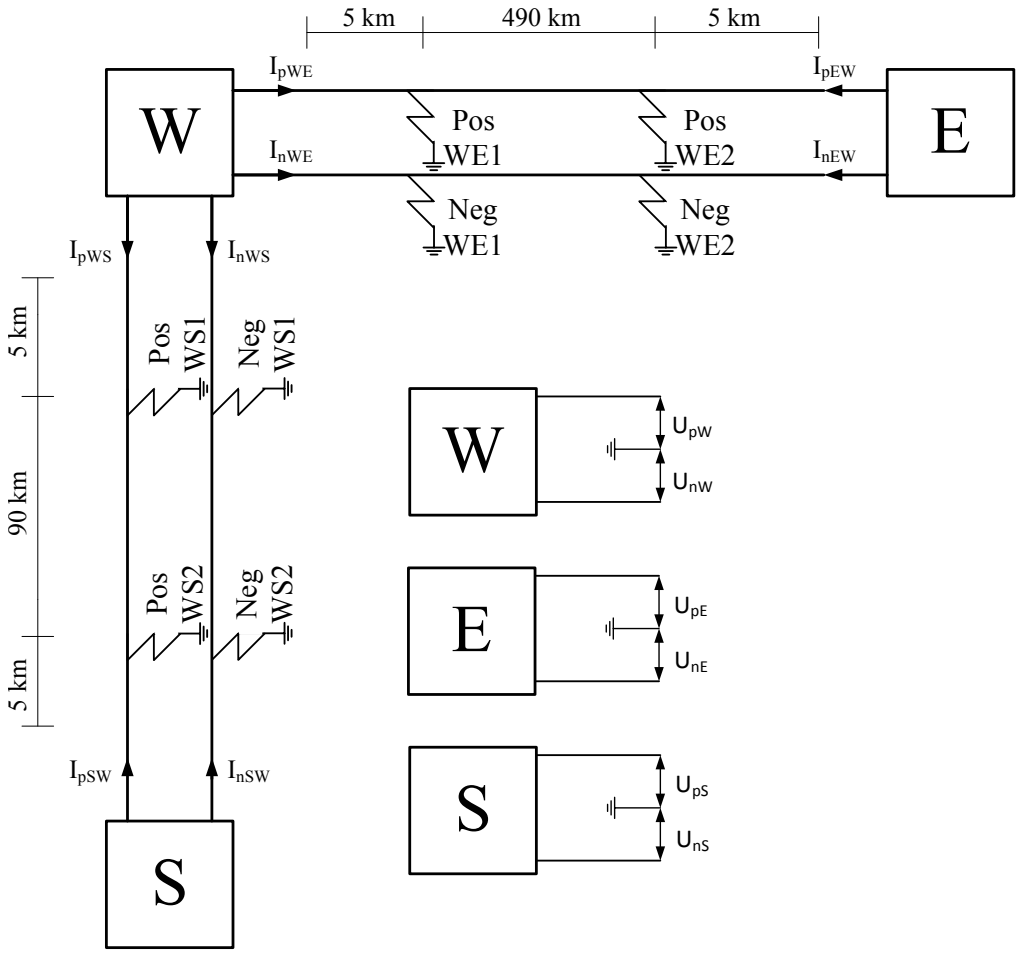

FIGURE 6.1: Layout of the implemented MTDC system

6.1 Currents and voltages

6.1.1 Base case

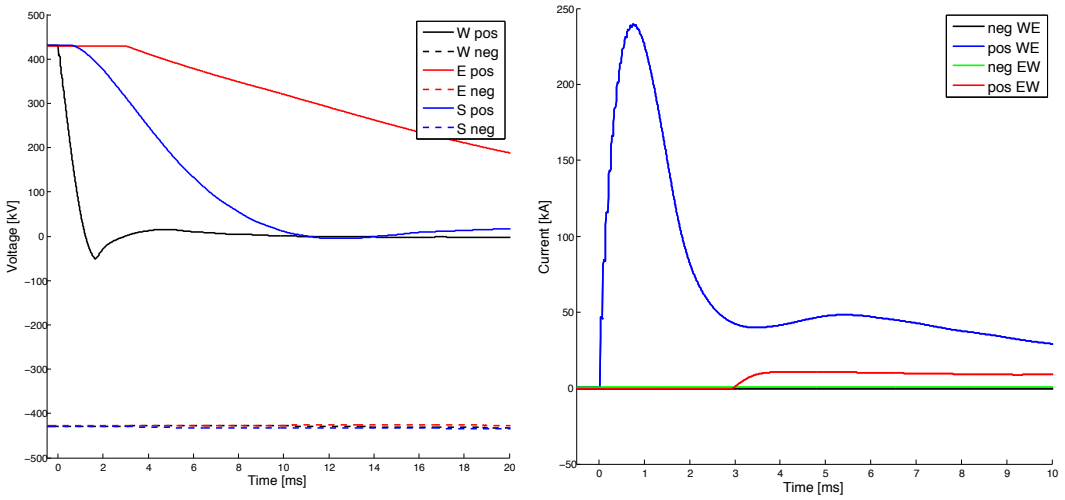

(A) System voltages

(B) WE line currents

FIGURE 6.2: Voltage and current recordings during fault at pos WE1

Fault currents and voltages recorded during a fault at pos WE1 are shown in figure 6.2. Recordings from other fault locations and fault types are located in appendix D. The currents and voltages recorded at converter W, which is only 5 km away from the fault, almost immediately experience a fast initial change as the capacitor at converter W is discharged into the fault. Distance between fault and converter E is much longer, and the transients appear later and are much less severe because there is a significantly larger resistance between fault point and the converter. For single pole faults, only currents and voltages in the faulted pole are affected by the fault. This is as expected according to the description of bipolar systems in section 2.2. For pole-to-pole faults, both poles experienced disturbance more severe than those experienced during single pole faults, with very symmetrical currents and voltages comparing the two poles. Since the primary difference between the different fault types were related to difference in current direction and small variations in severity for the pole-to-pole faults, the rest of this chapter will focus on positive pole-to-ground faults.

There are two contributing factors to the fault current in breakers at converter W, during the initial discharge of the converter capacitor. The primary source of

initial fault current is discharge of the capacitor, but there is also some current flowing from the connected WS line due to discharging of its cable capacitance, as was explained in section 3.1.4. This is illustrated in figure 6.3, showing the currents out of the positive pole of converter W. Once the capacitor is discharged, current flows through the diodes, powered by the inductive power of the cables for a short while, until the connected AC grid starts feeding the fault. The diode currents are better illustrated in section 6.1.4.

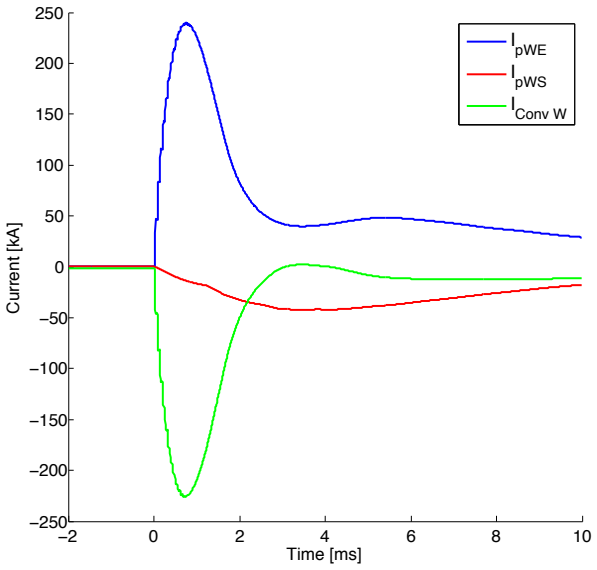

FIGURE 6.3: Current in breakers pWE and pWS, with current from converter W during fault pos WE1

Current I_{pWS} has a much slower rise rate than I_{pWE} because the cable capacitance is far smaller than the converter capacitor, and discharge occurs as the wave is travelling along the line, meaning there is no momentary discharge of a large capacitance. Once the fault has propagated to converter S, the capacitance at this station is discharged as well, into the positive pole of line WS. By inspecting I_{pWS} at t = 1.22 ms, the fault wave from discharging the capacitor at converter S can be seen arriving at the breaker and causing an increase in the currents rate of rise. Due to the increased resistance of the 100 km cable, currents from this discharge is not as large as those seen in cable pWE at the initial discharge. The current in pWE during fault at pos WS1 is not as severe as the other way around. This is due to the increased distance of line WE, which serve to purposes. First, it increases the total fault path impedance. Secondly, the increased distance means

the wave from discharging capacitor E will take more time to reach the breaker at converter W. The difference in these is illustrated in figure 6.4.

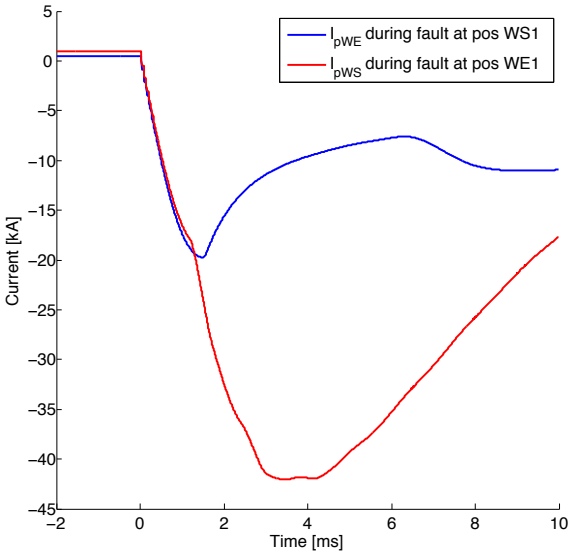

FIGURE 6.4: Currents in healthy lines during nearby faults

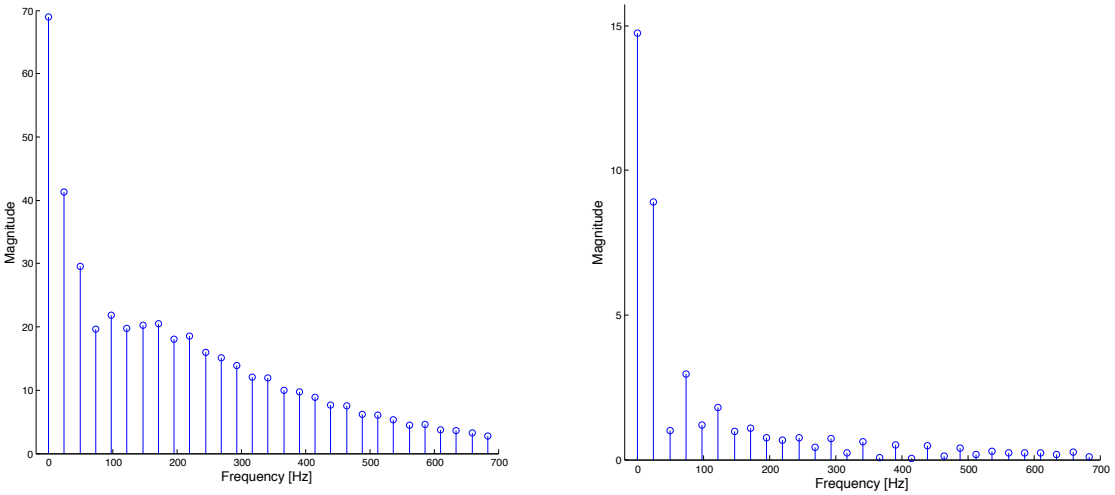

(A) Recorded at breaker pWE

(B) Recorded at breaker pEW

FIGURE 6.5: Frequency analysis of current on the positive pole WE line during fault at pos WE1

In figure 6.5 the frequency content for currents recorded at pWe and pEW are shown, calculated using Fast Fourier Transform in MATLAB (code in appendix B). Current recorded close to the fault has a higher amount of high frequency components than the one recorded far away. The high frequency components are

primarily caused by the discharge of converter capacitors and the amount depend on discharge time. It was explained in chapter 3 how discharge time of capacitors are dependent on capacitance and resistance, as well as the inductance in the circuit. Increased fault distance will increase all three of these, causing a larger time constant, τ.

Looking at frequency content of current recordings from breakers pWS and pSW during fault at pos WE1 in figure 6.6, it can be seen that the high frequency components are damped marginally faster than the low frequency components.

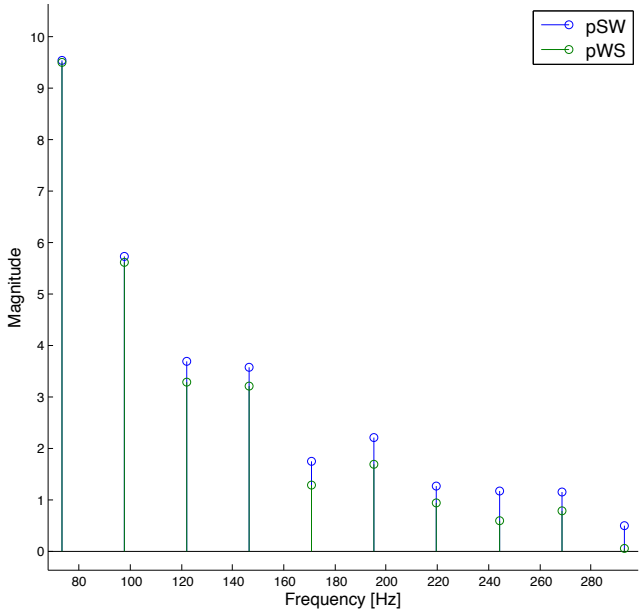

FIGURE 6.6: Frequency analysis of current in breakers pWS and pSW during fault at pos WE1

6.1.2 Varying converter capacitance

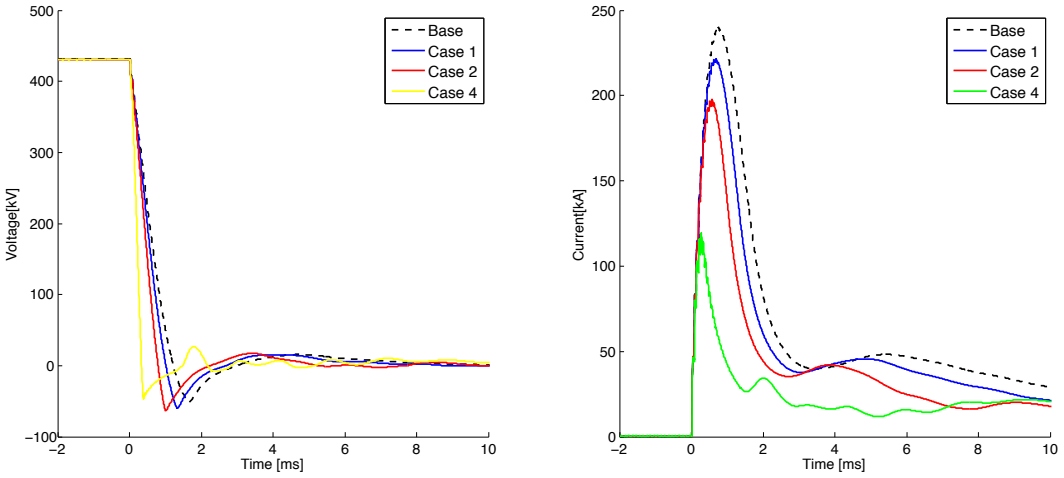

(A) Voltage pos W (B) Current pWE

FIGURE 6.7: Influence of filter capacitance on the fault currents and voltages. Fault location pos WE1

In figure 6.7, the effect of varying filter capacitance on fault current and converter voltage is illustrated. Reducing the filter capacitance results in lower fault peak current, but also a faster discharge. The lowest voltage value is not influenced by filter capacitance, but it is also reached faster. Only one current and one voltage is displayed in figure 6.7, but the effect is the same for the other measurements.

Due to the lowered discharge time, currents in the system would be expected to contain more high frequency components. This is illustrated for current I_{pWS} during fault at pos WS1 in figure 6.8. The frequencies displayed have been scaled to better express the relative frequency content of each signal. For frequencies above 1 kHz, the current components related to a small converter capacitor has a higher magnitude than those recorded with large capacitors. However, magnitude of the current components at these frequencies are only a small fraction of the total current. It is not necessarily the cause of the discharge, but could also be an effect of reduced noise filtering due to the lowered capacitance in the system.

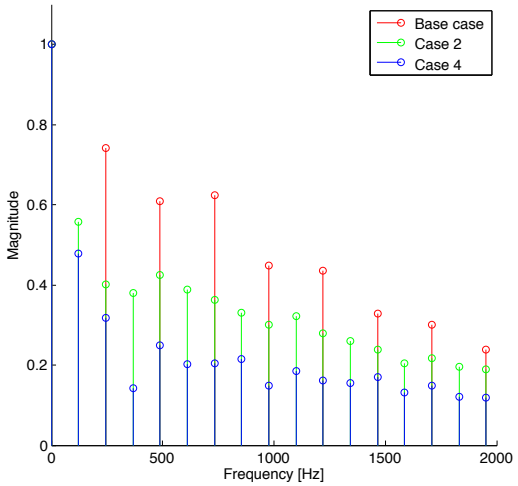

FIGURE 6.8: Frequency content of current I_{pWS} for fault at pos WS1

6.1.3 Varying fault impedance

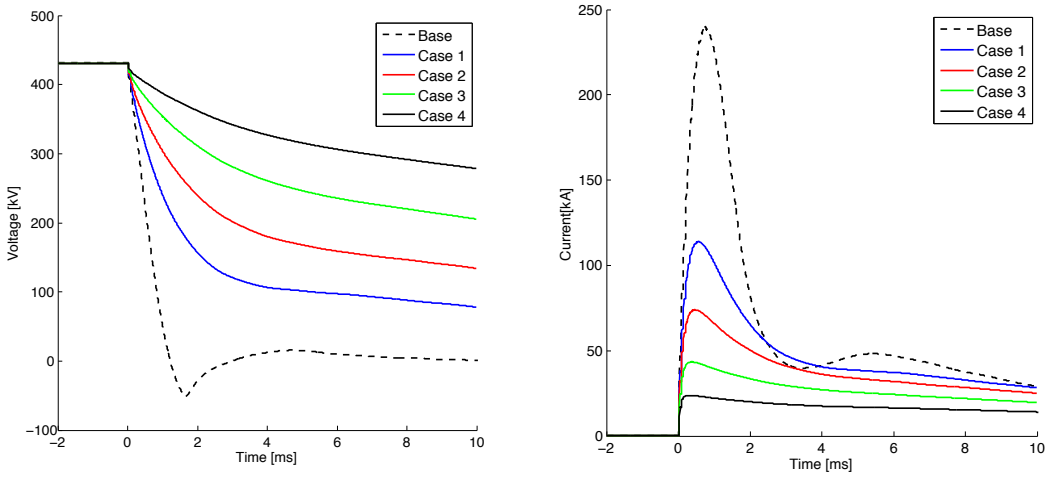

(A) Voltage pW

(B) Current at pWE

FIGURE 6.9: Voltage and current recordings from converter W during positive pole fault at location WE1 under varying fault impedance

In figure 6.9, the effect of varying fault impedance on fault current and converter voltage is illustrated. Time constant τ increases in accordance with the fault impedance. This leads to a decrease in the high frequency components in the recorded currents, illustrated in figure 6.10. The increased fault path impedance cause reduction in peak fault current as well.

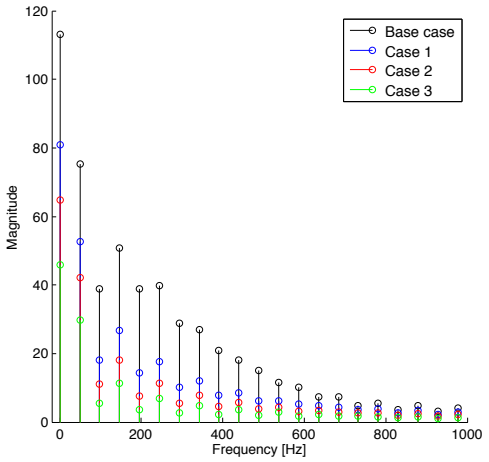

FIGURE 6.10: Frequency analysis for different fault impedances

For the converter voltages, similar observations are made. The voltage never drops to zero for cases 1 to 4, resmbling an overdamped system.

While figure 6.9 only shows one current and one voltage, the observations made here are true for the rest of the system as well.

6.1.4 Diode currents

Diode currents are displayed in figures 6.11-6.13 for different distances and converter capacitances. Diode current starts increasing once capacitor is discharged, which for low impedance faults close to the converter is between 0.34 and 1.53 ms, depending on capacitor size. As has been noted earlier, the smaller capacitor is discharged the fastest, leading to an earlier rise in diode currents. The currents reach a value between 32 kA for the smallest capacitor, and 41 kA for the 315.68 μF capacitor. These times increase for a larger fault distance. Roughly 1 ms after peak value the currents are different in the individual diodes, indicating that the fault is being fed from the connected AC network. The rise in current does not seem to be influenced by the reflected current waves, but while the current is dropping it is showing signs of a step wise reduction, indicating the presence of travelling waves.

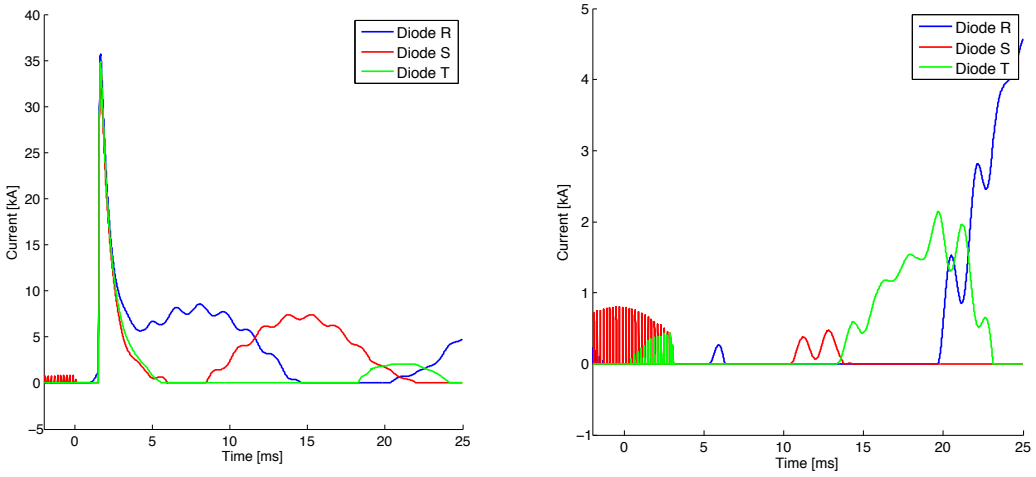

(A) 5 km

(B) 495 km

FIGURE 6.11: Diode currents with a converter capacitance of 631.36 μF

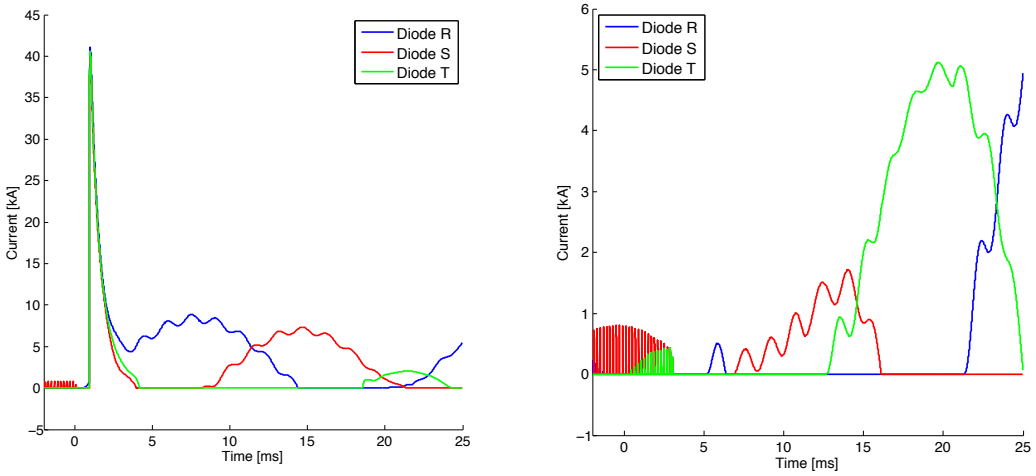

(A) 5 km

(B) 495 km

FIGURE 6.12: Diode currents with a converter capacitance of 315.68 μF

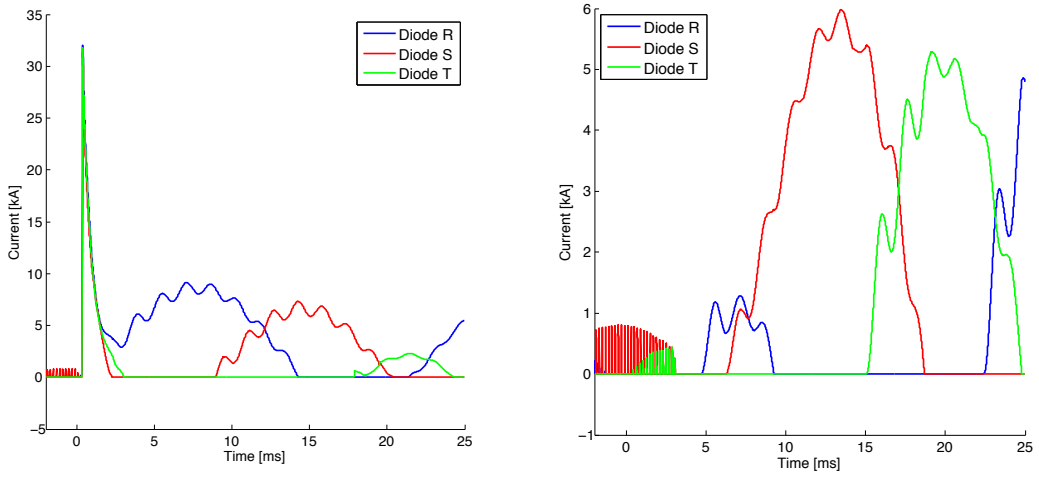

(A) 5 km

(B) 495 km

FIGURE 6.13: Diode currents with a converter capacitance of 63.14 μF

6.2 Wavelet protection

6.2.1 Base case

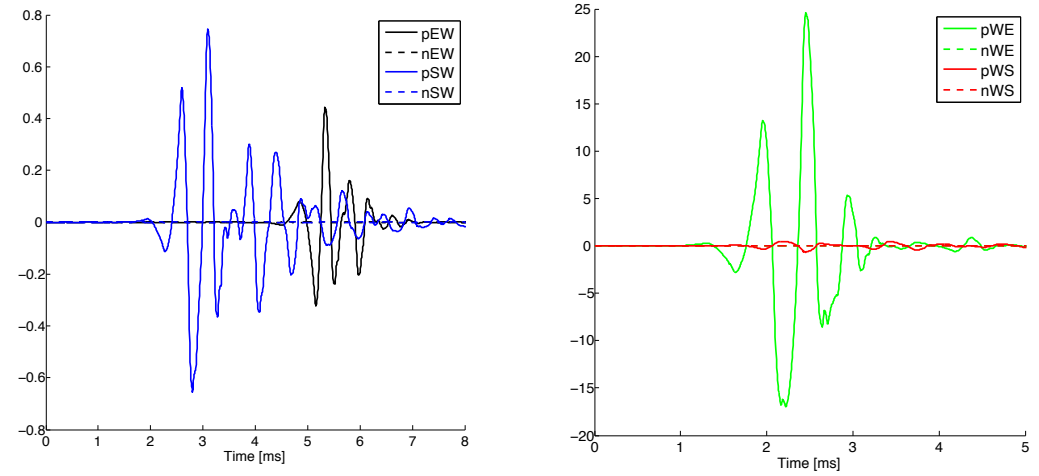

(A) Recorded at E and S

(B) Recorded at W

FIGURE 6.14: Wavelets recorded during fault at pos WE1

Figure 6.14 shows the level six wavelet coefficients recorded from all three converter stations during fault at pos WE1. From section 6.1.1 it is clear that a majority

of the high frequency components in the fault currents are found in the frequency range between 100 and 500 Hz for short distance faults, while long distance faults contain few components with a frequency higher than 300 Hz. This was reflected in the calculated wavelet coefficients, where lower level coefficients produced large oscillations for close faults, while long distance faults were only detectable using fifth or sixth level wavelets. For the longest distance of 495 km, the sixth level wavelets were preferred, while fifth level wavelets registered marginally higher peaks with fault distance of 95 km. Different wavelets for close and high distance faults are shown in appendix D.

Below is a list of some observations worth noticing.

1. There is a delay between arrival of the transient and increase in the wavelet value
2. The wavelets recorded far away from a fault are only a small fraction of those recorded close to the fault
3. Polarity depends on direction of fault
4. At converter W there is a large difference in peak value for recordings on either side of the converter

The first point is due to the need of a time window in order to calculate the wavelet coefficients. Size of the time window depends on sampling frequency, type of mother wavelet and the number of calculated levels. A high amount of levels require extra time to perform computations, increasing time delay of the wavelets. The second point is related to the lower magnitude of high frequency components in the currents at long fault distances, as was presented and explained in section 6.1.1. The third point is again due to the process of calculating wavelets and the equations used, which were presented in section 4.9. The fourth and final point is again related to the lack of high frequency components in the recorded current. The reasons for this was also discussed in section 6.1.1. These observations were made independent of fault type and location. Wavelets for different fault locations can be found in appendix D.

6.2.2 Varying capacitance

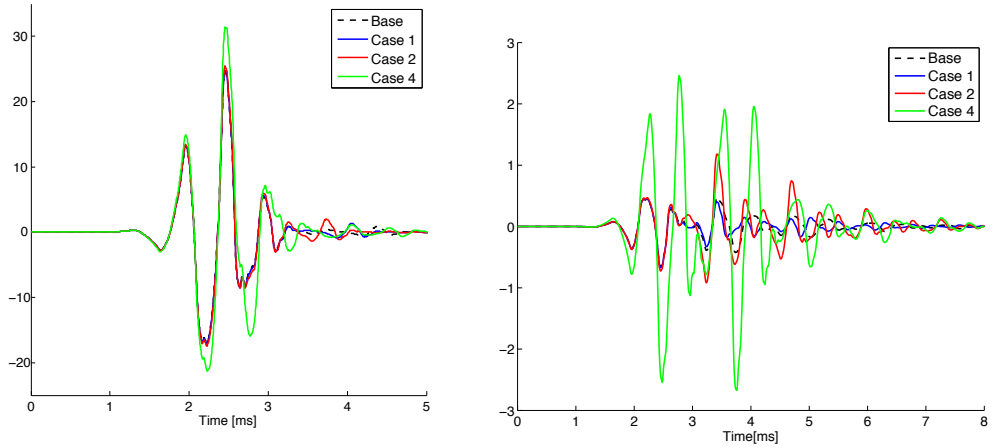

(A) Recorded at pWE

(B) Recorded at pWS

FIGURE 6.15: Wavelet analysis of fault currents following a fault at pos WE1. Recorded in pWE with varying filter capacitance

Wavelets following fault at pos WE1 is shown in figure 6.15 with different converter capacitors. A slight increase in the wavelets recorded at pWE can be seen with the reduction of capacitor size. The smaller capacitor will be discharged faster, leading to an increase in frequency components detectable with the sixth level wavelet coefficients. For close distance faults, the fifth level coefficients reached a higher peak value than the sixth level ones.

TABLE 6.1: Wavelet peaks compared to filter capacitance

Case	$\lvert Z_{cable}/Z_{conv} \rvert$	Absolute peak value wavelet pWE	Absolute peak value wavelet pWS
Base	$67f \times 10^{-3}$	24.59	-0.66
1	$50f \times 10^{-3}$	24.86	-0.67
2	$33f \times 10^{-3}$	25.43	1.18
4	$6.7f \times 10^{-3}$	31.41	-2.7

6.2.3 Varying fault impedance

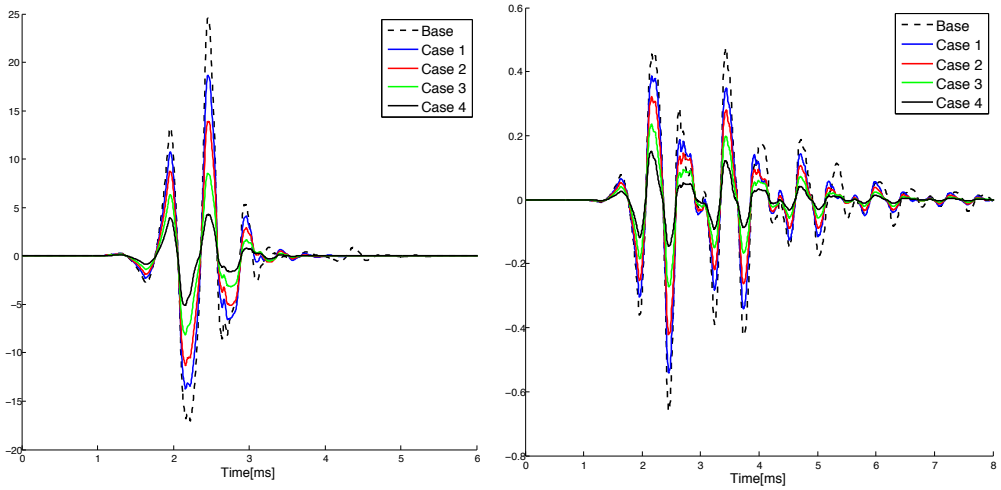

(A) Recorded in WE line, positive pole

(B) Recorded in WS line, positive pole

FIGURE 6.16: Wavelet analysis of fault currents following a fault at pos WE1. Recorded at converter W with varying filter capacitance

Figure 6.16 shows wavelets recorded at converter station W during a fault at pos WE1, and with different fault impedances. With the decline in high frequency components noted in section 6.1.3, as well as reduction of current magnitude for all frequencies, it is no surprise that magnitude of the detected wavelet coefficients decrease as well.

6.3 Derivative protection

6.3.1 Base case

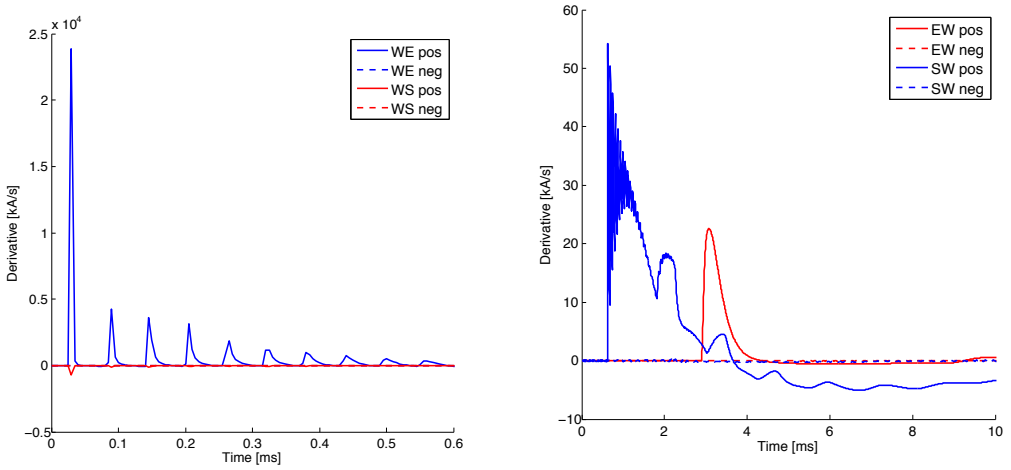

(A) Derivatives recorded at converter W (B) Derivatives recorded at converters E and S

FIGURE 6.17: Recorded derivatives during a positive pole fault at WE1

The derivatives recorded during a fault at pos WE1 are shown in figure 6.17. Polarity of the initial spike is determined by direction of fault, as a fault behind the breaker results in a negative current, as was illustrated in section 6.1.1. The recorded derivative peaks correspond with arrival of current waves.

Figure 6.17b shows the derivatives recorded on the positive pole at stations E and S. For a period starting 2 ms after the initial transient, the derivative of current I_{pSW} is negative even though the fault occurred in front of the breaker. This can be attributed to the drop in current after filter capacitance is discharged.

Due to the increased fault path impedance and subsequent increased discharge time of converter capacitor, long distance fault derivatives are smaller than short distance faults. This can be seen by comparing the derivatives of I_{pWE} and I_{pEW} in figure 6.17.

For faults along the WS line, a fault close to either of the converters initially caused a small negative derivative at the other end, before the positive surge. This is illustrated in figure 6.18. There were no indication of a drop in current

occurring in accordance with the derivative, so there is a possibility that this was due to amplification of noise caused by the PSCAD differential component.

To investigate this phenomena, distance between converter W and fault point WE1 was increased to 95 km, and a fault applied at pos WE1. The resulting derivative showed no sign of the negative spike in either end of the line, indicating that the spike is not related to fault distance, but rather distance to closest converter. This was further confirmed by increasing distance between WS2 and converter S to 40 km and applying a positive pole fault. The resulting derivative is illustrated in figure 6.19, and show no negative spike prior to the positive surge. Based on these results, it is theorised that the dip is either caused by an irregularity with the measuring derivative component in PSCAD, or by transmission and reflection of the transient wave at either one of the converters or the fault point. Derivative plots for different fault locations can be found in appendix D.

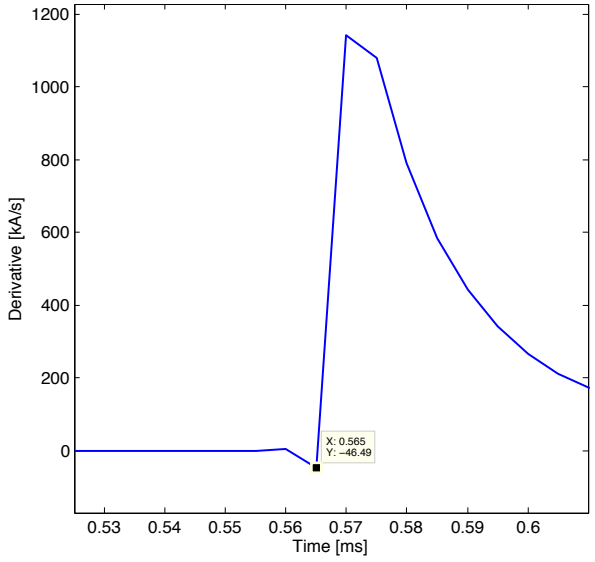

FIGURE 6.18: Negative derivative value just prior to arrival of transient wave at converter

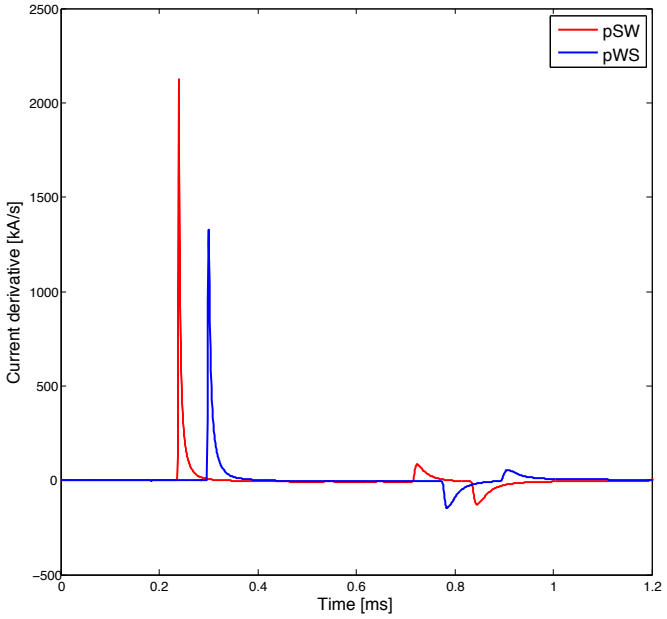

FIGURE 6.19: Derivatives recorded after fault 40 km from converter S, showing no negative spike prior to positive surge

6.3.2 Varying capacitance

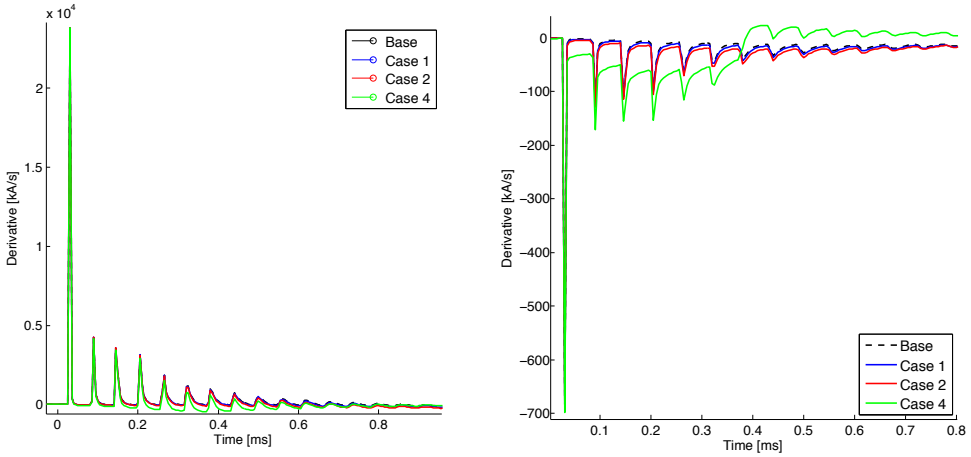

(A) Recorded in pWE

(B) Recorded in pWS

FIGURE 6.20: Fault derivatives with varying filter capacitance. Fault pos WE1

Derivatives recorded at converter W during a fault at pos WE1 with varying converter capacitance are illustrated in figure 6.20. The derivatives recorded at either side of converter W are only marginally affected. There is a certain increase in magnitude of the subsequent peaks for derivatives recorded in breaker pWS

when reducing capacitor size. Reducing capacitance also caused some positive derivative values for faults behind the breaker, roughly 0.4 ms after the fault occurred.

The smaller filter capacitance had no influence on the negative spike observed for faults close to either of the converters on line WS. This indicate that it is not caused by interaction with the converter.

6.3.3 Varying fault impedance

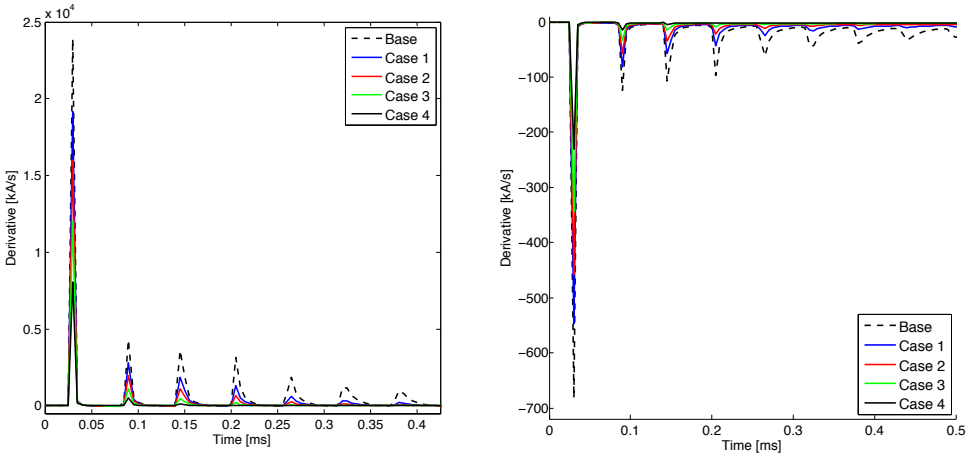

(A) Derivatives on line WE positive pole

(B) Derivatives on line WS positive pole

FIGURE 6.21: Derivatives at converter W, fault pos WE1, varying fault impedance

The recorded derivatives are reduced by increased fault impedance. This is again related to the reduction in fault currents and high frequency components noted in the previous sections. Derivatives recorded at converter W during fault at pos WE1 are shown in figure 6.21.

6.4 Travelling wave protection

6.4.1 Base case

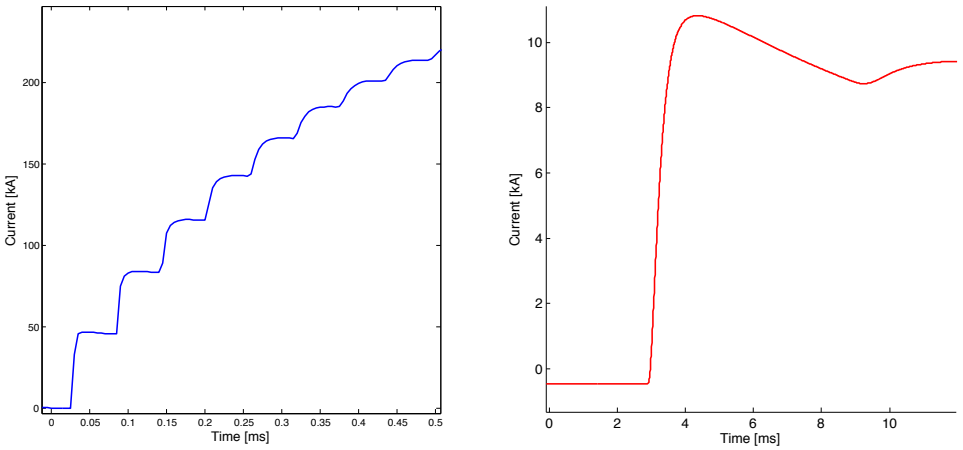

(A) Recorded at converter W

(B) Recorded at converter E

FIGURE 6.22: Detailed current development in the positive pole of line WE

In figure 6.22, the fault currents following a fault at pos WE1 are displayed in more detail than they were in section 6.1.1. The effect of arriving transient waves at breaker pWE are easily identified by the jumps in current. The derivative plot in figure 6.17a corresponded with this observation. By timing these jumps and taking into account the wave velocity in the cable, distance between fault and breaker pWE is found to be 5 km.

However, for the current measured at breaker pEW, the transient waves are not so easily identified. This is mostly due to the damping of high frequency components in the fault current. Because fault distance and wave velocity are known, it can be easily calculated that the transient should appear at breaker pEW at $t = 9ms$. There is an increase in current at this time, but its derivative is very small compared to the derivatives caused by faults closer to the converter.

For faults along the line WS, similar observations can be made, the arrival of transient waves are distinguishable at a distance of 95 km.

By adjusting the thresholds for detecting transient waves, it was possible to determine correct fault distance for all fault locations using the implemented MATLAB code.

6.4.2 Varying capacitance

The varying capacitance has only a small impact on detection of travelling waves, as the recorded derivatives are mostly affected for faults occurring behind the breaker. Using the MATLAB code gave the same results as in the base case.

6.4.3 Varying impedance

The increase in fault impedance reduced the transient current waves to the point where distinguishing their arrival from other variations in the current became impossible for long fault distances, using the implemented code. Thresholds could not be set low enough to distinguish the travelling waves, either leading to no identification of waves or a too short fault distance. For the shorter WS line the identification was still possible. This can be understood from inspecting currents for the two fault distances, illustrated in figure 6.23.

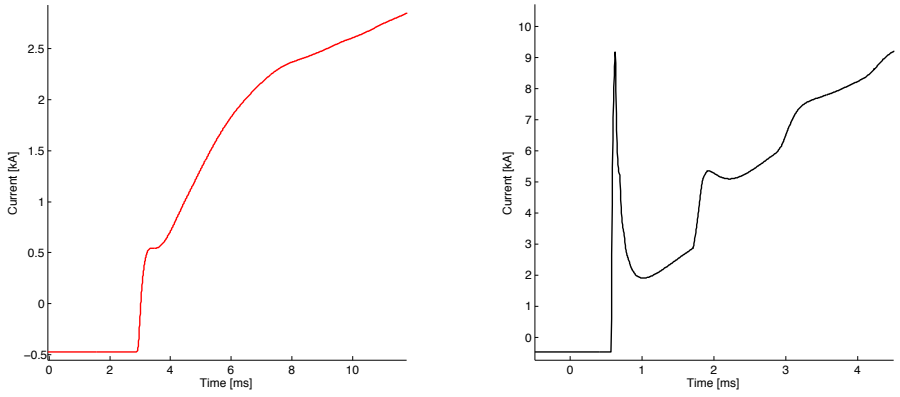

(A) Recorded in pEW (B) Recorded in pSW

FIGURE 6.23: Currents with fault impedance of 16 ohm and high fault distances. Distance is A) 495 km and B) 95 km

6.5 Other transient causes

There are other disturbances in a DC system which may cause transients that could be detectable by a protection system. In this section, converter W is tripped,

meaning all the IGBTs are blocked. Secondly, operating point of the different converters is changed as well by a factor of 1.6.

6.5.1 Tripping converters

Converter W was tripped, causing disturbances in current and voltages, illustrated in figure 6.24. Tripping the converter means it will function as an uncontrolled diode rectifier bridge, resulting in decreased voltage. Even though the system becomes inoperable, neither current nor voltage approach a level which is dangerous to equipment in the DC system. Therefore, the DC breakers should not be triggered by this event. Rather, breakers in the AC system should be opened in order to isolate the faulted converter.

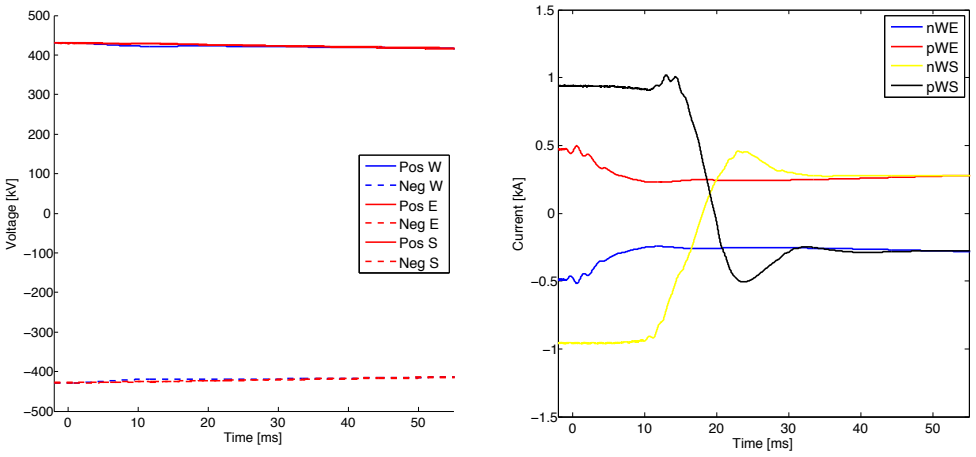

(A) System voltages

(B) Currents

FIGURE 6.24: Voltage and current recordings after tripping converter W

Looking at the recorded wavelets and current derivatives, it is clear that the obtained levels are far below those observed during short-circuit faults. This is illustrated in figure 6.25.

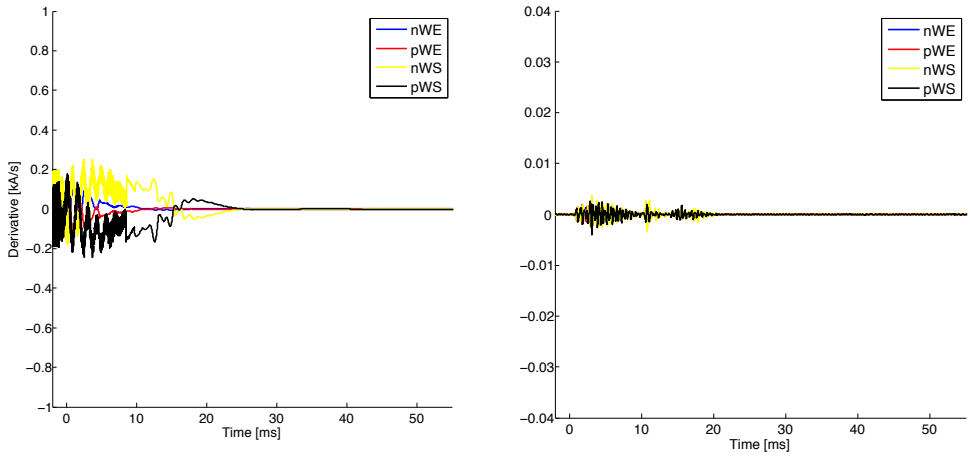

(A) Current derivatives

(B) Wavelets

FIGURE 6.25: Derivatives and wavelets recorded after tripping converter W

6.5.2 Changing operating point

The system operating point was varied in two different ways. First by changing voltage reference at converter W. Second by changing power reference at converter E. The resulting currents and voltages are illustrated in figures 6.26 and 6.27.

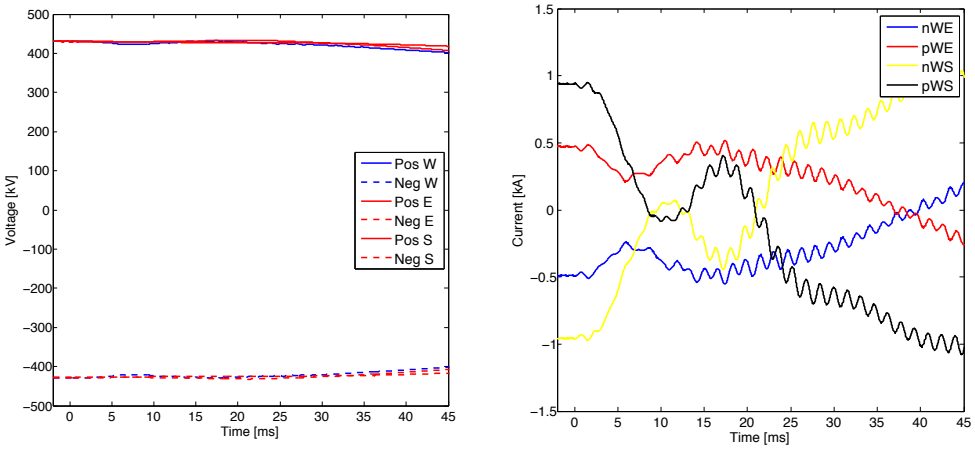

(A) Voltages

(B) Currents

FIGURE 6.26: Voltages and currents following change in voltage reference at converter W

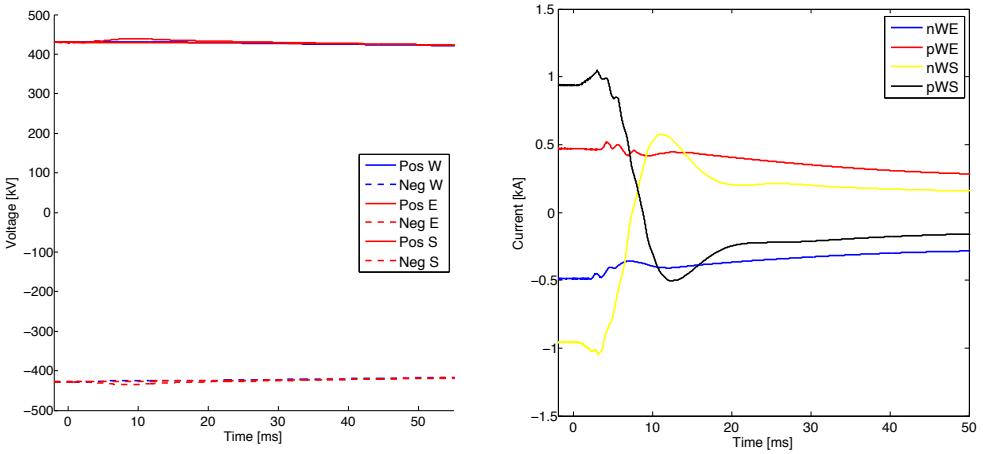

(A) Voltages

(B) Currents

FIGURE 6.27: Voltages and currents recorded after a change in power reference at converter S

In this case, the control system acts too slowly to cause any abrupt changes in currents or voltage, resulting in no high frequency transients on the line.

6.6 Summary and discussion of results

In these simulations, the pole-to-pole fault was applied with both poles also being faulted to ground with equal fault impedances. if only one pole was connected to ground, the resulting currents and voltages would be expected to be less symmetrical. However, this should have little impact on the evaluation of the protection methods.

6.6.1 Currents and voltages

The observed currents and voltages corresponded with earlier simulations performed by others and which were presented in chapter 3. Magnitude of the fault current primarily depended on fault path impedance and converter capacitance.

Fast Fourier Transformation revealed frequencies in the current ranging from 0 Hz up to 1 kHz for short distance faults, and up to 300 Hz for long distances. Fault currents in the healthy part of the grid was found to contain far fewer high frequency components. Size of the converter capacitors had a surprisingly low effect on the frequency content. Referring to the natural frequency of an RLC circuit, it was expected that the frequency would increase by a factor of $\sqrt{10} = 3.16$ when comparing base case with the lowest capacitance. The absence of such increase could indicate that the higher frequencies observed are due to the travelling waves, and not the natural response of an RLC circuit. The observed frequencies were well below the Nyquist frequency of 100 kHz, indicating that no information was lost.

Looking at the current, the system seems to be underdamped for all fault impedances when fault distance is 5 km. This is in stark contrast to the damping ratios calculated for these faults. However, the voltage recorded under the same conditions reveal that the system is in fact overdamped for all resistances except 0.01 Ω. The deviation from expected results is due to the build up of current resulting from reflection of waves at the converter. As was explained in 3.1.4, voltage and current behave differently when being reflected by a negative reflection coefficient. A possible reason the system appear to be underdamped for low resistance faults, is the fact that there is a current going through the line prior to fault. This means

there is energy stored in the system inductance, which need to be dissipated before a steady state is reached. Reduction of converter capacitance increase the underdamped behaviour of both voltage and current, as was expected.

Diode currents were recorded for short and long distance faults. Once the converter is discharged, current in the diodes reach damaging levels many times their rated current almost immediately. Discharge time depends on capacitor size and fault path impedance, as has been noted before, varying between 0.34 ms for the smallest capacitor up to 1.53 ms for the largest. These currents can be very damaging to the diodes, and should preferably be avoided. Compared to the reported operating times for the DC breaker in section 2.6 this is not possible for these discharge times, meaning some sort of current limiter, as presented in 2.7, must be installed.

6.6.2 Wavelet protection

The recorded current wavelets proved a very reliable means of detecting the high frequency transients. Increasing fault path impedance, either by increasing fault distance or fault impedance, produced lower magnitude wavelets as both current magnitude and frequency content was reduced. The polarity of the wavelets depended on fault direction, but numerous oscillations with varying magnitude makes it difficult to determine polarity quickly.

There was a time delay of around 1 ms from the transient arrived at the breaker until a difference in the wavelet could be detected. Another millisecond passed before the wavelet reached its peak value. Length of the time delay depends on sampling rate, choice of mother wavelet and the desired number of coefficient levels computed. Six levels were computed in these simulations. For faults 495 km away from the breaker, the sixth level coefficients produced oscillations with the highest magnitude, while the fifth level magnitudes were marginally higher for fault distance of 95 km. Lower level coefficients were only marginal for either fault distance. This is again related to frequency content of the fault current, as the higher level coefficients represent lower frequency content. For shorter lines it may therefore be unnecessary to compute all six levels, which would reduce the time delay.

Wavelets recorded on the faulted line were very similar to the Daubechies mother wavelet, while those recorded in the healthy line close to converter W appeared

more distorted. Magnitude of the oscillations were also significantly lower. This is caused by the different nature of the fault currents, as the fault current in a breaker at converter W on the healthy line is caused by discharge of cable capacitance rather than converter capacitance.

Reducing the converter capacitances increased magnitude of the wavelet coefficients, both in the faulted and healthy pole, indicating that the smaller capacitance produce more current components in the frequency range detected by the wavelets. Different VSC technologies were presented in 2.4, and the MMC was reported to have improved operational characteristics compared to the VSC used in these simulations. If the MMC is implemented, it will also have a much smaller effective capacitance as its distributed capacitors are connected in series. Also, the distributed capacitance will not be discharged in the same way as a concentrated capacitor, and may not produce an equivalent transient wave the wavelets can so easily detect.

6.6.3 Derivative protection

The recorded current derivatives increased rapidly to a very large magnitude for short distance faults. The magnitude decreased with an increasing fault distance.

For most fault locations, polarity of the initial derivative peak was a reliable means of determining fault direction. Derivatives following faults at locations WS1 or WS2 would show a negative spike at the converter on the far end of the faulted line. This spike was not affected by decreasing capacitance, and changes caused by increasing fault impedance was most likely related to the general reduction in magnitude caused by decreased currents. It is possible that this was caused by the PSCAD component used to compute the derivative, as the fault current showed no sign of a corresponding decrease.

Reduction of converter capacitance had very little influence on the derivatives recorded on the faulted line. For recording in the healthy line, the increased spread of fault current caused a significantly larger negative peak. With capacitances of 315.74 and 63.14 μF, a small positive value was observed for faults behind the breakers, following a few milliseconds after the initial negative peak.

6.6.4 Travelling wave protection

The travelling wave protection relies on the initial and first subsequent transient waves. These must be distinguished from other variation in the current. For low fault impedances this is possible to accomplish by measuring the derivative. For large fault distances and with a high fault impedance, the transient wave arrivals are indistinguishable from other variations. This indicate that there is a maximum distance for which the travelling wave protection method is applicable. In these simulations, it should be possible to protect line WS with travelling waves. Detection time for the fault will of course also increase with the line distance.

The wave speed calculated before the simulations was based on the assumption of loss less conductor and sheaths. With the recorded arrival times, fault distance was correctly calculated within a few hundred meters. Seeing how the error margin was 842 meters, the assumption was valid.

6.6.5 Effect of other faults

Both the computed wavelets and the derivatives showed only marginal impact following tripping of the converters or change in either voltage or power references.

Chapter 7

Proposed detection method

Based on the results, it seems a possible solution could be to determine direction of the fault using current derivative, and then the absolute value of the wavelet transform to determine if the fault has occurred within a given breakers protection zone. Such a solution was implemented in MATLAB, and is discussed below.

7.1 Description of method

Determining fault direction will be done by checking whether the current derivative exceeds a given threshold. In order to see if the fault is within the protection zone of the given breaker, absolute magnitude of the wavelets is checked against a separate threshold.

As mentioned in the results, the derivative could change polarity less than a millisecond after the initial transient arrival. To account for this, the derivative is checked against both a negative and positive threshold. Exceeding the negative threshold causes the system to ignore any following wavelet values which may reach the given threshold.

As was explained in the previous chapter, the peak value of derivatives does not occur simultaneously as peaks in wavelets. Assuming the DC breakers from section 2.6 are installed, this time delay could be utilised by putting the breakers in standby mode once a fault is indicated to have occurred in front of the breaker. Interruption will then occur within microseconds once fault location has been confirmed by the wavelet transform.

The decision algorithm is illustrated in figure 7.1, and was implemented in MATLAB in order to determine whether the solution was viable, see appendix B for the code. In addition to this, the system should have two timers. The detection of a negative derivative puts the system out of action, but it should be brought back within a few milliseconds, as the positive derivative surge will have passed by then. Also, if the wavelet threshold is not exceeded within a few milliseconds following a positive derivative, the system should resume checking the derivative.

7.2 Determining thresholds

In order to determine thresholds, two values have to be taken into account. First, the lowest value registered during a fault inside the protection zone. Second, the largest value found for a fault outside the zone. In order to successfully be able to determine a threshold, it is required that the first value is large than the second value.

Both wavelet and derivatives are minimised with high impedance, meaning high fault resistance and maximum fault distance. Maximum values detected at all breakers for single-pole faults at the opposite end of their protection zone and with fault impedance of 16 Ω are given in table 7.1.

To determine the second value, faults were applied closely behind the breaker and with fault impedance 0.01 Ω. This maximum value will also depend on size of the filter capacitor. Values from a filter capacitance of 63.14μF is used at first, but increased if necessary to satisfy the above mentioned requirement.

Table 7.1: Maximum values detected for faults within protection zone with large fault path impedance

Breaker	pWE	nWE	pEW	nEW	pWS	nWS	pSW	nSW
Wavelet Max	0.22	0.22	0.22	0.22	2.13	2.13	2.14	2.0
Derivative Max	5.5	5.5	5.5	5.5	399.5	399.5	399.5	399.5

Unfortunately, wavelets recorded at breakers in stations E and S were larger for the low impedance faults outside their protection zones than during high impedance faults inside their zones. This means it will not be possible to determine a wavelet threshold with the given capacitance. By changing the filter capacitance to 315.82

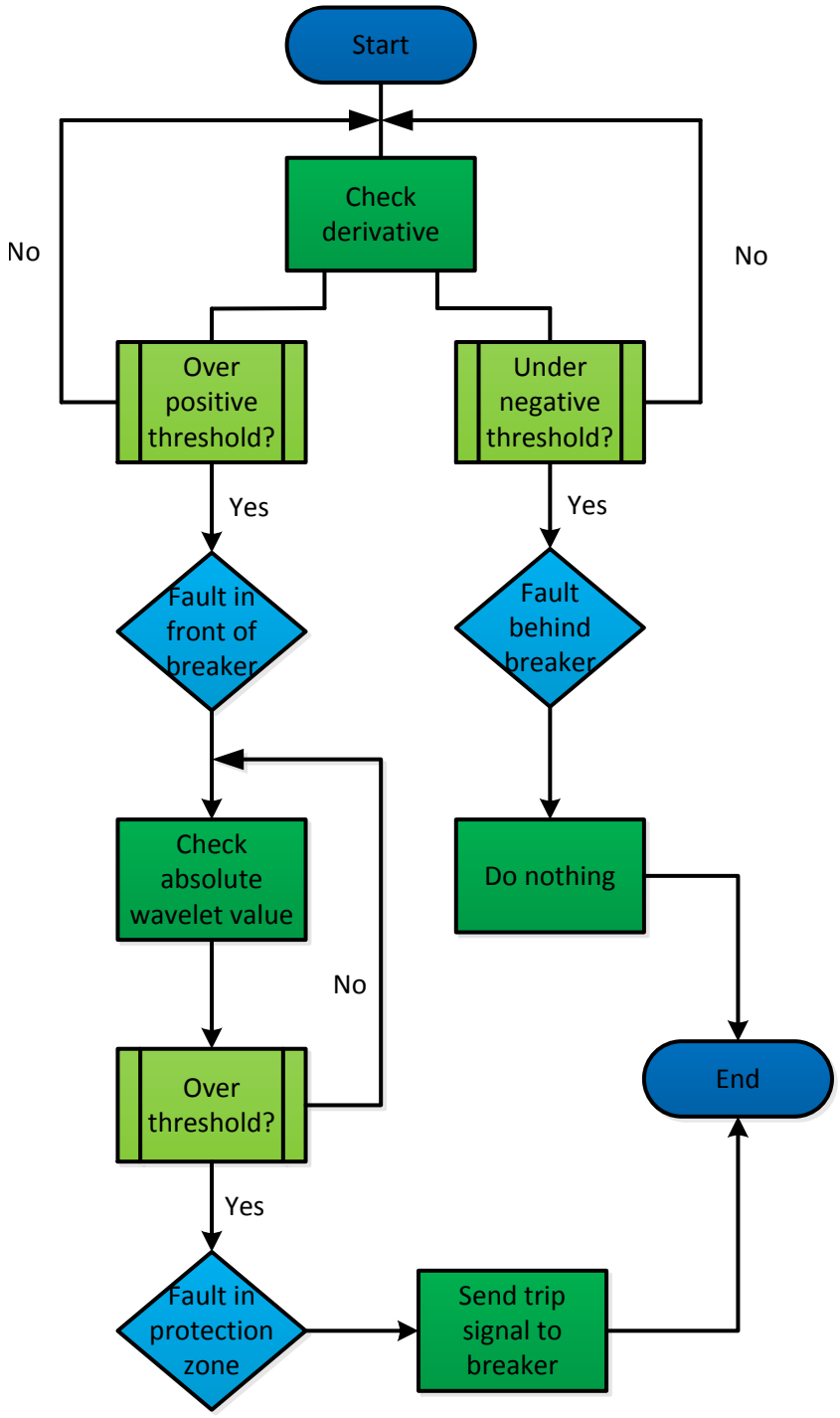

FIGURE 7.1: Decision algorithm for fault detection based on wavelet and derivative measurements

Table 7.2: Maximum wavelet and derivative values detected for faults outside protection zone

Breaker	pWE	nWE	pEw	nEW	pWS	nWS	pSW	nSW
Wavelet Threshold	0.85	0.85	0.12	0.12	1.19	1.19	1.19	1.19
Derivative Max	15	15	14	14	13	13	55	55

μF, the values in table 7.2 were obtained. The derivative values listed in this table is of lesser importance, as they are preceded by a negative surge whenever the fault occurs behind the breaker, which will cause the system to ignore any following measurements.

Due to the negative spike in the derivative recorded on the WS line, breakers connected to this line has to be given larger thresholds than those on the WE line. During low impedance fault, this spike reached a value of -60 kA/s, which has to be taken into account when determining thresholds. Since the spike was not detected for a fault distance of 100 km on the WE line, it is assumed that the spike will not appear here.

Based on these considerations, thresholds were determined for each breaker and listed in table 7.3. As can be seen from the code in appendix B, the derivative threshold for determining a fault behind the breaker is the same as for determining a fault in front of it, only with opposite polarity. For implementation in a simple system as the one used in these simulations, the derivative thresholds at converters E and S are in reality irrelevant, as faults can only occur in a single direction. However, the for the sake of testing the proposed method, the derivative threshold has been set to the same as for the breakers on the opposite end of either line.

Table 7.3: Derivative and wavelet thresholds for each of the breakers

Breaker	pWE	nWE	pWE	nWE	pWS	nWS	pSW	nSW
Wavelet Threshold	0.20	0.20	0.20	0.20	2.00	2.00	2.00	1.90
Derivative Threshold	5.30	5.30	5.30	5.30	70.0	70.0	70.0	70.0

7.3 Implementation and results

The MATLAB code was then used with the listed thresholds and converter capacitance set to 631.36 μF. All fault types and locations were tested, with fault impedance ranging from 0.01 Ω to 16 Ω. The recorded times from detection of first transient until opening of breakers are listed in tables in appendix C.3. The decision times range from 1.210 ms for low impedance faults occurring close to the breaker, and up to 2.345 ms for high impedance faults far away from the breaker. Current levels in the breaker reached up to ... for close low impedance faults. The proposed solution correctly located faults for all the tested scenarios.

7.4 Discussion of method

The decision to send final trip signal to the breakers was made before the converter diodes entered their freewheeling phase, based on comparison with the diode currents recorded for the large capacitor. For short distance, low impedance faults, detection was made in less time than the reported action time of DC breakers described in section 2.6. Long distance high impedance faults were detected slower, but their magnitude is also significantly lower, meaning components can sustain them for a longer period of time.

Since it was not possible to determine wavelet thresholds for a system with a converter capacitance of 62.14 μF, this method is clearly not applicable to all VSC based systems. Of the different converter technologies presented in section 2.4, the two-level VSC used in these simulations is the technology with the highest capacitance, as the other options use series connected capacitors. Also, the detection times were longer than the discharge time of smaller capacitors.

Since the system is turned off for a few milliseconds by a fault occurring behind the breaker, it becomes vulnerable to subsequent faults which may occur in front of the breaker as a consequence of the initial fault.

Chapter 8

Conclusions

In this thesis work, fault detection and localisation in VSC based MTDC networks has been investigated. Different proposed methods have been evaluated, and some of them were implemented in PSCAD and tested under various fault conditions.

System fault currents and voltages were investigated to determine time limits for which a protection system would have to locate a fault. Large fault currents were recorded as the converter capacitors were discharged. In order to avoid fault currents in converter diodes, current should be interrupted between 0.34 ms in systems with small converter capacitors, and 1.53 ms in system with large capacitors. Once the diodes became conducting, the fault immediately rose to damaging level. This is not possible to interrupt in time with current HVDC breaker technology, which has a reported action time of 2 ms, meaning current limiters must be installed. Variations in converter capacitances and fault impedance resulted in fault currents similar to what has been found in earlier work on the subject.

The three protection methods chosen for implementation were current derivative protection, current wavelet protection and travelling wave protection.

Derivative protection proved reliable at detecting the initial fault transient, and fault direction. It was not possible to distinguish high impedance faults within the protection zone from low impedance faults outside the zone.

Wavelet protection was implemented with fourth order Daubechies chosen as mother wavelet. Wavelet magnitude depends on both converter capacitor size and fault impedance. There was a significant magnitude difference for wavelets observed in faulted and healthy lines. A low converter capacitance reduced this

difference. There was also a significant time delay between arrival of the first transient wave and rise in wavelet magnitude. Shape and polarity of the wavelets depended on direction of fault, but determining polarity is complicated due to the numerous oscillations with varying magnitudes.

Travelling wave protection relies on successfully detecting the first two transients arriving at the converter and being reflected at the fault point. This was possible for a fault distance of 95 km, using the current derivative for detecting transients. This indicates that the travelling wave method could be a viable option for short distance lines. Localisation time depends on fault distance, and is equal to time the fault wave needs to travel from the breaker, to the fault and back again.

Of these methods, neither could be used for locating all faults within an acceptable time by itself. Using current derivative for determining fault direction and the magnitude of wavelet coefficients for determining distance, faults were successfully located in a high capacitance, radial three converter HVDC grid. In combination with IGBT based DC breakers capable of entering standby-mode on first detection of a fault transient, interruption could be achieved within 2.345 ms for all faults, independent of fault location and resistance, with lower times for close, low impedance faults.

While the combination of current derivative and wavelet protection proved successful in this simple system, it does in not mean the issue of locating faults in and MTDC system is solved. However, it does indicate that these methods are promising and should be considered in further work on the subject.

Chapter 9

Further work

In this thesis, three proposed methods for detecting faults in an MTDC system has been simulated in a simple, radial three converter system using PSCAD, which utilise one of the most accurate cable models currently available. The converters implemented in the simulations have been basic two-level VSCs with large DC capacitors.

It was determined that current limiters must be installed if the diodes are not to be exposed to damaging currents. Some examples of such technology was presented, but further work is needed in order to determine how these can be implmented in an effective manner.

Since there are more advanced converter designs available which have proven more favourable operational characteristics, it is highly recommended to implement these and redo the tests. The MMC is of special interest, not only because it is generally regarded as a superior converter design, but also because the results obtained here indicate that the MMC will cause quite different operational performance by the implemented protection systems.

One of the major challenges with fault detection and localisation in MTDC systems is the complexity of the grid. The radial grid used here is the simplest option available, and increasing complexity will make fault localisation more difficult.

Several different protection methods have been presented in this thesis in addition to those which were implemented. Artificial Neural Networks (ANN) seem promising, but as it is fairly complex it was determined too time-consuming to include

in this thesis work. However, the idea has some merit and should be considered for implementation and testing.

Results from computer simulations differ from those obtained in the real world, especially due to the lack of imperfections and noise. Testing the effect of DC faults and the performance of different protection systems in a laboratory setup is difficult, but absolutely necessary if these systems are to see real life implementation.

Appendix A

PSCAD models

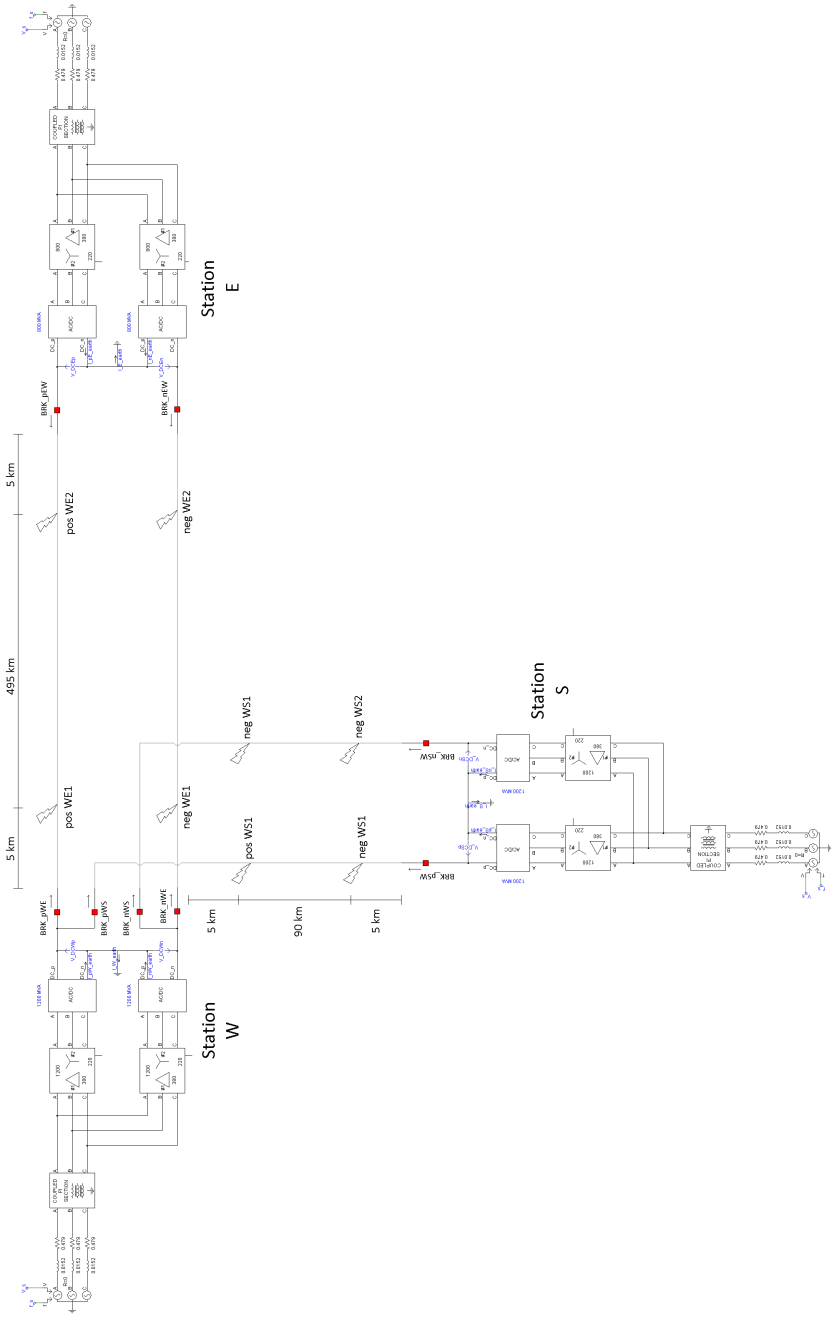

FIGURE A.1: The MTDC system implemented in PSCAD with all measurement and fault points indicated

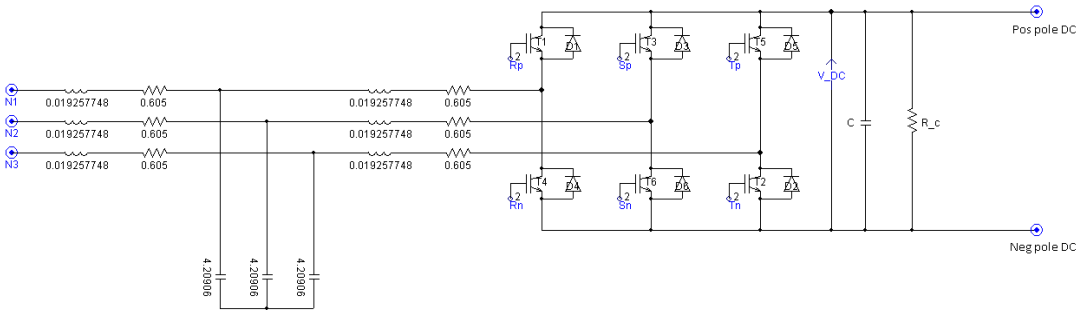

FIGURE A.2: The VSC model implemented in PSCAD with all measurement points indicated

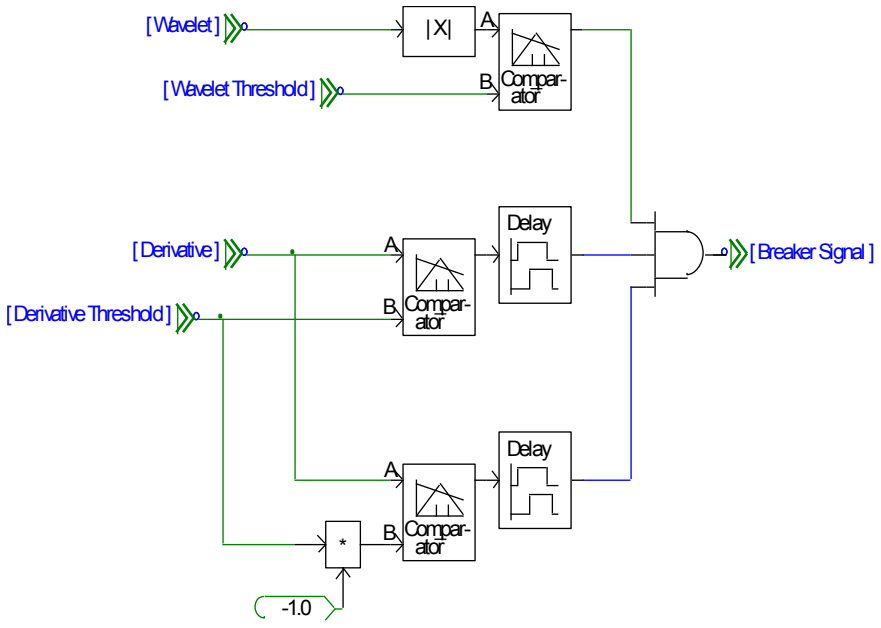

FIGURE A.3: Proposed detection method implemented in PSCAD

Appendix B

MATLAB code

Code for doing FFT analysis to determine frequency content of a signal

```
%% Inputs: table with recordings and time stamps, and column number of
%% recording to be analysed

function FFT_analysis(Table, i)
    Matrix=table2array(Table);  %% Convert into a matrix
    L=length(Matrix)-1;         %% -1 because table2array
                                %% inserts NaN at bottom of Matrix
    Mag=(Matrix(1:L,i));
    fs=1/(Matrix(2,1)-Matrix(1,1)); %% Time stamps are in the first column
    hold all
    NFFT = 2^nextpow2(L); %% Takes the next power of two after L
    FFT=fft(Mag, NFFT)/L; %% The FFT command in MATLAB
    f=fs/2*linspace(0,1,NFFT/2+1);
    stem(f,2*abs(FFT(1:NFFT/2+1))) %% Plots the results
end

```

Code for finding faults using wavelets and derivatives:

```
%% Input: Tables with recorded derivatives and wavelets,
%% column numbers specifying which breaker is being controlled
%% and thresholds for wavelet and derivative respectively
%% Output: Time in milliseconds from detection of first
%% transient until fault is detected
function Time = FindFault(WavTab,DerTab,WavCol,DerCol,WavThres,DerThres)
%% Make tables to matrixes:
%% Mat1 contains wavelets, Mat2 derivatives
    Mat1 = abs(table2array(WavTab));
    Mat2 = table2array(DerTab);
    Found = 0;
    Pos = 0;
    i = 1;
    Time = 0;
    Neg = 0;
%% The loop stops if a fault is found inside the protection zone
%% or if it is determined that a fault has occurred behind the breaker
while i < length(Mat1) && i < length(Mat2) && ~Found && ~Neg
%% Check derivative to determine a fault in front of the breaker
        if Mat2(i,DerCol) >= DerThres && ~Pos && ~Neg
            Pos = 1;
            Time1 = Mat2(i,1);
        end
%% Once a fault has been determined in front of the breaker
%% the wavelet is checked against the given threshold
        if Mat2(i,DerCol) < -DerThres && ~Neg && ~Pos
            Neg = 1;
        end
%% Determine if the fault is behind breaker
        if Mat1(i,WavCol) >= WavThres && Pos && ~Neg
            Time2 = Mat1(i,1);
            Time = (Time2 - Time1)*1000; %% Scaled to ms
            Found = 1;
        end
    i = i + 1;
    end
end
```

Code for finding arrival times of the transients:

```
function Ans = ArrTimes(Table, Col)
%Table is table with current vectors

Matrix = table2array(Table);
Count = 0;
Ans = zeros(1,2);
i = 3;
check = false;
DerTemp = 0;
Ts = 5e-6;

while Count < 2 && i < length(Matrix)
    Der = Matrix(i,Col) - Matrix(i-2,Col); %% Taking the derivative
    if Der/Ts > 150 && ~check
        check = true;               %% Detecting the initial transient
        Ans(1) = Matrix(i-1, 1);
        Count = Count + 1;
    end

    if Der/Ts > DerTemp && check    %% Increase in derivative is taken as
        Ans(2) = Matrix(i-1,1);     %% indication of new transient
        Count = Count + 1;
    end
    DerTemp = Der/Ts;
    i = i+1;
end
if Count < 2
    Ans(2) = Matrix(i-1,1);
end
end
```

Code for finding fault distance, using the previous function:

```
function Dist = FindDist(Table, Col)
%% Table is a table with current vectors
epsR = 3.17;    %% Cable insulation permittivity, used to determine wave velocity
c = 3e5; %% Speed of light in km/s
v = c/sqrt(epsR);
Times = ArrTimes(Table, Col); %% Previous function used to find arrival times

if Times(2) > Times(1)
    TravTime = (Times(2) - Times(1))/2;
    Dist = TravTime*v;
else
    Dist = 1e8;
end
end
```

Appendix C

Tables

C.1 Peak values for wavelets with different fault positions

Table C.1: Wavelet peaks for positive pole faults

	Fault location			
Relay	pos WE1	pos WE2	pos WS1	pos WS2
pWE	-8.0565	0.3140	-0.9893	0.2599
nWE	-0.0423	-0.0163	-0.0423	-0.0405
pWS	-0.9685	0.0305	8.3540	-2.9630
nWS	0.0413	0.0486	-0.0411	-0.0395
pEW	0.2845	-8.0539	0.1069	0.0095
nEW	0.0045	0.0032	-0.0045	0.0052
pSW	1.1687	-0.0332	-2.9477	8.4512
nSW	0.0467	-0.0508	0.0437	0.0442

Table C.2: Wavelet peaks for negative pole faults

	Fault location			
Relay	neg WE1	neg WE2	neg WS1	neg WS2
pWE	0.0422	0.0163	0.0422	0.0405
nWE	8.0564	-0.3139	0.9892	-0.2598
pWS	-0.0413	-0.0485	0.0411	0.0394
nWS	0.9685	-0.0305	-8.3539	2.9630
pEW	-0.0045	-0.0031	0.0045	-0.0051
nEW	-0.2844	8.0538	-0.1068	-0.0094
pSW	-0.0466	0.0508	-0.0436	-0.0442
nSW	-1.1686	0.0331	2.9476	-8.4512

Table C.3: Wavelet peaks for pole-to-pole faults

	Fault location			
Relay	ptpWE1	ptp WE2	ptp WS1	ptp WS2
pWE	17.8804	0.4617	-1.5708	0.4873
nWE	-17.8804	-0.4617	1.5708	-0.4873
pWS	-1.5754	-0.0405	18.2096	-4.0837
nWS	1.5754	0.0405	-18.2096	4.0837
pEW	0.4377	18.2126	0.2295	-0.0202
nEW	-0.4377	-18.2126	-0.2295	0.0202
pSW	1.9768	-0.0330	-4.0516	18.6641
nSW	-1.9768	0.0330	4.0516	-18.6641

C.2 Determining thresholds, proposed method

Table C.4: Minimum and maximum values for derivatives, positive pole faults

Breaker	Fault location							
	Pos WE1		Pos WE2		Pos WS1		Pos WS2	
	Max	Min	Max	Min	Max	Min	Max	Min
pWE	12 026.5	-48.3	8.5	-1.4	4.5	-174.8	2.4	-19.6
nWE	1.4	-1.6	2.2	-1.3	1.4	-1.6	1.4	-1.3
pWS	9.3	-351.9	2.0	-4.0	5 785.1	-72.3	590.6	-182.3
nWS	2.1	-1.4	2.3	-1.4	2.6	-1.4	2.2	-1.9
pEW	8.6	-1.3	11 948.9	-58.5	7.1	-1.2	3.3	-1.0
nEW	0.6	-1.4	0.7	-0.8	0.6	-0.9	0.7	-0.0008
pSW	34.0	-8.1	4.3	-1.8	589.6	-183.4	5 764.7	-75.9
nSW	1.5	-4.6	1.8	-2.5	1.6	-5.1	1.8	-2.6

Table C.5: Minimum and maximum values for derivatives, negative pole faults

Breaker	Fault location							
	Neg WE1		Neg WE2		Neg WS1		Neg WS2	
	Max	Min	Max	Min	Max	Min	Max	Min
pWE	1.6	-1.4	1.3	-2.2	1.6	-1.4	1.3	-1.4
nWE	48.3	-12 026.5	1.4	-8.5	174.8	-4.5	19.6	-2.4
pWS	1.4	-2.0	1.4	-2.2	1.4	-2.6	1.9	-2.2
nWS	351.9	-9.3	4.0	-2.0	72.3	-5 785.1	182.2	-590.6
pEW	1.1	-0.6	0.8	-0.7	0.9	-0.6	0.8	-0.7
nEW	1.3	-8.6	58.5	-11 949.0	1.2	-7.0	1.0	-3.3
pSW	4.5	-1.5	2.5	-1.8	5.1	-1.6	2.5	-1.8
nSW	8.1	-34.0	1.8	-4.3	183.4	-589.6	75.9	-5 764.7

Table C.6: Minimum and maximum values for derivatives, pole-to-pole faults

Breaker	Fault location							
	PtP WE1		PtP WE2		PtP WS1		PtP WS2	
	Max	Min	Max	Min	Max	Min	Max	Min
pWE	17 961.1	-153.8	13.7	-1.4	9.1	-258.6	3.0	-29.0
nWE	153.8	-17 961.1	1.4	-13.7	258.6	-9.1	29.0	-3.0
pWS	19.6	-525.7	2.0	-4.7	8 549.7	-162.2	870.4	-107.6
nWS	525.7	-19.6	4.7	-2.0	162.2	-8 549.7	107.6	-870.4
pEW	13.9	-2.2	17 845.6	-185.0	12.0	-2.8	4.6	-1.2
nEW	2.2	-13.9	184.9	-17 845.6	2.8	-12.0	1.2	-4.6
pSW	62.6	-17.7	5.7	-1.5	869.9	-109.2	8 519.7	-194.4
nSW	17.7	-62.6	1.5	-5.7	109.2	-869.9	194.4	-8 519.7

C.3 Detection times, proposed solution

Table C.7: Times in milliseconds from first fault transient until trip signal, fault impedance 0.01 ohm

Fault	Breaker							
	pWE	pEW	pWS	pSW	nWE	nEW	nWS	nSW
Pos WE1	1.210	2.175	-	-	-	-	-	-
Pos WE2	2.175	1.210	-	-	-	-	-	-
Pos WS1	-	-	1.555	1.975	-	-	-	-
Pos WS2	-	-	1.975	1.555	-	-	-	-
Neg WE1	-	-	-	-	1.210	2.175	-	-
Neg WE2	-	-	-	-	2.175	1.210	-	-
Neg WS1	-	-	-	-	-	-	1.550	1.975
Neg WS2	-	-	-	-	-	-	1.970	1.555
PtP WE1	1.210	2.175	-	-	1.210	2.170	-	-
PtP WE2	2.175	1.210	-	-	2.175	1.210	-	-
PtP WS1	-	-	1.555	1.975	-	-	1.550	1.970
PtP WS2	-	-	1.975	1.555	-	-	1.970	1.555

Table C.8: Times in milliseconds from first fault transient until trip signal, fault impedance 2 ohm

Fault	Breaker							
	pWE	pEW	pWS	pSW	nWE	nEW	nWS	nSW
Pos WE1	1.240	2.160	-	-	-	-	-	-
Pos WE2	2.160	1.240	-	-	-	-	-	-
Pos WS1	-	-	1.585	2.170	-	-	-	-
Pos WS2	-	-	2.170	1.585	-	-	-	-
Neg WE1	-	-	-	-	1.240	2.160	-	-
Neg WE2	-	-	-	-	2.160	1.240	-	-
Neg WS1	-	-	-	-	-	-	1.575	2.170
Neg WS2	-	-	-	-	-	-	2.170	1.585
PtP WE1	1.220	2.165	-	-	1.220	2.165	-	-
PtP WE2	2.165	1.220	-	-	2.165	1.220	-	-
PtP WS1	-	-	1.565	2.000	-	-	1.560	2.000
PtP WS2	-	-	2.000	1.565	-	-	1.995	1.565

Table C.9: Times in milliseconds from first fault transient until trip signal, fault impedance 4 ohm

Fault	Breaker							
	pWE	pEW	pWS	pSW	nWE	nEW	nWS	nSW
Pos WE1	1.270	2.160	-	-	-	-	-	-
Pos WE2	2.160	1.270	-	-	-	-	-	-
Pos WS1	-	-	1.585	2.170	-	-	-	-
Pos WS2	-	-	2.315	1.795	-	-	-	-
Neg WE1	-	-	-	-	1.270	2.160	-	-
Neg WE2	-	-	-	-	2.160	1.270	-	-
Neg WS1	-	-	-	-	-	-	1.790	2.315
Neg WS2	-	-	-	-	-	-	2.315	1.795
PtP WE1	1.230	2.160	-	-	1.230	2.160	-	-
PtP WE2	2.160	1.230	-	-	2.160	1.230	-	-
PtP WS1	-	-	1.575	2.165	-	-	1.565	2.165
PtP WS2	-	-	2.165	1.575	-	-	2.160	1.575

Table C.10: Times in milliseconds from first fault transient until trip signal, fault impedance 8 ohm

Fault	Breaker							
	pWE	pEW	pWS	pSW	nWE	nEW	nWS	nSW
Pos WE1	1.415	2.175	-	-	-	-	-	-
Pos WE2	2.175	1.415	-	-	-	-	-	-
Pos WS1	-	-	1.815	2.320	-	-	-	-
Pos WS2	-	-	2.320	1.815	-	-	-	-
Neg WE1	-	-	-	-	1.420	2.180	-	-
Neg WE2	-	-	-	-	2.180	1.420	-	-
Neg WS1	-	-	-	-	-	-	1.810	2.330
Neg WS2	-	-	-	-	-	-	2.350	1.815
PtP WE1	1.250	2.155	-	-	1.250	2.155	-	-
PtP WE2	2.160	1.250	-	-	2.160	1.250	-	-
PtP WS1	-	-	1.595	2.315	-	-	1.585	2.315
PtP WS2	-	-	2.315	1.595	-	-	2.180	1.595

Table C.11: Times in milliseconds from first fault transient until trip signal, fault impedance 16 ohm

Fault	Breaker							
	pWE	pEW	pWS	pSW	nWE	nEW	nWS	nSW
Pos WE1	1.440	2.340	-	-	-	-	-	-
Pos WE2	2.345	1.440	-	-	-	-	-	-
Pos WS1	-	-	1.850	2.510	-	-	-	-
Pos WS2	-	-	2.510	1.850	-	-	-	-
Neg WE1	-	-	-	-	1.440	2.340	-	-
Neg WE2	-	-	-	-	2.345	1.440	-	-
Neg WS1	-	-	-	-	-	-	1.810	2.330
Neg WS2	-	-	-	-	-	-	2.350	1.815
PtP WE1	1.405	2.160	-	-	1.405	2.160	-	-
PtP WE2	2.160	1.405	-	-	2.160	1.405	-	-
PtP WS1	-	-	1.800	2.315	-	-	1.800	2.315
PtP WS2	-	-	2.315	1.800	-	-	2.315	1.800

Appendix D

Plots

D.1 Currents and voltages for different fault types

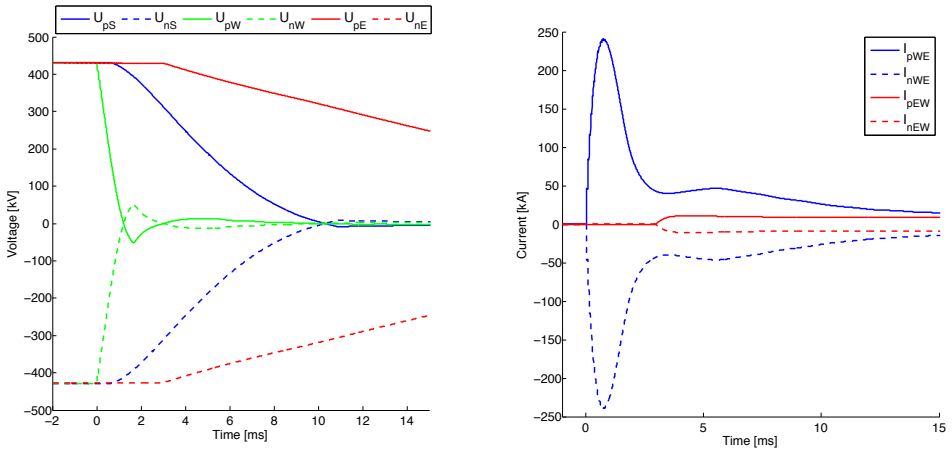

(A) Voltages (B) Currents, WE line

FIGURE D.1: Voltages and currents following pole-to-pole fault at WE1, Base case

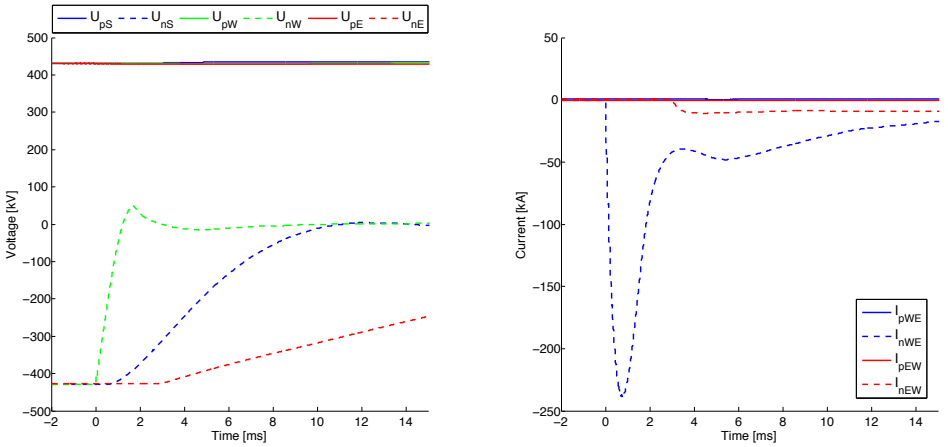

(A) Voltages (B) Currents, WE line

FIGURE D.2: Voltage and currents for fault at Neg WE1, Base case

D.2 Currents and voltages for different fault distances

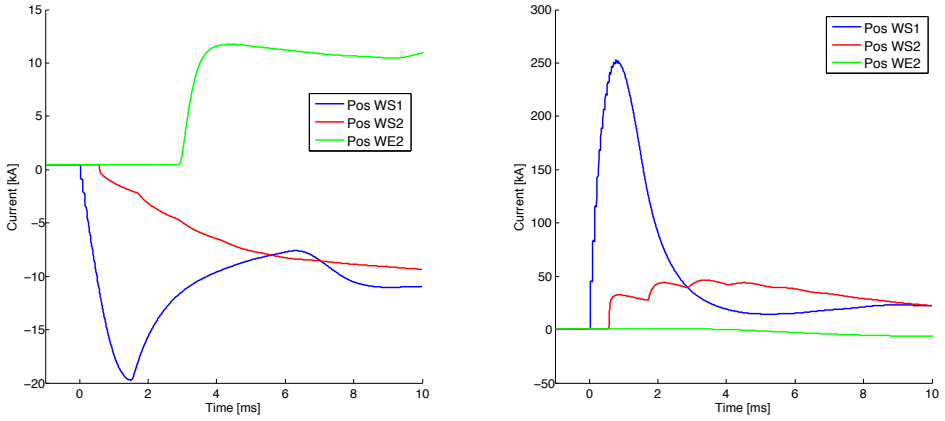

(A) Recorded in breaker pWE (B) Recorded in breaker pWS

FIGURE D.3: Currents in positive pole breakers at converter W for different fault locations

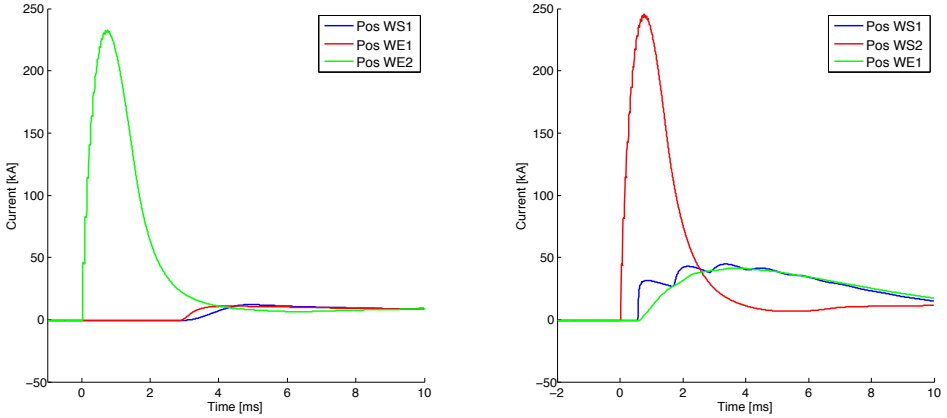

(A) Recorded in breaker pEW (B) Recorded in breaker pSW

FIGURE D.4: Currents in positive pole breakers at converters E and S for different fault locations

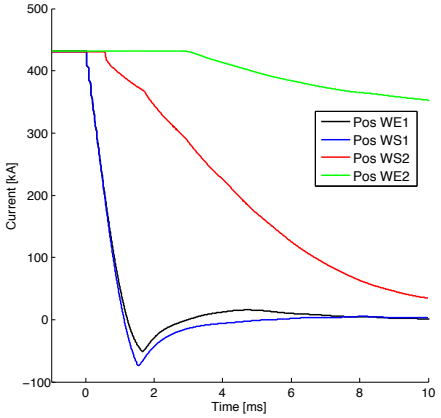

(A) Converter W

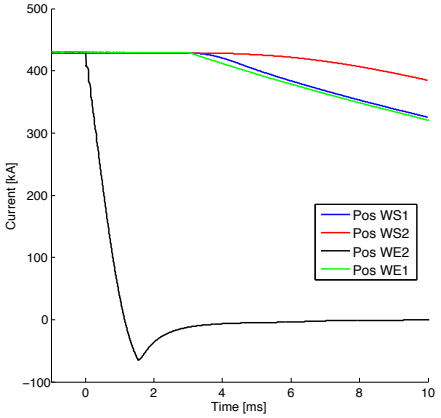

(B) Converter E

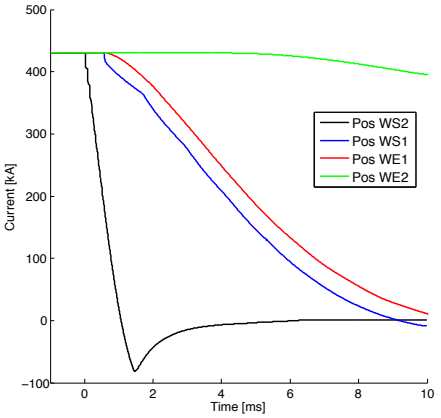

(C) Converter S

FIGURE D.5: Positive pole voltages for the three converters following faults at various locations

D.3 Wavelet plots for different fault locations

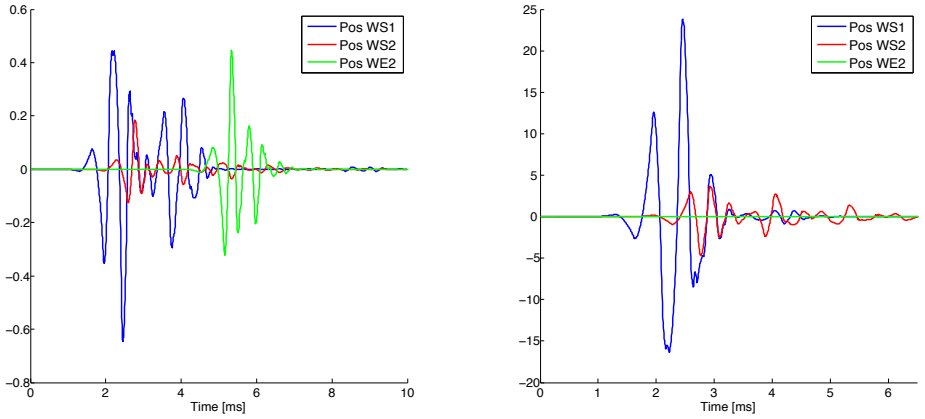

(A) Recorded in breaker pWE (B) Recorded in breaker pWS

FIGURE D.6: Wavelets recorded in positive pole breakers at converter W for different fault locations

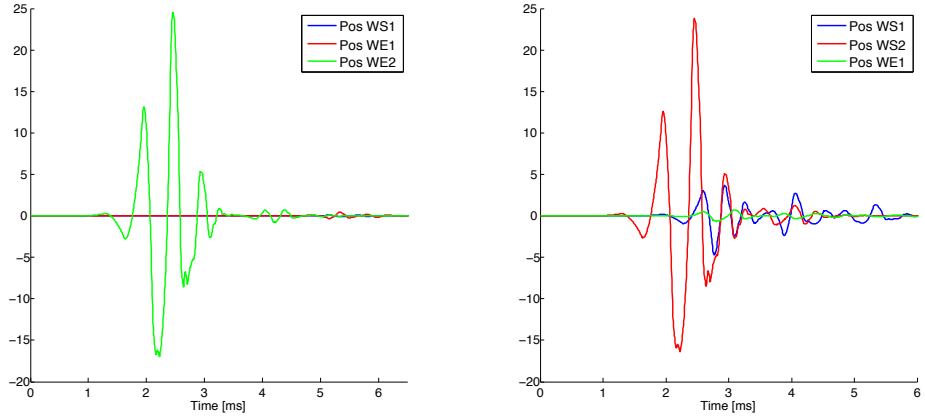

(A) Recorded in breaker pEW (B) Recorded in breaker pSW

FIGURE D.7: Wavelets recorded in positive pole breakers at converters E and S for different fault locations

D.4 Derivatives for different fault locations

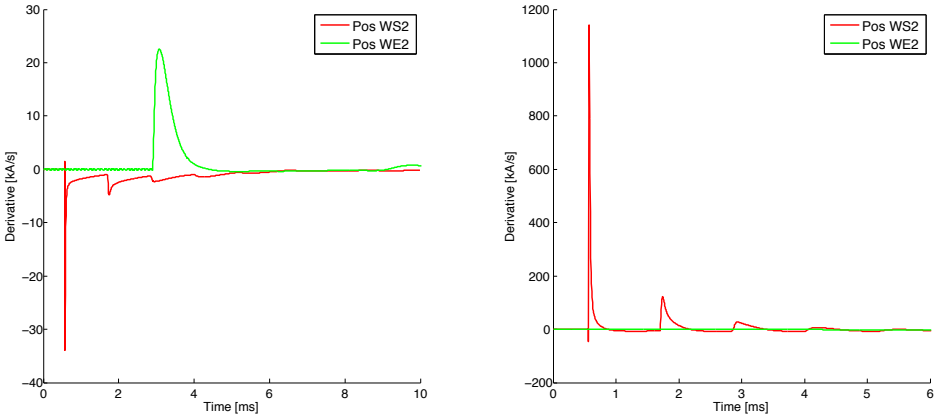

(A) Recorded in breaker pWE (B) Recorded in breaker pWS

FIGURE D.8: Derivatives recorded in positive pole breakers at converter W for different fault locations

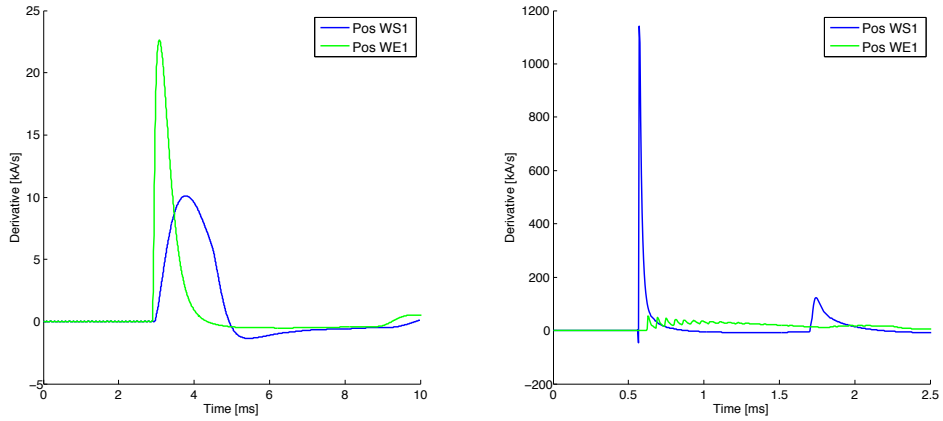

(A) Recorded in breaker pEW (B) Recorded in breaker pSW

FIGURE D.9: Derivatives recorded in positive pole breakers at converters E and S for different fault locations

Appendix E

Calculations and derivations

E.1 Equivalent resistance at converter station

Wave impedance healthy cable, Z_W, impedance converter capacitor, $Z_C = (j\omega C)^-1$

$$Z_{eq} = \frac{Z_W \times Z_C}{Z_W + Z_C} = \frac{Z_W \times (j\omega C)^-1}{Z_W + (j\omega C)^-1} \tag{E.1}$$

Multiplying both sides with $(j\omega C)$ yields

$$Z_{eq} = \frac{Z_W}{1 + j\omega C Z_W} \tag{E.2}$$

Multiplying both sides with the complex conjugate of the denominator gives the end result

$$Z_{eq} = Z_W \frac{1 + j\omega C Z_W}{1 + (\omega C Z_W)^2} \tag{E.3}$$

E.2 Damping factors

Damping factor is found by equation (3.13) which was found on page 30 and repeated below.

$$\zeta = \frac{\beta}{\omega_0} = \frac{CR^2}{4L} \tag{E.4}$$

Assuming $C \approx C_{Conv}$ the following damping factors are found for fault distance 5 km along the WE line with different fault impedances:

Fault impedance 0.01 Ω

$$\zeta = \frac{631.36\mu F \times (41.1 + 10.0[mH])^2}{4 \times 4.6nH} = 89.25 \tag{E.5}$$

Fault impedance 2 Ω

$$\zeta = \frac{631.36\mu F \times (2.041\Omega)^2}{4 \times 4.6nH} = 1.43 \times 10^5 \tag{E.6}$$

Fault impedance 4 Ω

$$\zeta = \frac{631.36\mu F \times (4.041\Omega)^2}{4 \times 4.6nH} = 5.60 \times 10^5 \tag{E.7}$$

Fault impedance 8 Ω

$$\zeta = \frac{631.36\mu F \times (8.041\Omega)^2}{4 \times 4.6nH} = 2.22 \times 10^6 \tag{E.8}$$

Fault impedance 16 Ω

$$\zeta = \frac{631.36\mu F \times (8.041\Omega)^2}{4 \times 4.6nH} = 8.83 \times 10^6 \tag{E.9}$$

Bibliography

[1] Working group B4-52. Hvdc grid feasibility study. *Cigré Tech. Rep.*, 2012.

[2] 3E, EWEA, ForWind, IEO, NTUA, Senergy, and SINTEF. Offshore electricity grid in europe, October 2011. URL `http://offshoregrid.eu/images/FinalReport/offshoregrid_fullfinalreport.pdf`.

[3] ABB. Abb québec-new england, 2013. URL `http://www.abb.com/industries/ap/db0003db004333/87f88a41a0be97afc125774b003e6109.aspx`.

[4] ABB. History of abb's hvdc expertise. URL `http://www.abb.co.uk/cawp/seitp202/7cfd9a3a7416a383c1256e8600406f4f.aspx`.

[5] D. Jovcic, D. Van Hertem, K. Linden, J.-P. Taisne, and W. Grieshaber. Feasibility of dc transmission networks. In *Innovative Smart Grid Technologies (ISGT Europe), 2011 2nd IEEE PES International Conference and Exhibition on*, pages 1–8, 2011. doi: 10.1109/ISGTEurope.2011.6162829.

[6] M. D. Pfeiffer, M. K. Bucher, and C. M. Franck. The effect of grid topology on transient fault currents in multi-terminal vsc-hvdc offshore networks. International Conference on Power Systems Transients, Vancouver, Canada, July 2013.

[7] M.P. Bahrman and B.K. Johnson. The abcs of hvdc transmission technologies. *Power and Energy Magazine, IEEE*, 5(2):32–44, 2007. ISSN 1540-7977. doi: 10.1109/MPAE.2007.329194.

[8] S. De Boeck, P. Tielens, W. Leterme, and D. Van Hertem. Configurations and earthing of hvdc grids. In *Power and Energy Society General Meeting (PES), 2013 IEEE*, pages 1–5, July 2013. doi: 10.1109/PESMG.2013.6672808.

[9] N. Flourentzou, V.G. Agelidis, and G.D. Demetriades. Vsc-based hvdc power transmission systems: An overview. *Power Electronics, IEEE Transactions on Systems, signals and devices*, 24(3):592–602, 2009. ISSN 0885-8993. doi: 10.1109/TPEL.2008.2008441.

[10] B. Jacobson, B. Westman, and M. P. Bahrman. 500 kv vsc transmission system for lines and cables. In *Cigre San Fransisco colloquium 2012, B4-6*, 2012.

[11] N. Mohan, T. M. Undeland, and W.P. Robbins. *Power Electronics*. John Wiley & Sons, 3rd edition, 2003.

[12] Lidong Zhang and Lars Dofnas. A novel method to mitigate commutation failures in hvdc systems. In *Power System Technology, 2002. Proceedings. PowerCon 2002. International Conference on*, volume 1, pages 51–56. IEEE, 2002.

[13] A. Lesnicar and R. Marquardt. An innovative modular multilevel converter topology suitable for a wide power range. In *Power Tech Conference Proceedings, 2003 IEEE Bologna*, volume 3, pages 6 pp. Vol.3–, 2003. doi: 10.1109/PTC.2003.1304403.

[14] A. Yazdani and R. Iravani. *Voltage-Sourced Converters in Power Systems*. Wiley, 1st edition, 2010.

[15] E. N. Abildgaard. Exploring the properties of a modular multilevel converter based hvdc link, June 2012.

[16] M. K Bucher and C. M. Franck. Analysis of transient fault currents in multi-terminal hvdc networks during pole-to-ground faults. In *IPST 2013, Vancouver, Canada*, pages 1–7, 2013.

[17] Fujin Deng and Zhe Chen. Design of protective inductors for hvdc transmission line within dc grid offshore wind farms. *Power Delivery, IEEE Transactions on*, 28(1):75–83, 2013. ISSN 0885-8977. doi: 10.1109/TPWRD.2012.2224384.

[18] Sajib Barua. Single-phase full-bridge vsc, April 2013. URL `http://protorit.blogspot.no/2013/04/single-phase-full-bridge-vsc.html`.

[19] Acha E., V. G. Agelidis, O. Anaya-Lara, and T. J. E. Miller. *Power Electronic Control in Power Systems*. Newnes, 2002.

[20] D. Schmitt, Y. Wang, T. Weyh, and R. Marquardt. Dc-side fault current management in extended multiterminal-hvdc-grids. In *Systems, Signals and Devices (SSD), 2012 9th International Multi-Conference on*, pages 1–5, 2012. doi: 10.1109/SSD.2012.6198125.

[21] E. Ildstad. Tet4195 high voltage equipment - cable technology, 2009. Compendium in High voltage equipment subject at Norwegian University of Science and Technology.

[22] M. Runde. Tet4195 high voltage equipment - current interruption in power grids, 2013. Compendium in High Voltage Equipment subject at Norwegian University of Science and Technology.

[23] Lianxiang Tang and Boon-Teck Ooi. Locating and isolating dc faults in multi-terminal dc systems. *Power Delivery, IEEE Transactions on*, 22(3): 1877–1884, 2007. ISSN 0885-8977. doi: 10.1109/TPWRD.2007.899276.

[24] C.J. Greiner, T. Langeland, J. Solvik, and O.A. Rui. Availability evaluation of multi-terminal dc networks with dc circuit breakers. In *PowerTech, 2011 IEEE Trondheim*, pages 1–8, 2011. doi: 10.1109/PTC.2011.6019340.

[25] ABB. Abb solves 100-year-old electrical puzzle – new technology to enable future dc grid, 2013. URL `http://www.abb.com/cawp/seitp202/65df338284e41b3dc1257aae0045b7de.aspx`.

[26] J Häfner and B. Jacobson. Proactive hybrid hvdc breakers - a key innovation for the reliable hvdc grids. The electric power system of the future, International symposium, Bologna, September 2011.

[27] M. Y. Haj-Maharsi. *Novel DC Ring Topology and Protection System – a Comprehensive Solution for mega city power grids.* PhD thesis.

[28] University of Technology Eindhoven. Ptc thermistor, Desember 2013. URL `http://www.resistorguide.com/ptc-thermistor/`.

[29] J. W. Nilsson and Riedel S. A. *Electric circuits, 7th edition.* Pearson Prentice Hall, 2005.

[30] H. K. Høidalen. Tet4130 high voltages and high voltage protection, 2012. Compendium in High voltages and high voltage protection subject at Norwegian University of Science and Technology.

[31] M. M. Saha, J. Izykowski, and E. Rosolowski. *Fault Location on Power Networks*. Springer, 1st edition, 2009.

[32] A. Alefragkis. Transient analysis of multi-terminal hvdc vsc-based networks during dc faults. In *IET conference - DPSP 2014*, March 2014.

[33] AGH department of electronics. Damped oscillations in rlc circuits, May 2010. URL `http://en.wikipedia.org/wiki/File:RLC_transient_plot.svg`.

[34] Wikipedia. Rlc transient plot, May 2010. URL `http://en.wikipedia.org/wiki/File:RLC_transient_plot.svg`.

[35] N. Kumar. *Comprehensive physics XII*. Laxmi Publications, 2003.

[36] Jin Yang, J.E. Fletcher, and J. O'Reilly. Short-circuit and ground fault analyses and location in vsc-based dc network cables. *Industrial Electronics, IEEE Transactions on*, 59(10):3827–3837, 2012. ISSN 0278-0046. doi: 10.1109/TIE.2011.2162712.

[37] Ibrahim Farhat. Fault detection, classification and location in transmission line systems using neural networks. 2003. URL `http://spectrum.library.concordia.ca/1920/`.

[38] U Astrom, B Westman, Victor Lescale, and Gunnar Asplund. Power transmission with hvdc at voltages above 600 kv. In *Power Engineering Society Inaugural Conference and Exposition in Africa, 2005 IEEE*, pages 44–50. IEEE, 2005.

[39] K Bohnert, P Gabus, H Brändle, and Aftab Khan. Fiber-optic current and voltage sensors for high-voltage substations. In *16th International conference on optical fiber sensors*, pages 752–754, 2003.

[40] D Naidoo. Protection of ultralong hvdc transmission lines. Master thesis, University of Kwazulu Natal, March 2005.

[41] J. Suonan, J. Zhang, Z. Jiao, L. Yang, and G. Song. Distance protection for hvdc transmission lines considering frequency-dependent parameters. *Power Delivery, IEEE Transactions on*, 28(2):723–732, 2013. ISSN 0885-8977. doi: 10.1109/TPWRD.2012.2232312.

[42] G. Krzysztof, R. Kowalik, D Rasolomampionona, and S. Anwar. Traveling wave fault location in power transmission systems: An overview. *Journal of electrical systems*, 7(3):287–296, 2011.

[43] D.C. Robertson, O.I. Camps, J.S. Mayer, and William B. Gish. Wavelets and electromagnetic power system transients. *Power Delivery, IEEE Transactions on*, 11(2):1050–1058, 1996. ISSN 0885-8977. doi: 10.1109/61.489367.

[44] K. De Kerf, K. Srivastava, M. Reza, D. Bekaert, S. Cole, D. Van Hertem, and R. Belmans. Wavelet-based protection strategy for dc faults in multi-terminal vsc hvdc systems. *Generation, Transmission Distribution, IET*, 5(4):496–503, 2011. ISSN 1751-8687. doi: 10.1049/iet-gtd.2010.0587.

[45] F.H. Magnago and A. Abur. Fault location using wavelets. *Power Delivery, IEEE Transactions on*, 13(4):1475–1480, 1998. ISSN 0885-8977. doi: 10.1109/61.714808.

[46] M. E. Abdelsalam. *Power Transmission Line Fault Location based on Current Traveling Waves*. PhD thesis.

[47] AM Gargoom, N Ertugrul, and WL Soong. Comparative study of using different mother wavelets on power quality monitoring. *Signal*, 2:2, 2004.

[48] Ying Zhang, Nengling Tai, and Bin Xu. Fault analysis and traveling-wave protection scheme for bipolar hvdc lines. *Power Delivery, IEEE Transactions on*, 27(3):1583–1591, 2012. ISSN 0885-8977. doi: 10.1109/TPWRD.2012.2190528.

[49] T.S. Sidhu, H. Singh, and M.S. Sachdev. Design, implementation and testing of an artificial neural network based fault direction discriminator for protecting transmission lines. *Power Delivery, IEEE Transactions on*, 10(2): 697–706, Apr 1995. ISSN 0885-8977. doi: 10.1109/61.400862.

[50] H.W. Dommel and W. Scott Meyer. Computation of electromagnetic transients. *Proceedings of the IEEE*, 62(7):983–993, July 1974. ISSN 0018-9219. doi: 10.1109/PROC.1974.9550.

[51] A. Fujimori, T. Tanaka, H. Takashima, T. Imajo, R. Hata, T. Tanabe, S. Yoshida, and T. Kakihana. Development of 500 kv dc pplp-insulated

oil-filled submarine cable. *Power Delivery, IEEE Transactions on*, 11(1): 43–50, Jan 1996. ISSN 0885-8977. doi: 10.1109/61.483999.